Three-dimensional electrode array for brain slice culture

Vazquez Rodriguez, Patricia; Dimaki, Maria; Svendsen, Winnie Edith

Publication date:
2011

Document Version
Publisher's PDF, also known as Version of record

DTU Nanotech
Department of Micro- and Nanotechnology

Three-dimensional electrode array for brain slice culture

Ph.D. Thesis

Patricia Vazquez,

Supervisors:
Associate Prof. Winnie Edith Svendsen
Assistant Prof. Maria Dimaki

NaBIS Group
February 1, 2011

Preface

This thesis is submitted as a partial fulfillment of the requirements for obtaining the PhD degree from the Technical University of Denmark (DTU). The research reported has been conducted at the Department of Micro and Nano Technology (Nanotech) at DTU in the period from October 2007 to January 2010. The project has been supervised by Associate Professor Winnie E. Svendsen and Assistant Professor Maria Dimaki, and financed by a Marie Curie European grant within the project CellCheck.

These last three years have been the culmination of a personal search in life. I am privileged that I could do it and be surrounded by so many fantastic people that have taught me so much, both at a professional and at a personal level. It is truly never too late to learn and drive your life the way you want it.

First of all, I would like to thank my supervisor Winnie E. Svendsen for having the idea of this project and believe in me. None of this would have happened without her great support and humanity, and I am always in debt with her for that.

I would also like to thank my second supervisor, Maria Dimaki, for her professional support and dedication. She has earned my highest respect through all these years (which I don't give away so easily), and I had the opportunity to see her as an excellent professional and a human being.

There are particular areas of my work that wouldn't have been done without the help of many people, and I would like to acknowledge them in this space.

For the development of a movable mechanism for electrode arrays I was lucky to count on two great master students, Karsten Brandt and Giovanni Altamura. It was a great satisfaction to see this project coming to a good end, as a way of acknowledgment to all our efforts.

Polymerization of three dimensional electrodes was a beautiful little adventure in science that gave me the chance to work with Luigi Sasso. It was truly a pleasure, both professionally and personally, and he showed me that, sometimes, to believe in peaks is good. Thanks for being a friend.

All experiments of brain slice culture were done at the Neurobiology Research Institute of Molecular Medicine, at the University of Southern Den-

mark. They wouldn't have been done without the help from Jan Bert Gramsbergen, and his advice on the topic has been extremely useful. Also, thanks to Indumati Vedarethinam, a gentle, great spirit in a tiny body, for her help with some neuronal culture and the preparation for my first experiment for brain slice culture. Not to mention her smile throughout these years.

Gracias to Romen Trujillo for his knowledgeable help in the impedance measurements and analysis. The struggle with a micro-needle wouldn't have been as much fun without him. A second set of tests were done by Marco Carminati at the Politecnico di Milano, and his mesurements were extremely useful in their clarity of presentation. Also in relation to the characterization of the electrodes, I would like to mention Henrik Hartmann Henrichsen for helping me in performing the penetration test. His robotic set up saved me a great deal of effort in devising a testing platform.

Most part of my activities took place in the clean room, and it was a pleasure to use such equipment and work with the personnel at Danchip. It was great to work with people that smile and are professional (both at the same time). In particular, I'd like to mention Jonas Lindhart, as a guest start in the fabrication of silicon pillars; Helle Vendelbo Jensen and Katharina Nilson for her sympathy and readiness to help; Rune Christiansen for the metal deposition an bonding knowledge, apart from the pleasure of his company, and the rest of the working team who always behaved in a most professional way.

It was also a great experience to know all the collaborators at the european project of which this work is part of, CellCheck. It was very motivating to meet so many different disciplines of science working together.

I will always remember the NaBis group. I feel privileged for having being surrounded by so many warm people with so much curiosity for life. It will be hard to find again another place where such a contagious open atmosphere surrounds me. I never had to say no to cake so many times.

Thanks, dad, for keeping me in track with the last developments in La Liga. Thanks, Cristi, for being such a beautified reflection of myself, and for bringing new life to our family. New generations take the relay.

And...Thanks John, you have always been there.

Last, I will like to thank myself for having given me the chance to pursued my dreams.

Lyngby, 01-02-2011,

Patricia Vazquez

Contents

Abstract (Danish)

Multielektroder arrays (MEA) er rækker af elektroder mest i mikrometer størrelse, som er blevet brugt i stor omfang til at stimulere og måle elektrisk aktivitet fra neuronale netværker.

Brug af disse for at analysere hjerne slices (hjerneskiver) kan give indsigt i interaktioner mellem neuroner, eftersom dyrkninger af hjerneskiver in vitro beholder funktionaliteten af netværkerne i den levende hjerne.

Elektroder var designet og fabrikeret med det formal at optimere MEA præstationen ved stimulering af og måling fra hjerneskiver in vitro. Meget af arbejdet beskrevet her beskæftiger sig med studiet af silicium mikrofabrikations teknikker for at opnå$3D$ elektroder med en høj dimensionsforhold, som er de mest egnede til at interagere med hjerneskiver.

Elektroderne blev karakteriseret bade elektrisk og mekanisk for at demonstrere deres bedre egenskaber ved elektriske malinger og væv indtrægningsevne.

Ved et andet sæt eksperimenter, det fabrikeret MEA system blev forsøgt integreret med et dyrkningsplatform som skal gøre længerevarende målinger mulige. Baseret påeksisterende litteratur mange forskellige platformer blev udviklet og tested med hjerneskiver. Selvom dyrkningen af væv ikke var mulig i disse systemer, eksperimenterne viser at de mikrofluidiske dele af systemet var funktionelle og det var muligt at integrere MEA systemet med ved at modificere den og lave den del af gennemstrømningsmekanismen.

Til sidst en mekanisme som var I stand til at flytte elektroderne ind og ud af hjerneskiveren blev udviklet, simuleret og testet. Systemet var i stand til at flytte MEA chippen. Selvom mindre modifikationer vil være ønskelige for at forbedre bevægelsespræcisionen, integrering af denne mekanisme med MEA chippen var mulig og funktionaliteten af systemet blev påvist.

Abstract

Multielectrode arrays (MEA) are arrays of electrodes, usually with dimensions in the micro scale, that have been extensively used for the stimulation and recording of electrical activity in neuronal networks.

Their application in the analysisn of brain slices can provide great insight into network interactions, as cultures of brain slices *in vitro* preserve the network functionality of the living brain.

Electrodes were designed and fabricated with the aim of optimizing the MEA performance in recordings and stimulation of brain silces *in vitro*. A major part of this work is based in the study on silicon microfabrication techniques to obtain the high-aspect-ratio, three dimensional electrode structures that are most suitable for interaction with brain slices.

These electrodes were characterized electrically and mechanically in order to demonstrate their improvement in performance for electrical recordings and penetration of tissue.

In a second set of experiments, efforts were made for the integration of the fabricated MEA with a culture platform that would allow long term experiments. Several designs were proposed, based on existing literature, and were tested with the culture of brain slices. Although the culture of the tissue proved unsuccessful, the experiments show that the fluidic systems were functional from the conceptual point of view, and it was possible to integrate the MEA in the system by adapting it within the perfusion mechanism.

Ultimately, a novel mechanism with the capability of moving the electrode array inside the brain slice culture was designed, simulated and tested. It was proven that this system was able to move the MEA, and although the design needs minor adjustments in order to obtain precise control of deflection, the integration of such mechanism with the MEA array was realized and tested to prove functionality.

Chapter 1

Introduction

The nervous system in mammals is one of the most important parts of the body. It is the central mechanism that assimilates all the information comming from the functional body, and modulates the interaction of all its senses with the exterior. It is then no wonder that as many as 10^{12} neurons compose the huma brain.

The influence of the brain in the organism reaches deeper levels than pure physical functionality, as it affects cognitive behaviour like learning [1, 2], language skills, and even the way we think and feel [3]. All of this is due to multiple, tiny electrical signals sent over neuronal connections.

Neurons are the basic cells that construct the nervous system. The neuron is an electrically active cell, is very unique in its behaviour and properties in regard to other cells in the body. For instance, the neuron response to external stimuli varies from hundreds of milliseconds to days; they are connected in networks to other neurons, and these networks are extremely dynamic in creating and destroying interconnections. These networks process information amazingly quickly: the electrical signal generated by a neuron may travel within the nervous system with a velocity as fast as 100 m/s, and the communication from cell to cell takes only in the hundreds of microseconds [4].

Technology has shown an interest in this field for along time now. It is a very appealing area for many reasons: it defines who we are, it governs our physical reactions the potential for the investigation of mental diseases is very encouraging. But maybe it is the electrical nature of the activity of neurons that makes it approachable to the engineering mind. In fact, many of the contributions to electrophysiology are due to the application of new methods supported by technology that was first developed for other purposes, as in the case of microfabrication.

In this chapter, a brief introduction to the biological aspect of neurons is given, discussing mainly their anatomy and functionality. However, a thorough review of this field is beyond the scope of this work, and the main

focus of attention will be driven towards the solutions that technology has provided for the facilitation of electrical measurements of neuronal activity. More precisely, the introduction will be based around the developments and characteristics of microectrode arrays (MEAs), since it is the main motivation of this project to develop a new MEA configuration for the analysis of the electrical activity from brain slices.

1.1 Neuronal electrical activity

The most amazing property of neuronal cells resides in its electrical nature. Most neuronal processes are driven by the propagation of electrical signals generated by other neurons, and it is due to this electrical activity that they are able to behave so dynamically. Although the anatomy of neurons varies throughout the brain, the main features that describe them are [5]:

Soma The body of the neuronal cell varies its dimensions, but it is usually about 20 μm in diameter. As in other cells, it contains the basic organelles of the cell (including the nucleus). In here, all the main activity of the neuron is generated and processed, like the generation of energy or the release of neurotransmitters.

Dendritic tree The dendritic tree is a complex web of cellular extensions with short branches (thereby the name of dendritic *tree*), whose diameters range from 1 to 20 μm. The incoming signals arrive from the outside to the cell from its dendrites.

Axon The axons of a neuron start off from the soma of the cell, in the shape of a filament that spreads out at its end in a tree-branch configuration. Axons are the paths from where neurotransmitters are sent out to the external environment of the neuron, and as such, they adapt their length in order to reach other parts of the body. This is why lengths of up to 1 mm can be found, although their diameter is usual about 1-20 μm, as in the case of the dendrites.

The electrical signals generated in a neuron, called *action potentials*, are short waveforms of about 1 ms of duration and approximately 80 mV of amplitude at the maximum peak. A typical shape of this waveform is shown in figure 1.2.

The basic mechanisms of creation of the action potential will not be explained here, since it is not within the scope of this work. Nevertheless, it should be mentioned that it is caused by an ion gradient between the exterior and interior of the cell. In this situation, the neuron reacts by releasing an ionic flux through its membrane, which forms the electrical signal, called

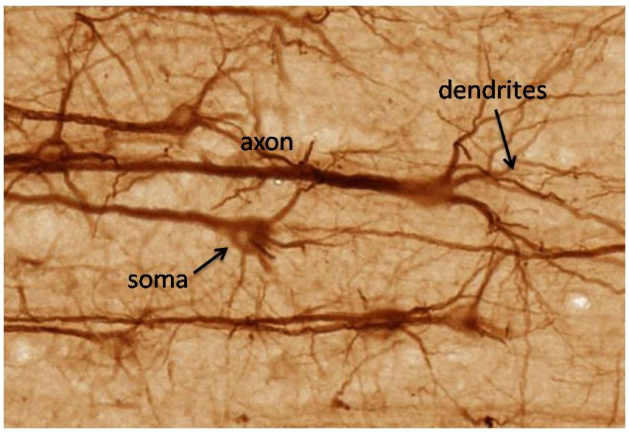

Figure 1.1: Image of a neuronal network. The arrows indicate the main parts of a neuron: soma, dendrites and axon (modified image from wikipedia).

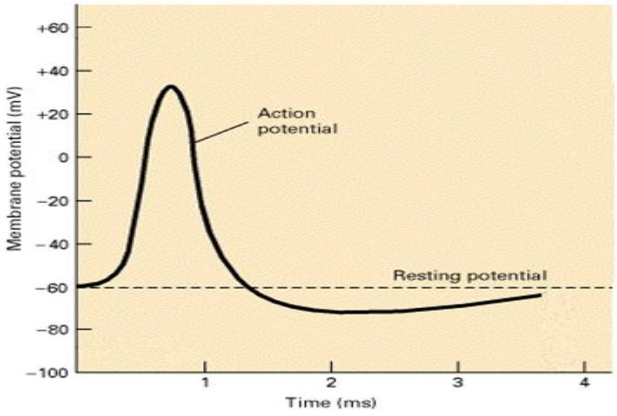

Figure 1.2: The action potential shows a pronounced peak of about 80 mV in amplitude that lasts 1 ms. The broken line shows the resting potential, which marks the transition between the resting state and the excitated phase. A neuron produces an action potential when the voltage of its membrane reaches this voltage level, and by sending out the electrical signal it returns to its original balance (modified from [6]).

action potential. This action potential is then propagated down the axon of the cell, until it reaches the end of it, in a structure called synapse. The signal is transmitted to the synapse of another cell either by chemical release of neurotransmitters or by purely electrical propagation.

1.2 Brain slices

Within *in vitro* techniques, brain slices cultures have become an important tool for the study of neuronal circuits. The benefit of using brain tissue instead of single cell cultures resides in the preservation of intrinsic neuronal circuitry that doesn't exist in single cell cultures. This fact facilitates the study of the neuronal network response as a whole against a particular stimulus, be it chemical or electrical.

The use of brain slices in electrophysiology has been expanding since normal electrical activity was first recorded in brain slice from a mammalian Central Nervous System (CNS) *in vitro* [7]. Plasticity behaviour (dynamic connectivity of the neuronal networks), as well as the effects of drugs or pathologies in the brain alter the structure and functions of the neuronal tissue and can be studied with the availability of brain slices [8]. The same applies to brain development, where thick explants of brain tissue give a more accurate model for the dynamics of the cerebral cortex tissue than thin ones [9]. The great advantage of electrical recordings of neuronal activity is that they can provide a detailed time-course of the events leading to cell death or survival [10].

Among slice preparations, the hippocampus area is of great interest. Its development and characteristics have received more attention than any other region of the brain[11]. This area of the brain has an enormous impact on the regulation of processes in the brain; it seems to play an essential role in the process of behavioral learning and memory [12, 13], and thus studies of neurotoxicity applied to the hippocampus [14] have high relevance for the understanding of the effects of harming substances in the brain.

The hippocampus area offers also easy access for analysis, since it is organized in different, very easily distinguished layers of neuronal cell types. When cut into thin slices (of about 400 μm) in the correct direction, neuronal networks remain well preserved, and can be observed under a normal microscope, without the need of any additional instrumentation or chemical modifications. Due to the wealth of information on this part of the brain, its relevance and the easy access for monitoring purposes, this work will be focused on the hippocampus.

In a brain slice, the entire neuronal network within the tissue is communicating constantly from one point to another. Like the lights of a city viewed from a plane, this activity signals the presence of the neurons and

shows their lives and the mesh of interactions, but individual cells cannot be pinpointed. Therefore, studies of brain slice activity aim for the stimulation and recording of local populations of neurons.

Therefore, studies on neuronal cultures and brain slice cultures should be seen as complementary, as each provides with different type of information about neuronal activity.

Acute slices and organotypic slices

In order to prepare brain slices, the animals are killed and the whole brain immediately extracted. In the case of the preparation of hippocampal slices, the hippocampal area is located and subsequently removed from the rest of the brain. Thin slices are usually obtained in a specialized cutting equipment that is well calibrated to obtain the desired thickness of the slice. The difference between acute slices and brain slices is that the former ones are used for electrophysiological measurements immediately after the cutting, whereas the latter are preserved in an appropiated culture environment for at least 1-2 weeks until the recordings are made.

Since acute slices are used immediately, the original structure of the brain is preserved in the tissue under analysis. Nevertheless, the cutting process creates a dead cell layer that impedes the acquisition of good quality of signals (this fact will be commented later on). On the other hand, if given the appropriate time, organotypic slices are able to regenerate the damaged tissue.

1.3 Multielectrode arrays for neuronal studies

The action potentials generated by neurons are, after all, electrical signals. As such, it is possible to measure them by placing a conductive surface nearby. This idea was embraced for the development of multielectrode arrays for electrophysiological applications.

The measurement of electrical signals from neurons in vitro with electrode arrays started in the seventies with the first original work by [15], and was followed soon after by many others [16, 17, 18]. The first works were prompted by the emergence of microelectronic technology that made possible to fabricate electrodes in the subcellular size of less than 10 μm.

The concept that defines a multielectrode array is very simple: a group of electrodes, usually in the micro meter range, are distributed homogeneously and placed in the center of a chip. From their sites, wires embedded in the chip go to the outside world through pads of bigger dimensions, which are manufactured for ease of connection. This typical configuration can be

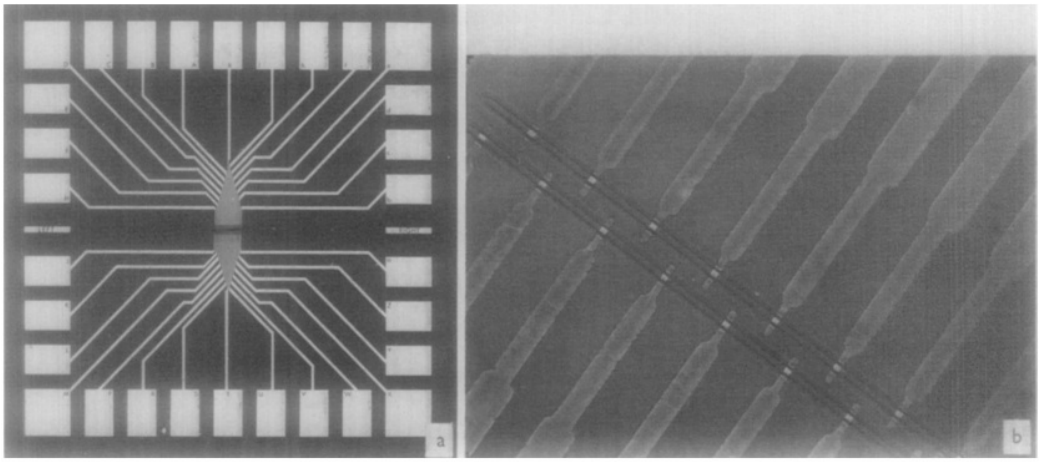

Figure 1.3: First microelectrode array. The left shows a view of what would be a typical MEA, with the pads surrounding the perimeter of the chip for accesible connection, and wires going from the pads towards the center of the design, where the microelectrodes are distributed. On the right, a detail showing a group of microelectrodes (from[15]).

observed in figure 1.3, which has been chosen as example and to pay tribute to the first fabricated MEA.

One of the first differences between this technique and the more traditional method of patch-clamping is that in this case the recordings are extracellular, which means that is a non-invasive method that allows long-term recordings. This comes in stark contrast to mirco-pipetting, which consists of impaling a single cell in order to record its signals from its internal environment, which unfortunately causes its death after a brief lapse of time.

Due to the extracellular character of the recordings obtained, though, measurements are limited to electrical activity that comes often from multiple neurons, since the electrodes of the system are placed in the open space of the culture environment, and therefore exposed to neighbouring cells [19]. This is undesirable in the case of studies where the main interest lies in single cell analyisis or membrane properties, but it offers a wealth of information about neuronal network dynamics. Therefore, different techniques are pursued for different purposes.

On the downside, as measurements are extracellular there is a typical loss of the strength of the signal between 100 and 1000 %. This is due to the fact that the cells don't attach perfectly to the surface of the electrodes; the distance between both bodies introduces what is called the seal resistance (basically, an opposition to the current flow). This problem can be paliated by using specific coatings that promote the adhesion of neurons to the substrate[18], but the nature of the extracellular recording will always carry some loss of signal. On top of that, it must be taken into consideration that

the reach of the action potential, once it comes out of a neuron, is in the range of 10-50 μm. Therefore, the sensor must be placed as close as possible to the cell [4, 17]. Even then, the amplitude range of these signals is not great: typical recordings range from 100 μV to 1 mV.

One of the key features that defines a MEA is the feature of having muliple electrodes that can be used simultaneously. This configuration allows recording from many disparate points within the same culture, something that, until their introduction in the field of neurophysiology, wasn't possible. In this way, travel propagation of a signal can be traced from one initiator site to the final destination, and the effect of an stimulus in a particular area can be studied in the broader range of the neuronal network.

Technological advances in materials, recording techniques and on-chip stimuli has driven research in the field, although the main concept of a MEA remains as the original design. One of the most prominent alterations, though, is the incorporation of CMOS technology [20, 21] to improve the quality of the signal recorded. This is done by offering the amplification of the recorded signals on stage. Moreover, the number of electrodes available for recording is much larger with CMOS technology, reaching few thousand electrodes at least.

Despite the great advantage of this type of chip, their fabrication is not easy and limits the range of materials and temperatures for post-processing, since the circuitry built inside is quite sensitive.

1.4 3D electrodes

Although three dimensional electrodes have been used extensively in microelectrode arrays for *in vivo* implants in the brain since the 90's [22], developments for applications *in vitro* show only few examples [23, 24]. Although the realm is different for *in vivo* recordings of the brain than for *in vitro* applications, the concept of using sharps stuctures for ease of penetration in the tissue is of equal importance.

1.4.1 Dead cell layer

It is a well known fact that the use of three dimensional structures improves the efficiency of electrical systemswith regard to the sensitivity of the measurements.

The use of three dimensional electrodes has many advantages in the realm of brain slice recording. First of all, the fact of having a system able to penetrate the tissue closes the distance between cells and the surface of the electrodes, reducing the leakage of signal that impedes the quality of the recordings. This is a very common problem found in MEAs, and it is usually

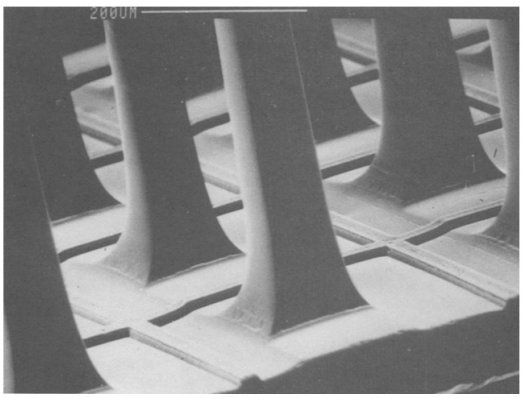

Figure 1.4: One of the first implantable MEA device, the well known Utah array (from[22]).

adressed by coating the surfaces of the electrodes with layers that promote the adhesion of neurons to the surface.

Unfortunately, in the case of brain slices, this measure is of no help, as when cutting the tissue to obtain slices, a layer of death cells is produced. This layer, that may range from 50 μm [24] to μ [25], is placed at the outside of the brain slice. Its presence makes planar electrodes inefficient because they lie far from the active sites within the tissue. Moreover, it acts to attenuate the signal detected by the electrodes. This is so because it isolates like a dielectric layer, impeding the passage of the signal through it. Recordings made with planar MEAs [18, 26] in brain slices showed amplitudes much lower than those achieved with a glass micropipette.

It seems, therefore, that using penetrating electrodes for brain slice recordings may improve the quality in the signals obtained, at least with regard to their amplitude. On top of that, the closer proximity to active, live neurons has the benefit of allowing a more efficient, local stimulation in the tissue. This is so since the intensity of the current needed as a stimulus is reduced, as it reaches easier the targeted area. Using low currents is not only beneficial for the culture, but for the electrode itself, since, as it will be seen in chapter 3, the use of high currents may trigger faradaic processes that can release toxic ions into the culture environment [27].

1.4.2 Reduction of noise

The use of high aspect-ratio structures also has another benefit in that, when compared with planar electrodes, they offer better recording quality as a consequence of the reduction of noise. This may not seem obvious, and therefore a careful explanation will be included here.

Let's take as an example the comparison of a disk-electrode with a cone-

electrode. Although for conceptual demonstration any other three dimensional shape could have been chosen, the use of a cone profile is of high relevance for electrodes in the domain of brain slice recordings. It is intuitive to think of sharp structures as the optimal for penetration of brain tissue. Other more blunt structures would only increase the tear and damage during their insertion (this fact will be studied in detail in chapter 3).

Therefore, let's consider an electrode of a conical profile, as shown in figure 1.5,

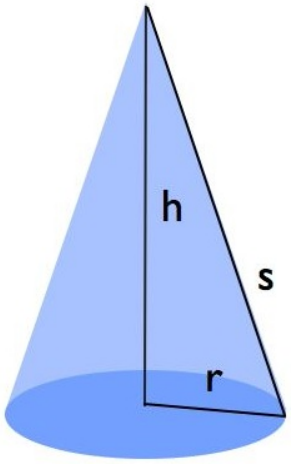

Figure 1.5: Conical electrode of height h, radius r and slant height s.

According to notation from the image, the slant height s is calculated by Pythagoras' theorem:

$$s = \sqrt{h^2 + r^2} \tag{1.4.1}$$

The surface area of a a conical electrode would be given by the following expression:

$$A_{3D} = \pi r s \tag{1.4.2}$$

and by considering the area of a planar disk-electrode of the same radius r

$$A_{2D} = \pi r^2$$

the ratio between both surfaces areas can be calculated. Substituting equation 1.4.1 into 1.4.2, the ratio between the planar electrode and the three dimensional can be expressed as:

$$G = \sqrt{\left(\frac{h}{r}\right)^2 + 1} \tag{1.4.3}$$

The expression of the ratio G between the 3D and 2D electrodes reflects the effect of the height of the cone in the increase of the gain in surface area.

The increase in surface area affects the resulting impedance of the electrode, and this is an important factor in any system that aims at reducing noise with the recording of the signal of interest.

The relation between the impedance of the electrode and noise is due to the expression of the thermal noise. Thermal noise, otherwise known as Johnson noise, accounts for most of the noise in an electrical system. It is originated from the movement of the charges inside the electrode, and can be calculated by the expression given by equation 1.4.2.

$$U_{th} = \sqrt{4kTRB}$$

where k is Boltzmann constant, T the temperature, R the resistance of the electrode and B the bandwidth of measured frequencies. Therefore, this is the link between the impedance of the electrode and the noise introduced in its measurements. But how does this relate to the surface area mentioned before?

The answer to this lies in the relation of the resistance of a conductor to the surface area. For a conductor of resistivity ρ, length l and cross-sectional area A, the resistance is expressed as in equation 1.4.4.

$$R = \rho\frac{l}{A} \tag{1.4.4}$$

The equation is shown here for illustrative purposes. It makes clear that by increasing the surface area, the resistance R is reduced G times (as per eq. 1.4.3).

It can be therefore concluded that the thermal noise U_{th} is also reduced, in this case in a proportion of $\sqrt{G}$.

After the previous analysis, the fact that should be remembered is that G, the gain factor introduced by using three dimensional electrodes instead of planar ones, directly impacts the quality of the recording signals by reducing the thermal noise.

This fact was also proven experimentally by [24]. In this paper it was shown that signals measured from acute hippocampal slices with three dimensional electrodes presented an increase in amplitude in comparison with planar electrode recordings.

In conclusion, the use of three dimensional electrodes seems a very suitable technology for the recording and stimulation of brain slices *in vitro*. Sharp structures of high aspect-ratio are an advantageous feature since they

penetrate the dead cell layer of the brain tissue, which impedes electrical measurements. Three dimensional electrodes are able to reach active cells and, by positioning closer to them, capture stimuli and recordings that are more accurate than in the case of planar electrodes. Moreover, their high surface area contributes to a reduction in the electrical noise, as it has been shown.

However, the use of out-of-plane structures that are able to penetrate tissue and cells is relatively new, as it will be explained in the following section.

1.5 Three dimensional electrode MEAs

Few works can be found in relation to three dimensional electrodes in MEAs for brain slice recordings. There is a well established field in the development of three dimensional structures for *in vivo* applications, but this is a slightly different concept. Mainly, these electrodes need to be very long, in the range of the millimiter, in order to penetrate the skin layer and reach the brain. Therefore, most of these fabrication techniques are unsuitable for the creation of out-of-plane electrodes in the micrometer range. There are exceptions where applied silicon microtechnology is used to obtain very sharp and tall structures. This is the case, for instance, of [28], where microfabrication techniques were used to create electrodes 250 μm of height and tips of less than 1 μm (in fact, the technique used in this article will be applied during part of this project). However, this work didn't show any results in regard to electrical recordings, and it may be due to the fact that such tall, sharp structures may prove hard to metalize.

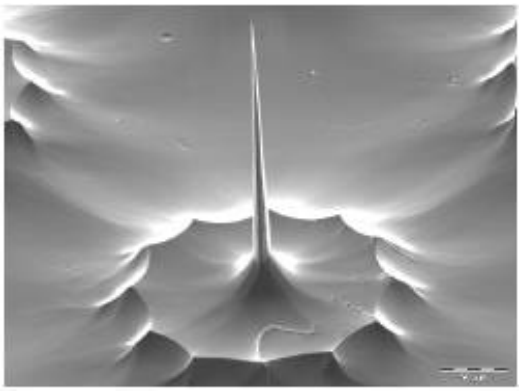

Figure 1.6: Very high aspect-ratio needles made of silicon were fabricated by microfabrication techniques. [28]

[29] took an original approach to the design of a 3D MEA for electrophys-

iology. Very tall, sharp stuctures were made of SU8 (a negative photoresist used commonly in microfabrication techniques). This work shows the tallest fo all electrodes published for brain slice recording, with reported dimensions of up to 570 μm and 120 μm in diameter. An image of the obtained array can be seen in figure 1.7, where the SU8 pillars have been electroplated with nickel. Although this report is worth mentioning, difficulties in metalizing these structures need to be considered. As shown in the image, it is possible to coat the whole array with a thin layer of metal, but to pattern it in order to obtain independent electrodes is another matter. This problem is not addressed on the mentioned reference, but that is most likely due to the fact that the design focused in the aim of integrating a perfusion system that could penetrate the brain slice culture (it should be mentioned, though, that the use of SU8 raises questions about biocompatibility, and the fact that the hollow needles are made of this material could compromise the survival of brain slice culture). On top of that, the fabrication of such device is not trivial and requires many steps for its fabrication.

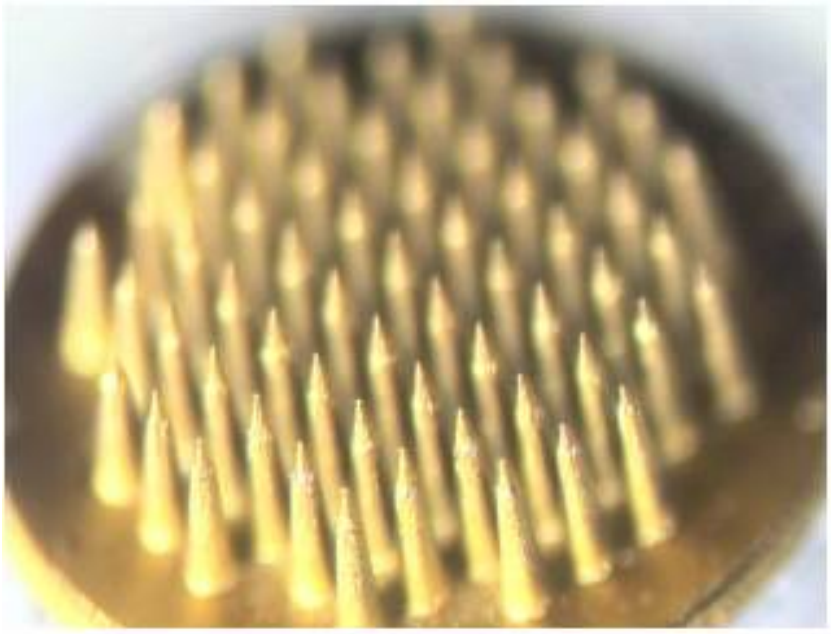

Figure 1.7: This image shows an array of SU8 towers mounted in a fuse silica substrate. Although in this picture the surface of the array is covered by a metal layer, the high aspect ratio of the structures is likely to impede proper wiring that would lend independent connections to each of the towers [29].

Work done by [30, 24] inititated the application of three dimensional MEAs for the recording of acute brain slices, and their contribution to the field is still relevant. In the former approach, electrodes were fabricated in

silicon and processed by common microtechnology processes. In the latter, the substrate of choice was glass for the transparency of the material, which allows for inspection of the array under a microscope. In both cases, the dimensions of the electrodes were between 47 and 60 μm in height, which is sufficient to bypass the dead cell layer mentioned earlier. Figure 1.8 shows the array of needles fabricated on a glass substrate [24]. This fact is reflected in the quality of the results shown. Their measurement showed a significant improvement in comparison with planar recordings. For instance, signals reported by [18] presented amplitudes not higher than 200 μV, whereas the above mentioned articles produced stable recordings of at least 400 μV (reaching 700 μm in [24]).

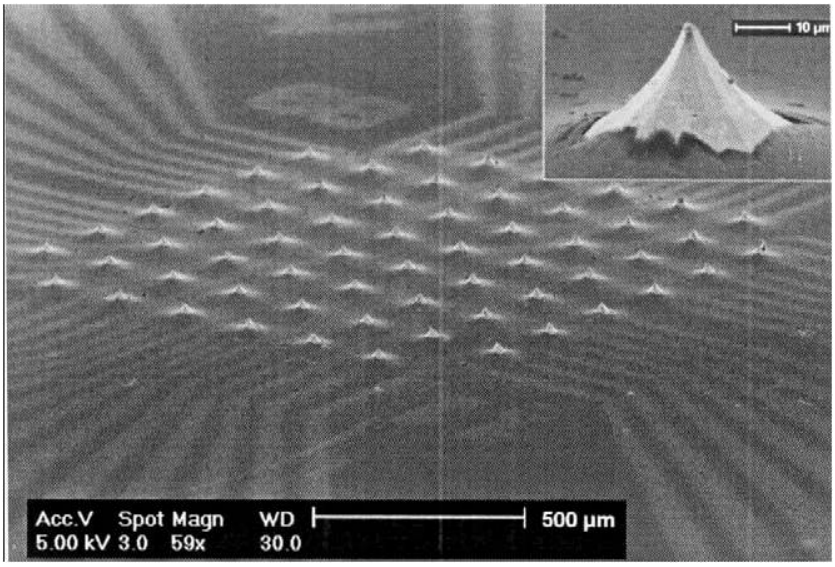

Figure 1.8: Multielectrode array with three dimensional electrodes, fabricated on a glass substrate. The insert shows one of the electrodes in detail. The height of the pyramid is 60 μm, although only the top 40 μm can actively record signals as the rest of the surface is covered by an isolating material [24].

Despite the good results, some improvements can be made in these designs. As can be seen in figure 1.8, the profile of the electrodes is quite flat at the base. This profile, which is inherent in the fabrication process, may hinder the penetration of the electrodes to active layers of the brain tissue. This is also the case with [30], with the electrodes just tall enough to reach inside the active part of the brain slice.

Nontheless, the most remarkable shortcoming in this area is the lack of studies in long term recordings of brain slices. This is due to the fact that the integration of a MEA platform with a suitable culture environment is not easy. Usually, this problem has been tackled by simply attaching a vial

to the MEA chip, whith the array lying in the center. This solution is not ideal from the point of view of optimization of the culture environment and long term measurements with the culture on-chip.

In none of the literature presented in this section was work done with the aim of obtaining long recordings. This is not due to lack of interest, as it will be commented on extensively during chapter 4.

1.6 Overview of the thesis

In this work, the development of a novel microelectrode array with three dimensional electrodes is presented. The fabrication technique is based on silicon methods, due to its biocompatibility and the availability of the equipment. In fact, the greater part of the project is based on mastering these techniques.

The electrodes obtained present a novel profile for the recording of brain slice signals, and from their characterization it seems that this shape could promote better signal recording. Moreover, since this profile is not completely smooth, it is hypotesized that it may improve the adhesion and anchoring of the tissue to its surface.

Nevertheless, the main motivation of the project was due to the lack of a reliable solution that takes care of culture on-chip specifically. This is desired for the aim of long time recordings, where there is no need to interrupt the measurements or damage the tissue by unnecessary manipulation of the tissue. Efforts on the optimization of MEAs and design of novel microfluidic devices for culturing brain tissue *in vitro* have been reported, but few works have tried to blend both approaches into one solution. A detailed review of methods of culture and proposed alternatives is given in chapter 4.

The structure of this thesis is as follows:

Chapter 1. Introduction.

> A brief introduction of the state of the art in relation with MEAs and three dimensional electrodes has been given. This introduction justifies the efforts for obtaining three dimensional electrodes for brain slice recording.

Chapter 2. Fabricaton.

> This chapter explains all the experiments done in the pursuit of a three dimensional structure for a MEA of silicon that is most suitable for brain slice recordings. Most relevant experiments done during the fabrication of the multielectrode array is presented, with issues and alternatives to standard methods.

In a second set of experiments, the fabrication of the novel MEA is modified in order to adapt it for the integration with a culture system.

Last, an alternative to standard metalization processes is shown, which solves step coverage issues in the presence of very sharp and tall profiles in few simple steps.

Chapter 3. Characterization.

As with any electrical system, the impedance of the electrodes defines the quality of the recordings that will be obtained. In this chapter, experiments to mesaure the impedance are realized and the modelization of the impedance presented.

In a second test, the electrodes were analyzed for penetration performace. The details of the experiment and the results are shown.

Chapter 4. Brain slice culture.

A thorough introduction on standard culture methods for brain slices is presented here. Also, an extensive research in literature of alternative methods leads to the design of two culture chamber prototypes, which have been tested for brain slice culture. The experiments done for this purpose are described too.

Chapter 5.Movable electrodes

In this chapter, a novel system with the ability to move the array of electrodes is presented. In order to do that, a brief description of types of actuation mechanisms is given.The design, simulations and fabrication are shown and the device obtained tested.

Chapter 6. Conclusions

A brief summary of the results obtained from all work presented, with conclusions and outlook.

Chapter 2

Fabrication

2.1 Introduction: silicon etching

The etching process is performed with the aim of shaping a silicon substrate with a desired pattern. This is the reason why in most cases it is done after a previous mask patterning on the surface of the wafer; the mask exposes areas that are desired to be removed in the silicon.

This mask is usually made with a deposition of materials that are resistant to the silicon etching species, such as resist, silicon oxide or silicon nitride. Depending on the etching method, the selectivity between the mask material and the silicon varies, but silicon oxide and silicon nitride are the most resilient in all cases.

Of course, nothing comes for free, and once the process is done, resist can be removed by simply dipping the silicon substrate in acetone, whereas silicon oxide and nitride need to be etched away with specific chemical etchants and it may take slightly longer to remove the mask completely.

Two main techniques are available for etching silicon: wet etch and dry etch. Their name is quite self-explanatory: for wet etch, the wafer is dipped into a bath full of a chemical etchant, whereas in dry etch, etching atoms are provided in the form of a plasma cloud that is created inside a low-pressure chamber of a specialized equipment.

2.1.1 Wet etch or dry etch?

Wet etch has the advantage of its simplicity in the concept and set up necessary to carry out the process. The only thing required is the chemical etchant, a temperature controlled cuvette in which to dip the wafer is submerged, and the safety precautions from the user to handle the chemicals.

Different types of chemical compounds can be found for etching either isotropically or anisotropically (although pure anisotropy doesn't exist; see

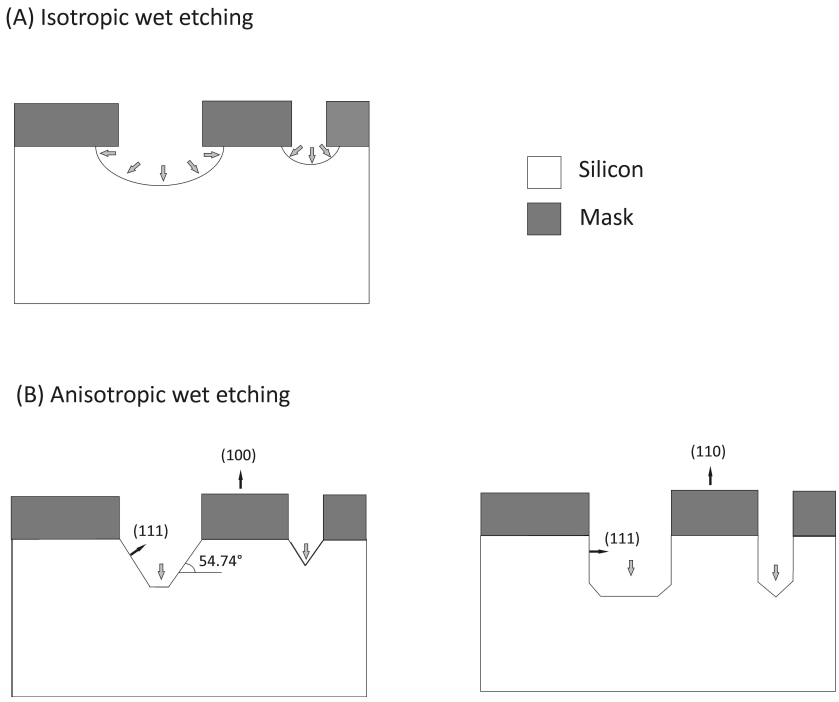

Figure 2.1: Wet etching with (A) isotropic etchant, and (B) anisotropic etchant. In the latter case, the inclination of the walls is affected by the wafer orientation chosen. If the silicon is of type (100), angles of 54.74° appear, whereas if using a wafer (110), the walls rise almost perpendicular to the surface.

Figure 2.1, where the anisotropic steps present some mild curvature at the side walls). Etchants for silicon can be either bases or acids. As examples of acidic etchants, HF, HNO_3 and acetic acid can be used. Nevertheless, bases are most commonly used due to lower cost and safety reasons. Common etchants are (NaOH, (KOH, ethylenediamine pyrocatechol (EDP) and tetramethylammonium hydroxide (TMAH) [31]. Nevertheless, for high aspect ratio structures (etch depth vs. feature width), only anisotropic etch is an appropiate technique. The chemical etchant attacks the silicon crystal planes at different speeds depending of their orientation, thus forming structures with walls at particular angles.

One of the problems of using this technique is the stringency in the angle formation. For instance, when aligning a square mask perfectly with the primary flat of a (100) wafer, a v-groove is obtained (see again Figure 2.1), with side walls at an angle of 54.74° [31]. The imposition in the value of the angle affects not only the design flexibility. In the case of using KOH as etchant, if misalignment happens, under etch of the mask will occur in a space approximately equal to the depth of the etching, and this fact will limit the density of pillars.

Among anisotropic etchants, only KOH is able to fabricate vertical walls, with etched angles of 80°; this may be the reason why it is the most popular etchant. However, the selectivity between silicon and SiO_2 is not very good, and its use should be discarded if the device contains any CMOS circuitry, since it would be attacked by the alkali ions of the solution. This problem could be solved by using tetra methyl ammonium hydroxide (TMAH), as it is devoid of metallic ions, but uniformity and reproducibility are not as good as with KOH. Even worse, the fact that the etch occurs at an angle of 30° [31] would only allow to fabricate small pillars.

In opposition, dry etch improves control over the process in regard to height and profile of the structures obtained, since it doesn't depend on the crystal orientation of the silicon as it happens with wet etching. It also offers a higher selectivity between silicon and its masking materials. In comparison with wet etch, the equipment is more complicated and expensive, but this is a technology developed with the specific purpose of producing high aspect ratio structures in silicon, and such specialization yields a fast and (relatively) easy process to control.

For all the reasons mentioned above, dry etch was considereded as the most suitable method for the fabrication of high aspect-ratio, three dimensional electrodes with a specifically tailored profile for the application of brain slice recordings. It is then a good idea to go a bit in depth with this technology and how do different parameters affect the outcome of the process. As mentioned, dry etching is easier to control than wet etching, mainly because all the specific parameters of the process are defined by the user. However,

the optimization of the ensemble of these factors is not trivial and requires a good amount of understanding of the effects that they provoke.

2.1.2 Deep Reactive Ion Etching

The main idea behind dry etch technology is very simple. If one wants to achieve high directionality of etching, the side walls should be protected from the etching process. The way to achieve this is done with a pair of gases where one of them behaves as active etchant and the other one blocks the first, but only at the side walls, as a sort of shell.

Among all the systems in dry etching, Deep Reactive Ion Etching (DRIE) is particularly efficient in directional etching since it counts with two separate power sources that provide independent control of ion flux and ion energy in a high-density plasma cloud. The plasma cloud is the etching agent of silicon, and the ability to control its energy and density independently enhances the results of the etched surfaces.

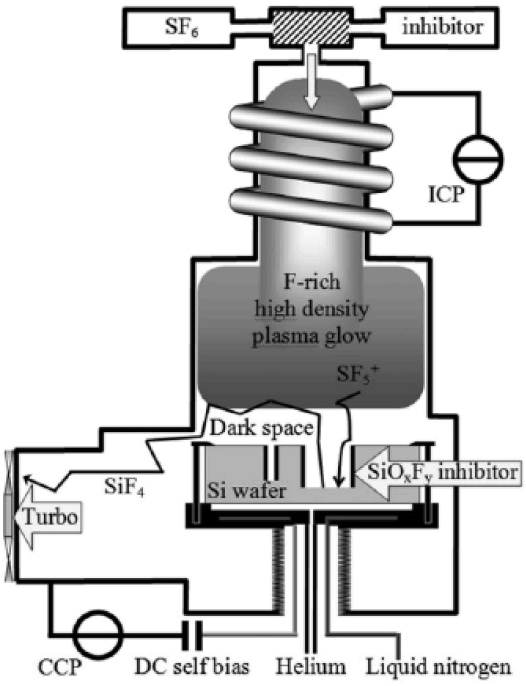

Figure 2.2: Schematic of a dry etch chamber (from [32])

The first power source is an inductive coupled plasma (ICP, also called coil power, is represented in Figure 2.2 with a coil wrapped around the chamber, top) that ionizes the incoming gas, which creates a cloud of highly dense plasma. The ions created will react with the silicon atoms and thus etch

the wafer surface. The second power source, a capacitive coupled plasma (CCP, or platen power), directs the ions from the plasma towards the wafer by creating a difference of voltage between the plasma and the wafer. During the process the wafer is clamped to a chuck with its backside cooled by a constant stream of helium gas in order to ensure a stable temperature on the wafer.

Two main modalities of etch have spread with the use of this equipment: continuous mode and pulse mode. The first one introduces in a continuous way both the etchant gas (in the case of the available equipment, SF_6) and an inhibitor gas (O_2 or C_4F_8) that counteracts the isotropy of the etching gas.

The second modality, introduced by Tsujimoto [33], but patented with the use of flouorocarbon gas by Laermer[34], uses a sequence of passivation cycles (protecting the side walls with polymer-building fluorocarbon gases) and active isotropic etching steps.

Although the continuous mode can obtain high directionality with the right proportion of O_2 (C_4F_8 is never used in this case as the etch rate is too slow), it is only reached at cryogenic temperatures [32]. This range of temperatures requires equipment able to handle them, and on top of that, the surfaces suffer of thermal stress. Additionally, the constant use of both power sources erodes the masking material on the wafer much faster than when performing an alternating, on-off process.

On the other hand, the pulse mode process is particularly easy to tune for the obtainment of very straight profiles with a good control of the undercut. It is for this reason that, although the pulse mode loses some etch speed by introducing a passivation time, it is generally preferred and widely used. It will also be the operating mode of all the experiments that will be explained throughout this work, and it is therefore worthwile to focus into this technique and the parameters that govern it.

Pulse mode

The pulse mode creates a very characteristic pattern. The fact that the two alternating phases are delivered sequentially creates vertical walls embedded with scallops (Figure 2.3), like a footprint of each step. During the active etch (first and third step on the image), most of the gas ions end up colliding with the horizontal flat surface of the floor of the trenches, whereas the walls are less affected. In this way, the protective passivation layer that was deposited in the previous cycle is removed at the bottom of the structure, but not at the side walls (step 3 of image). Unprotected, the bottom is etched at much greater speed than the side walls, and it is this way that tall structures with very vertical profiles are risen.

Up to now, only vertical walled structures have been mentioned, but in the

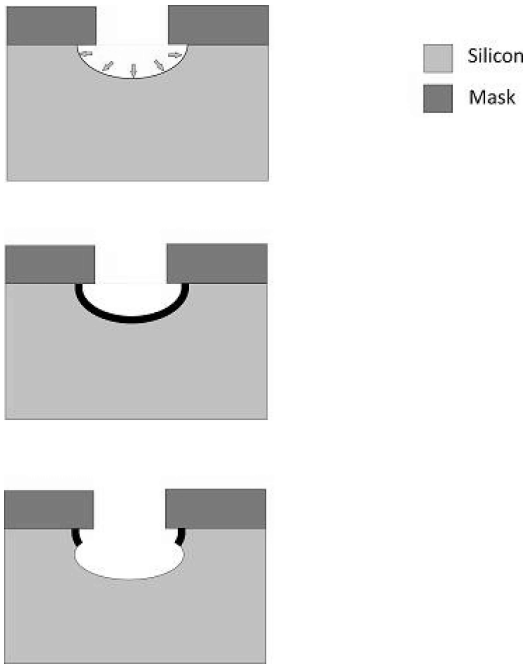

Figure 2.3: Pulse mode scalloping

application of concern here, that is, the penetration and recording of brain slices *in vitro*, it would be extremely valuable to obtain sharp structures, more in a conical fashion than a cylinder for ease of penetration (this fact is explained in detail in chapter 3. In this regard, it is possible to obtain some slope gradient by adjusting the parameters of the etching process [32, 35], but fine tuning needs to be done for each design. This is so, since the results are not only affected by intrinsic parameters of the process (times of etch vs. passivation, pressure, power, gases ratio), but also the amount of etched silicon and the layout of the design [36] play an important role.

Let' take a close look up at the influence of the main parameters that drive the etching process in pulse mode.

2.1.3 Parameters to consider in dry etch

Two type of etching phenomena occur simultaneously inside the chamber: chemical etching and physical etching. The first one happens as a consequence of the chemical reactions between the etchant gas and the silicon atoms, and as such, it occurs in all directions when the ions of the gas come in contact with the silicon atoms. This essentially means that it is an isotropic etch.

On the other hand, physical etching is due to the ion bombardement of the

silicon surface. The ions are directed towards the silicon surface, attracted by the electrical field created between the plasma cloud and the wafer. It is the main cause of directional or anisotropic etch. Only the surfaces that are parallel to the wafer surface will be etched away.

Chemical etching will be directly affected by the ion concentration of the plasma cloud, whereas it can be intuitively predicted that the power will have a great influence in the physical etching, as it accelerates the ion species of the etchant gas towards the substrate.

Yet, the whole picture develops into something a bit more complicated when several factors interact, and therefore a deeper analysis of these interactions is essential to understand the behaviour of a given set of parameters.

Gas ratio and time-multiplexing

Although there are several choices for gas etchants of silicon, the most commonly used is SF_6, due to the fast isotropic etch that it produces. Nevertheless, to control the isotropy of the process, a gas inhibitor counterpart is required if high directionality is desired. In the case of SF_6, its gas inhibitors are, as mentioned before, O_2 and C_4F_8.

Although the pair SF_6-O_2 presents interesting properties in the etching of silicon, the discussions held hereby will center around the pair SF_6-C_4F_8, since it is the fastest and mostly used in pulse etching modality.This is due to the fact that C_4F_8 is an excellent promotor of the inhibition layer that protects the side walls during the etching.

As the main chemical etchant, the concentration of SF_6 affects greatly the speed of the etch of silicon. It obviously follows that, for longer times of active etching, the etch rate increases too.

In opposition, the use of the inhibitor C_4F_8 will slow down the process, since its main function is to produce a teflon-like layer on the silicon surfaces that will protect them from the next ion bombarding during the active etch phase.

Nevertheless, the increase in concentration of this gas doesn't seem to have a great impact in the speed of the process [37]. This is not the case with the passivation time, that in regard to the etching process is a "dead time" and will delay the whole process.

It is also common to mix a concentration of SF_6 and O_2 gases during the active etch phase. The addition of O_2 has the purpose to control the isotropy of SF_6. This is clearly shown in Figure 2.4, where progressive increase in concentration of O_2 changes the profile into straighter walls.

In any case, independently of the concentration of gases, there needs to be a reasonable balance between the active etching time and the passivation phase, if one aims to achieve a good control of the profile and avoid mask undercutting [38]. The combination of both active and passivation time

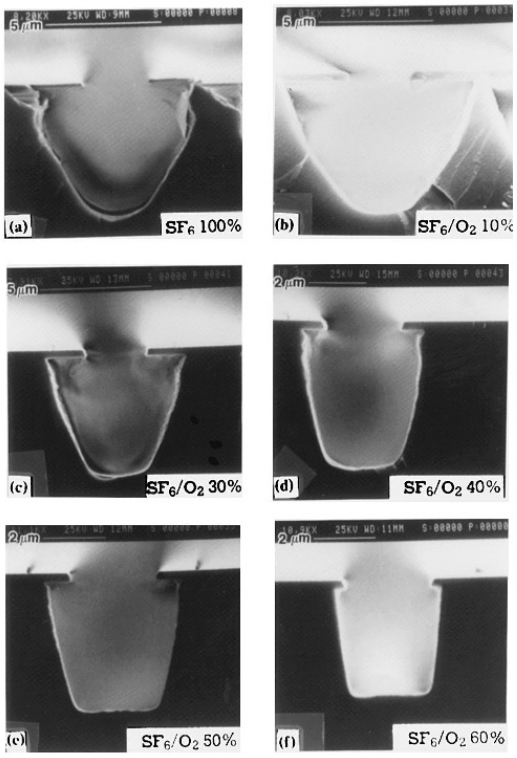

Figure 2.4: Effect of adding O_2 to the active etchant. The sequence of images shows how the increase in the concentration of O_2 translates into smooth, straighter walls, cancelling the insotropy effect of the main etchant gas [38]

needs to be tuned in order to obtain the desired sidewall inclination. This tuning needs to be tailored to each machine and design of the wafer. In

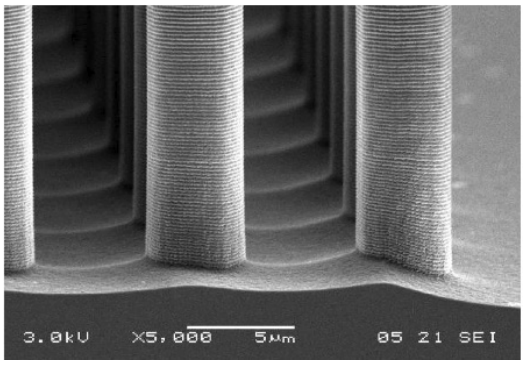

Figure 2.5: Typical scalloping profile formed by a pulse mode etch (modified from [32])

addition, time switching introduces a very typical scalloping profile (see figure 2.5), which can be minimized by adjusting the switching times if this were a feature to be avoided.

Power

The ICP coil, with an RF source of 5 kW at 13.56 MHz, generates a power to create the plasma cloud. As this power increases, the atomic density of both the etching and inhibitor gases in the cloud rise. The consequence of this is an increase in the etch rate, as it could be expected. However, this is only true until a maximum is reached. The reason behind it lies in the fact that the concentration of SF_6 is the limiting factor in the amount of chemical etch that can happen, and therefore, if there is not enough presence of fluorine ions available for reacting with the silicon surface, the increase in power doesn't have any impact in the process.

As for the CCP source (or platen power), its main function is to direct the ionic species in the plasma towards the wafer, which enhances the physical etching and thus the vertical profile of the obtained structures. In other words, it promotes the removal of the inhibitor layer that is deposited during the passivation phase.

The platen power has a radio frequency (RF) source operating at 13.56 MHz.The frequency of the RF source is too high for the ionic species to follow it, and therefore this source will not produce directly ionic bombardment. On the other hand, the electrons from the plasma are captured by this field. The migration of these charges leaves the plasma cloud with a positive potential bias, referred often as self-bias potential. It is this self-bias potential that will drive the ionic species against the surface of the wafer.

Pressure

The ASE can control the pressure value at which the process is run. At high pressures the etch rate will generally increase, with the advantadge of reducing the needs on the operating power that accelerate the bombardment species onto the silicon surface. This is due to the fact that the voltage at which the wafer will be is dependent on the pressure and RF power. Therefore, for a high value of pressure (which increases the voltage on the surface of the wafer) will require less power for the same ionic acceleration of the etching species. This would minimize the potential damage onto the etched surfaces. Another advantadge of operating at high pressure values is that high gas flow rates are easier to obtain. Nevertheless, directionality is better under low pressure operation and the selectivity of silicon against its masking material could be worsened by using high pressures [39]

Temperature

Temperature is a factor that can affect the etch ratre of the etching process. This is due to the fact that the chemical reactions between silicon and fluorine etchants are initiated when an energy threshold is reached, the activation energy, which depends exponentially on the temperature. If the temperature of the substrate is lowered, this chemical activity will decrease. Nevertheless, according to Jansen *et al.*[32], for temperatures in the range of room atmosphere down to $-120°C$, the etch rate decreases only about 10 percent, and therefore the impact of this factor is not very relevant for the speed of the process.

Nevertheless, temperature will have an important impact in the profile of the structures etched. If lowering the temperature decreases the chemical etching reactions, it has no effect on the physical bombardment. Since physical bombardement is the main etchant of the parallel surfaces on the substrate, this fact will only enhance the directionality of the overall etching. That said, operating at low temperatures comes with a cost. It may require the use of specific equipment able to handle cryogenic temperatures, but worst of all is the thermal stress that is introduced in the materials etched, due to the difference in thermal expanssion coefficients of silicon and its masking materials. In any case, since the equipment available for this project is only able to produce temperatures between 0 and 10 °C, the option of using cryongenic temperatures will not be considered.

Loading

Two phenomena are related to the pattern distributed along the surface of the wafer to be etched: macroloading and microloading. Macroloading is the effect caused by the total amount of silicon etched from the wafer. The

quantity of silicon ions etched away may end depleting completely the free ionic fluorine species in the plasma, therefore decreasing the etch rate of the process [39]. This could create problems if, for instance, silicon were to be etched all the way through until reaching a buried layer of another material. The progressive consumption of the silicon would create significant changes in the etch rate, making hard to predict the optimal end of the process. It will also affect the amount of under etch on the structures, as a small load would encourage this effect in comparison with a higher percentage of exposed area [40].

Microloading behaves in a similar fashion, but applied to a local area, where the structures may be affected by the depletion of etchants due to the design of the mask on that particular point.

These effects will be taken into account only in order to avoid an excess of loading, which would slow down the etch rate. A reasonable loading of at least a 10 % is adviced [40] . As for microloading, the design will be done in a symetrical fashion as to equilibrate this effect.

2.1.4 Undesired effects

For structures of high aspect ratio, be it deep trenches, or as in the case of this work, tall towers (in all experiments carried, consistently happening after reaching 50 μm of height), the appearance of undesired side-effects hinders a full control of the profile. These effects are called the RIE lag and the image force (IF). Both of them are a consequence of the etching ions colliding at an angle with the side walls of the trenches formed during the process, instead of the ideal situation where the impacts of the bombarding etching occurs perpendicuarly to the surfaces. But here is where the similarity ends, since each effect is caused by different deflection mechanisms, which will be explained in the following paragraphs. Figure 2.6 shows two examples of the appeareance of these two effects. RIE lag appears when the features etched are very different in diameter. The left side of the image shows how wider trenches tend to be etched faster than the small ones. On the other hand, the IF effect affects the directionality of the etching, making it more pronounced at the bottom side of the vertical walls (right hand side of image).

The mechanism behind the RIE lag occurs as a consequence of the ionic species coming in contact with the silicon surfaces at an angle. The deviation from the perpendicular direction is due to random collisions of the ions with gas particles. This angle produces a certain etch under the mask, and as the process continues, when the trenches acquired the necessary height, the top part of the narrower structures stops the incoming ions and thus the etching. This effect is represented in Figure 2.7 as shadowed areas that the incoming ions aren't able to reach. Also notice how the side walls are not totally vertical, and the inclination is slightly more pronounced in the wider

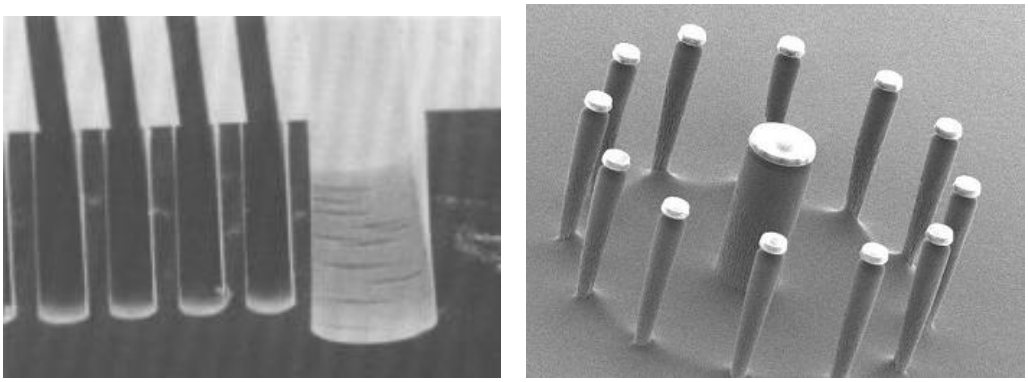

Figure 2.6: Undesired effects in silicon etching. Left, RIE-lag effect showing wide trenches that are etched faster (deeper) than the narrow ones (image taken from [40]). Right, IF effect seen repeated times in the mask design used for the 3D electrode array. The outside pillars are openly exposed to the effect, showing an uneven etch that attacks their base much faster than their top

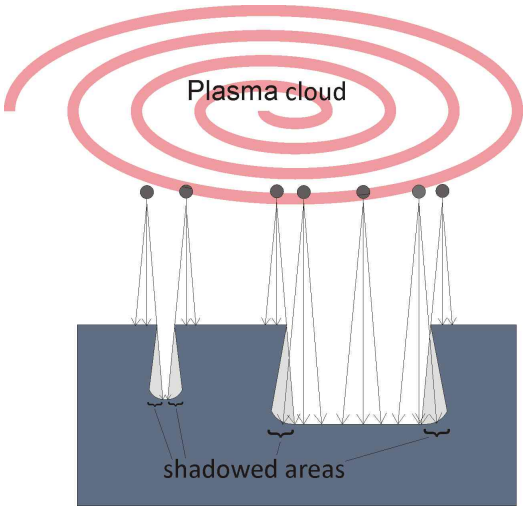

Figure 2.7: RIE lag effect

trench.

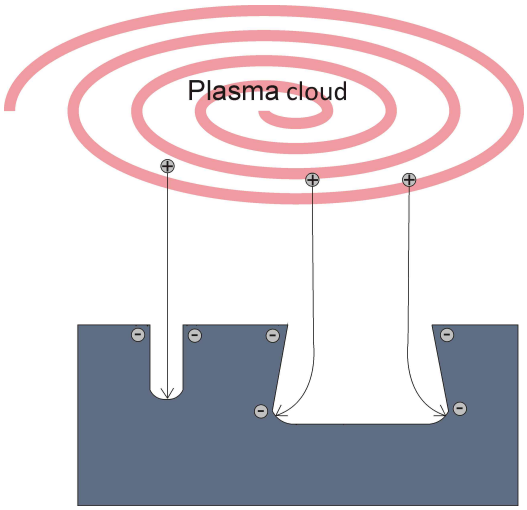

Figure 2.8: IF effect caused by the attraction of the positive ionic etchant species towards the negatively charged side walls of wide trenches. On narrow trenches, the walls are close enough to each other to cancel out their electrical field, and thus the ionic species aren't deviated.

On the other hand, IF affects wide trenches where walls don't cancel out each other's electrostatic attraction to the ionic species. Under these conditions, the ionic etchants are accelerated toward the wall with increasing speed as they reach further down the trench. As Figure 2.8 shows, the IF effect is cancelled out in narrow structures due to the closeness of the walls to each other, which balances the attraction of the ionic etchants towards their electrical potential. On the other hand, for wide trenches like the one on the right hand side of the figure, the bombardement of the attracted ionic species into the side wall produces a negatively tapered etch. This effect is also illustrated on the right hand side of Figure 2.6. A typical pulse-mode process was run to etch pillars of heights of about 100 μm, but the outermost structures were severely affected by the IF negative tapering.

Llet's define a convention for the sign of the angle at trenches and sharp structures. The inclination of the structure shown in figure 2.9 will be referred from now on as a "positive" inclination, and thus the angle will be also considered positive. Therefore, as commented, the RIE-lag and IF effects produce a negative tapering, which means that the structures obtained will have the inverted shape of the one shown in the image.

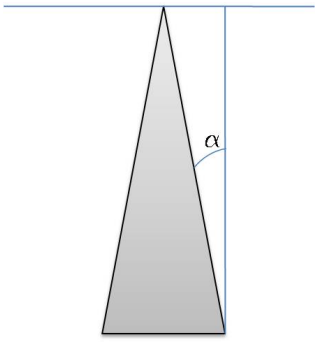

Figure 2.9: The image shows a structure with what will be referred to from now on as a "positive angle".

2.2 Experimental work: Electrodes fabrication

The main purpose of the experiments that will be explained here is to fabricate three dimensional, high aspect-ratio electrodes in silicon. The shape of these should be as sharp as possible, in order to minimize the damage of brain tissue when penetration by these structures occurs.

Heights over 50 μm would be desirable for the possibility to trespass the outer layer of dead cells that grows after cutting the brain slices [24]. The fact of obtaining these heights would also be beneficial from the point of view of the quality of the recorded signals, since higher disponibility of surface are of the electrodes translates into a better discrimination between signal and noise (section 1).

The requirements of the design in regard to electrode density wasn't specified, and as such it left room for freedom to chose the spacing between the structures. It should be considered that highly populated arrays complicate the interconnections on the chip, and it was therefore thought as a good approach to start with a matrix of 8x8 electrodes, which is also a very common configuration in commercially available arrays (Multichannel Systems, MED65).

This part of the experimental work will present and discuss the different problems that rose during the fabrication of these structures and what solutions were used to solve them. As a departing idea, it was thought to create the electrodes in two steps: one, that would make tall cylindrical structures of vertical profile; two, a sharpening, maskless process as it has been reported in literature [28, 41].

The sharpening step consist in removing the mask material once the first etch is completed. The wafer is then put back to be etched in continous mode for the time required, therefore exposing all areas of the wafer to the

effect of the process. This translates into a sharpening of the tall structures.

Having this last step in mind, it was necessary to aim for taller structures than the final desired height. The final isotropic etch, without the presence of any mask, reduces the height of the structures and needs to be taken into account.

2.2.1 Fabrication of tall cylinders

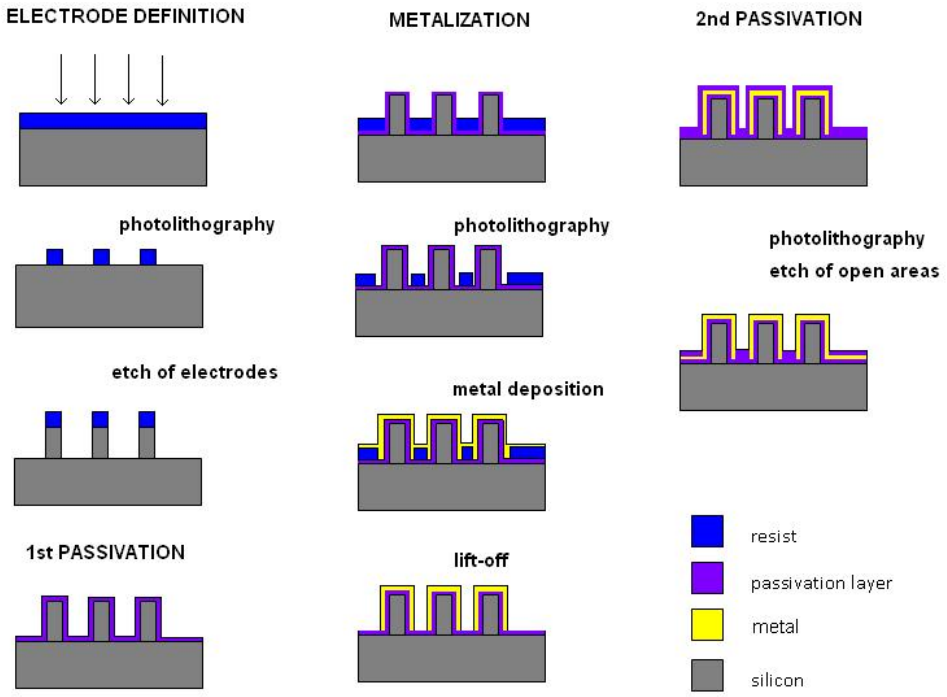

Figure 2.10: Fabrication steps on a single wafer of cylinder electrodes

The first goal to obtain was therefore the fabrication of very tall cylinders. This was done in single wafers. The process flow is described in figure 2.10, and it is composed of the following main steps:

Definition of electrode sites The first step consists of defining the areas of the electrodes by photolithography.

This is done by spinning a thick resist layer of 4.2 μm (a long etching time requires either a thick layer of resist or another kind of mask material such as silicon oxide. As it was commented at the beginning of this chapter, the use of resist simplifies the process). The resist is

processed by standard photolithography that transfers the patttern of the design to the surface of the wafer.

Etch of electrodes The second step is the etching of the electrodes by dry etch.

The etching is then performed in an inductively coupled plasma etcher (ICP). Pillars constructed in this way, with heights of about 60 μm, form the skeleton that will shape the final array of electrodes.

Passivation Deposition of an isolation layer.

The electrodes are all connected through a common substrate of silicon, which renders them not independent from each other. In order to isolate them, a thin layer of a non conductive dielectric is deposited on top.

Silicon nitride was deposited in a plasma-enhanced chemical vapor deposition (PECVD) equipment. The recipe used provided a low stress layer of 200 nm of silicon nitride (thickness measured by multiple angle reflectometry, Filmtek 4000).

Metalization The structures obtained are metalized.

Wires were patterned and metalized by standard negative photolithography. Metal deposition follows by using a e-beam evaporation machine or with a sputtering method. Usually, a very thin layer of Ti is deposited previously to the desired metal, with the purpose to promote its adhesion (in the experiments done, the thicknesses of both layers were 5 and 200 nm respectively). The metal of choice was gold, for biocompatibility reasons and availability in the laboratory.

Finally, the non-desired metal areas were removed from the wafer by a lift-off process. This is a step where the wafer is introduced in an ultrasound bath with acetone.The removal of the resist mask from unwanted areas takes away with it the metal that lies on top of it. In this way, only the designed areas (wires and electrode sites) hold the metal layer on top of them.

Passivation A thin layer of silicon nitride is deposited on the surface of the wafer.

Silicon nitride is used as the final passivation layer for its ability to form a good moist and sodium barrier and protect from scratches. However, this material accumulates a very high tensile stress (about 10^{10} $dynes/cm^2$ [42]). This fact is the cause that thicker layers than 200 nm be prone to cracking.

By using the same method as in the first passivation, a layer of 200 nm of nitride is deposited on top of the metalized electrodes. In this case, though, the step differs from the first passivation in that the electrodes need to be exposed in order to be able to contact the outside environment. To do this, the wafer is patterned with a photolithography that leaves openings only at the electrode and pad areas. After this, a short etch in a reactive etch machine (RIE) removes the nitride from these areas, leaving the MEA ready.

The realization of tall cylinders, in the range of 80-100 μm in height, was set as the cornerstone for ensuring the consequent sharpening step. As it has been explained during the introduction of this section, a slack height is necessary in order to provide for the after-sharpening processs,where an isotropic, continuous etching would decrease the initial height of the strucutres few μm.

The starting point for the etching was taken from a standard recipe given by the manufacturer of the Advanced Silicon Etcher ASE HC250M (from Surface Technology Systems). This recipe has a set of parameters aimed at obtaining trenches 50 μm wide and 300 μm deep, and needed to be optimized in order to adapt to the design and demands of the goal in mind. The manufacturer recipe, *deep*, is shown in table 2.1

Table 2.1: parameters for recipe *deep*

Parameters (units)	*etch step*	*passivation step*
Gas flow (sccm)	SF_6, 230; O_2 23	C_4F_8, 120
Cycle time (s)	8	5
Pressure (% APC opening [1])	87.7	87.7
Coil power (W)	2800	1000
HF Platen power (W)	19	0

Nevertheless, before starting the quest for the perfect recipe to etch high aspect-ratio structures, it was necessary to consider the appearance of undesired effects, as it would surely happen in the presence of the tall structures that were required. In fact, reentrant etching was noticed at the early attempts to etch a simple tall column, and it soon became obvious that if no solution was found, this effect would hamper the progress towards the obtainment of perfect structures.

The effect of this unwanted irregularity is that the base of the structures starts being etched much faster than other areas, with the consequent inverted profile to the one wanted. This is most likely due to the IF effect, that, as explained in section 2.1.3, is caused by the attraction of the etching ions to the side walls by the electrostatic force coming from the walls.

[1] the presssure is controlled by the aperture of a throttle valve (APC)

In the case of the design used for the experiments, this was a sure problem, since the pillars weren't opposed by any other physical structure that could cancel out the electrical field coming from their walls. The electrode array was composed of a maximum of 64 electrodes, with a distance between each other of 500 μm. In comparison with the dimensions of the pillars to be created, this pitch is too broad to consider a possible cancellation of the IF effect.

A possible solution could have been to use a higher density of electrodes-structures, but this would have proved difficult from the point of view of laying out connections between the functional electrodes and the outside pads of the chip, necessary to collect the signals recorded from the electrodes.

2.2.2 Use of sacrificial structures

The use of sacrificial structures to compensate the reentrant etching in the presence of tall structures has been reported on literature in several occasions [28, 43]. In 2003 Hanein *et al.* proposed this method to compensate the reentrant etching in high aspect-ratio silicon pillars, with a very similar aim as the one this project has. In their case, they were able, by applying their technique, to obtain microneedles 250 μm high, with sharp tips of 100 nm.

Their idea is based in surrounding the main pillars with protective structures to avoid the reentrant etching. This work also claims the sure success in the results without the need of adjustment of the pulse-mode times (etch/passivation), and therefore seemed a good method to guarantee high aspect-ratio pillars.

In the mentioned article, main pillars of 70 μm were used, surrounded by protection pillars of 30 μm in diameter. As for the distances in pitch, two values were tested, of 250 and 750 μm, of which the former was the one to give best results.

Following this example, the design was modified to include a set of similar sacrificial structures surrounding the main pillars in a circular pattern. The distances between the main pillar and the sacrificial structures is given in table 2.2.

Table 2.2: distances of main pillars-sacrificial pillars

Diameter main pillar (μm)	*Diameter sacrificial pillar(μm)*	*Circle around main pillar(μm)*
30	10	120; 100
50	20	250; 150
70	30	250; 350

The design included three different diameters of electrodes, 30, 50 and 70

μm, in order to test what would be the appropriate dimension of the final tower. The most important point of adjusting the diameter dimension is to have a value broad enough to endure the etching process, without the towers being destroyed, and at the same time not being too wide so that the final sharpening won't become cumbersome and long.

From all the possible parameters in the etching, it seemed plausible that the platen power (CCP source) would have a major impact in the obtained angle at the side walls. Recalling from section 2.1.3, the CCP source controls the directionality of the etching ions. With high values, it produces high directionality, by bombarding mostly the surfaces that are parallel to the wafer substrate.

It is also logical to consider that by increasing the passivation time in relation to the etch time during the pulse-mode process, the inclination of the wall should become more positive, since the active etch phase is an isotropic process and attacks the side walls. Therefore, by increasing the passivation time, a thicker layer protects the side walls for longer time during the following etching process.

Therefore, the ratio of etch/passivation time was taken as a second parameter to play for optimization.

The standard recipe, *deep*, was set to a lower platen power, of value $P_{platen} = 13$ W (compared to the inital value of 15 W), in order to allow for some isotropic etching during the active etch phase. As for the couple t_e/t_p (etching/passivation times), a test with just varying the passivation time, t_p, was performed, in order to simplify the settings of the experiment.

The method of characterization of the results used visual inspection in a Scanning Electron Microscope (FEI Nova 600 NanoSEM). This method is good for measuring heights and evaluating the topography of the surfaces (smoothness, profile). The possibility to tilt the wafer inside the chamber of the microscope helped to observe the electrodes in profile, which was essential for the obtainment of conclusions after the experiments.

The etch rate was characterized in terms of the variation of the passivation time. The calculations of this parameter are based in the heights of the pillars, obtained during a process run the same time at different values of the passivation time. A linear relationship was found between these two parameters, which can be seen in figure 2.11. The linear regression helps to predict the etch rate for a particular t_p. The negative slope of the curve is only reasonable, since the etch rate should decrease with an increment of the passivation time. This is due to the fact that the longer t_p allows the growth of a thicker protective layer, which the final etch step is less effective in removing.

As expected, the results showed that the inclination of the side wall was affected strongly by this parameter. The increment of t_p showed a tendency

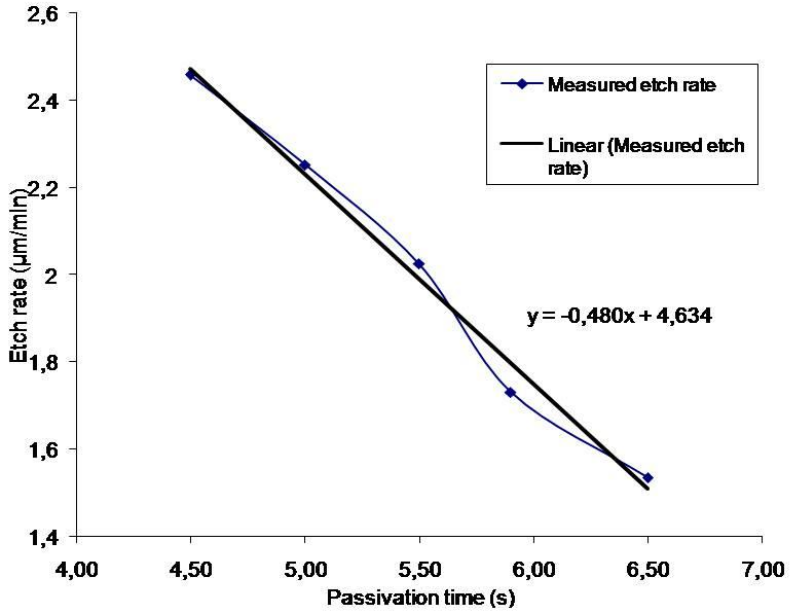

Figure 2.11: Etch rate in relation to passivation time

towards a positive slope, as it can be appreciated in Figure 2.12.

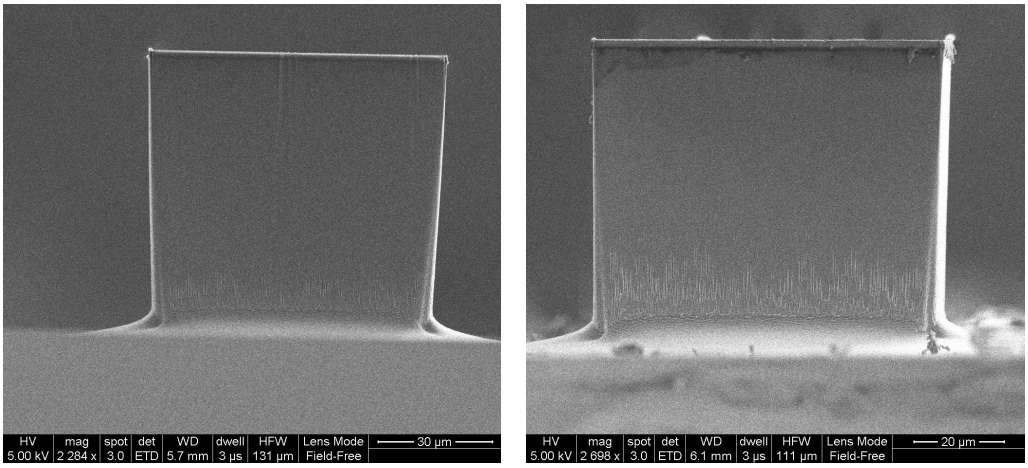

Figure 2.12: The passivation times modify the pillar slope. Left, t_p of 4.5 s, right, 5.5 s. The walls become more vertical as the passivation time increases.

It was also found that for the layout of the design, values of t_p higher than 6 s introduced silicon grass in the resulting structures (figure 2.13). It is a very important saddle point to find, as it is an indicator of a change in the sign of the slope from positive to negative [40]. Silicon grass, also called black silicon, is formed as a consequence of the presence of native oxide,

dust, particles of etched resist, etc.These particles behave as a mask themselves during the etching process, and as the etch reaches its most directional behaviour (perpendicular to the wafer), silicon spikes are created. Since this is a very visible phenomenon it gives a strong cue of the status of the process (black silicon receives its name for its appearance; the surface of the wafer looks gray-black due to the absorbance of light by the spikes, not letting it reflect).

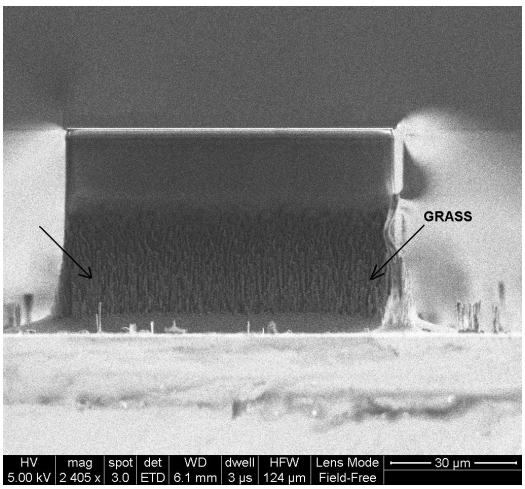

Figure 2.13: Silicon grass can be seen at the bottom of the structure. It appeared after a 30 min process with t_e/t_p of 7/6 s. It is a sign to stop increasing the passivation time in relation with the active etch time

Therefore, a passivation time of 6 s was set as the limit value. It was also noticed that, as the passivation time approached this limit value, the surfaces became rougher, and a good balance between smoothness of the walls and a vertical profile was found in the final optimal value of 5 s. The etch rate associated to the process was found to be 2.25 $\mu m/min$.

The finally adjusted set of parameters is given in table 2.3, forming the new recipe *sacrif*.

Table 2.3: parameters for recipe *sacrif*

Parameters (units)	*etch step*	*passivation step*
Gas flow (sccm)	SF_6, 230; O_2 23	C_4F_8, 120
Cycle time (s)	7	5
Pressure (% APC opening)	87.7	87.7
Coil power (W)	2800	1000
HF Platen power (W)	13	0

In conclusion, a recipe was obtained where structures of quite vertical walls were achieved, as in figure 2.14 and 2.15, which reached heights of about 60 μm.

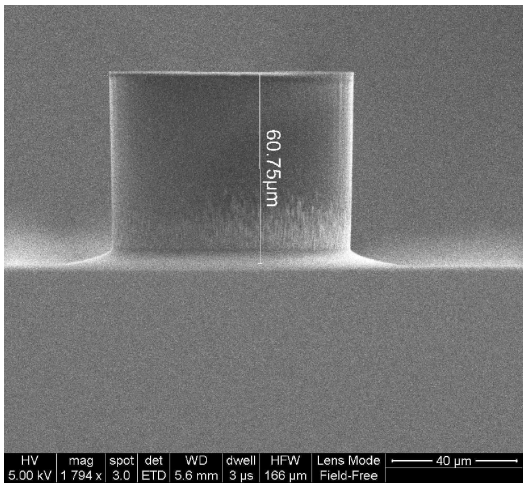

Figure 2.14: First optimization of recipe resulted in cylinder shapes of heights in the range of 60 μm in height, for structures with diameters of 70 μm. The image was taken in profile with a SEM, after cleaving the wafer.

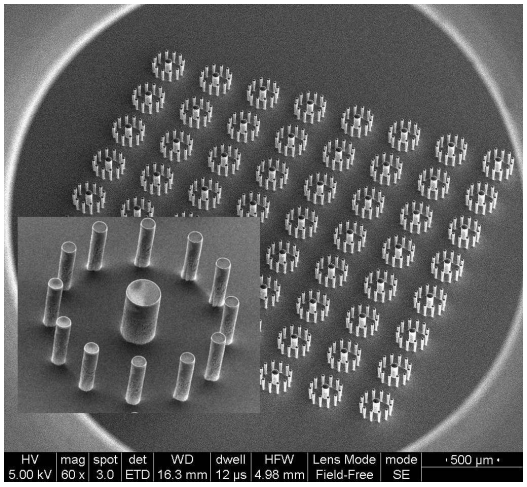

Figure 2.15: Array of 8x8 cylindrical electrodes with sacrificial structures. The inset shows in detail a single main pillar-electrode encricled by sacrificial structures.

Despite the obtainment of a recipe able to fabricate structures with vertical walls and high aspec-ratio, the second step of sharpening proved difficult to handle. Even though the use of sacrificial structures helped in avoiding

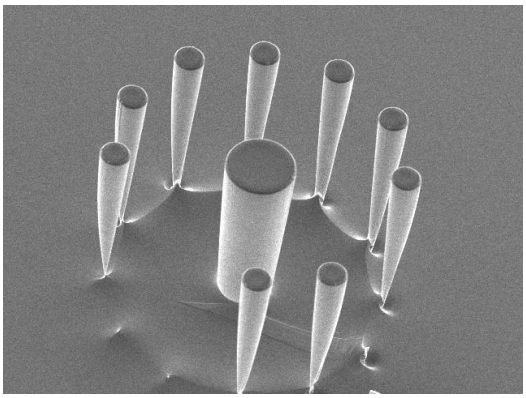

Figure 2.16: Surrounding sacrificial pillars protect the main strucutre (center) from the reentrant etch effect. As it can be seen, the base of these protective structures has been etched faster than other areas.

reentrant etching up to some extent, this effect started affecting the structures severely after reaching heights of about 80 μm. The outcome of this was the progress of the structures towards an inverted pyramid, in the opposite direction of what it was intended to be achieved.

The appereance of this problem is shown clearly in figure 2.16. The most outside structures have been etched much faster at the base of the cylinder, which is the reason why they were included in the design. Unfortunately, the central pillar is affected too; although less obvious, the shape of the main cylinder presents a slightly smaller diameter at the base than at the top.

This effected proved persisten in its appearing at the etching processes. The continuation of the etching for the intended sharpening step was unfruitful in avoiding the reentrant etchig, regardless of the variaton of parameters to try to palliate it. Changes in gas proportions or power rendered ineffectual to control this effect, and it proved impossible to progress in this line of work.

After this conclusion, the target of the etching was reconsidered, and it was decided to reach heights in the range of 60-70 μm in order to avoid this problem. There was no particular reason to obtain electrodes taller than this value, other than having the confidence of providing a generous margin for the second sharpening step. If previous works are taken into account, functional electrodes of MEAs are usually about 50-60 μm tall, enough to overcome the barrier of dead cell layers in the brain tissue, as it was commented in chapter 1.

Conclusion

The use of sacrificial structures as a way to compensate the reentrant etching wasn't particularly helpful. This may be due to the fact that for the

work of reference [28], the aim of the design was to obtain extremely tall needles, in the range of 250 μm. In the case of the experiments explained here, the electrodes needed to reach no more than 100 μ. It was noticed that the structures of 70 μm of diameter, which are comarable in size with the ones of the referred work, were the ones to show less sensitivity to the reentrant etching. Nevertheless, this dimension was too broad for the sharpening process intended. Optimal structures would be the ones of 30 and 50 μm, but these were affected by the reentrant etching effect. It is most likely, though, that by adjusting the distances from sacrificial pillars to main pillars, the mechanism of compensation would work.

2.2.3 Sharpening process

It is essential for the purpose of this work to obtain a method where a control over the slope of the side walls is attainable. It is the only way to create high aspect ratio electrodes that are sharp and able to penetrate brain tissue. As mentioned in the conclusions from the previous experiments, it was soon obvious that the sharpening of the structures fabricated with a vertical profile wasn't an easy task.

In a different approach to the one observed until now, where a first etch would reach the desired height, and a second one would aim at sharpening the structures, it was decided to devise a process that would achieve both effects at the same time. This implies the introduction of a gradual lateral etch during the process that would take care of the addition of a slope to the walls of the towers.

The method followed here is based on previous work done by Roxhed *et al.* [41], as the most straight forward and easy technique to create side wall slopes with a controlled inclination. It is based in an alternation between phases of anisotropic etching, using the pulse-mode process, and phases of standard isotropic etching (see figure 2.17). Thus, this procedure can be seen as a hybrid between pure isotropical etching and anisotropic etching, with the advantage of full control of the effect of the isotropy on the inclination of the walls.

The anisotropic step is made of a sequence of substeps as it has been explained earlier, where an active etching phase with SF_6 and applied bias voltaged is followed by a passivation time with gas C_4F_8. The otpimization of the pulse-mode step leads to the resulting anisotropy as a single step. The additionally new isotropic step is performed with an unbiased etch of SF_6. The combination of these steps lends a progressively risen slope with the desired inclination, where the isotropic step takes charge of the inclination of the walls, and the depth of the etched structures is given by the combination of both isotropic and anisotropic steps.

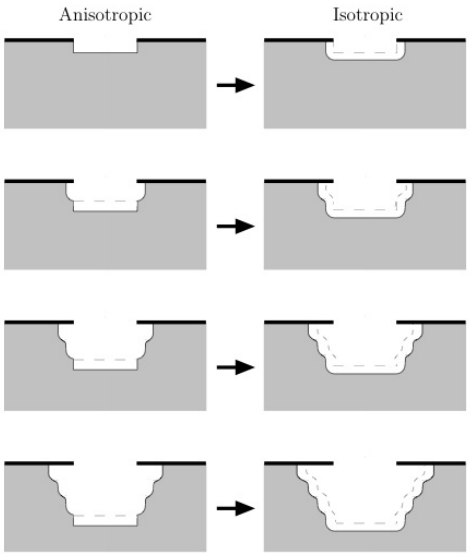

Figure 2.17: tapered technique. The combination of anisotropic and isotropic steps produces angled, rippled side walls [41]

The tuning of each phase is very straight forward, and it is easy to obtain control over the sidewall angle for very high aspect ratio structures.

Interestingly, this technique is a useful tool as a compensation for reentrant etching. Roxhed *et al.* demonstrated this by fabricating high aspect

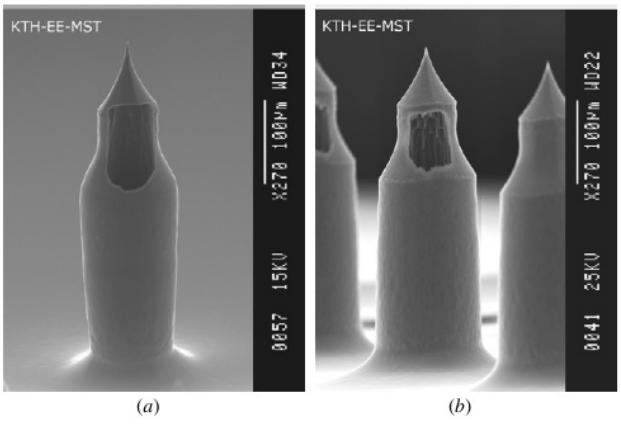

Figure 2.18: Compensation of reentrant etching by using the tapered etch technique. (a) Microneedle etched without compensation shows the reentrant etching effect at the base. (b) The same design with the application of a tapered mode cancels the reentrant etching (from [41])

ratio, hollow needles with very smooth sidewalls. Figure 2.18 shows how the

reentrant etching is compensated by using their technique. Also worth to notice is that the scalloped bands formed as a consequence of the switching between the different processes can be manipulated by tuning the lengths of periods of the anisotropic and isotropic steps, obtaining such smooth side walls.

In a slightly different approach, though, this technique will be used with a pronounced scalloping effect. This scalloping increases the surface area of the electrodes, and consequently the signal-to-noise ratio. Not only that, but it could promote a better anchoring of the brain tissue to the final electrodes, which is important to avoid movement of the slice during recordings, and also for attachement purposes.

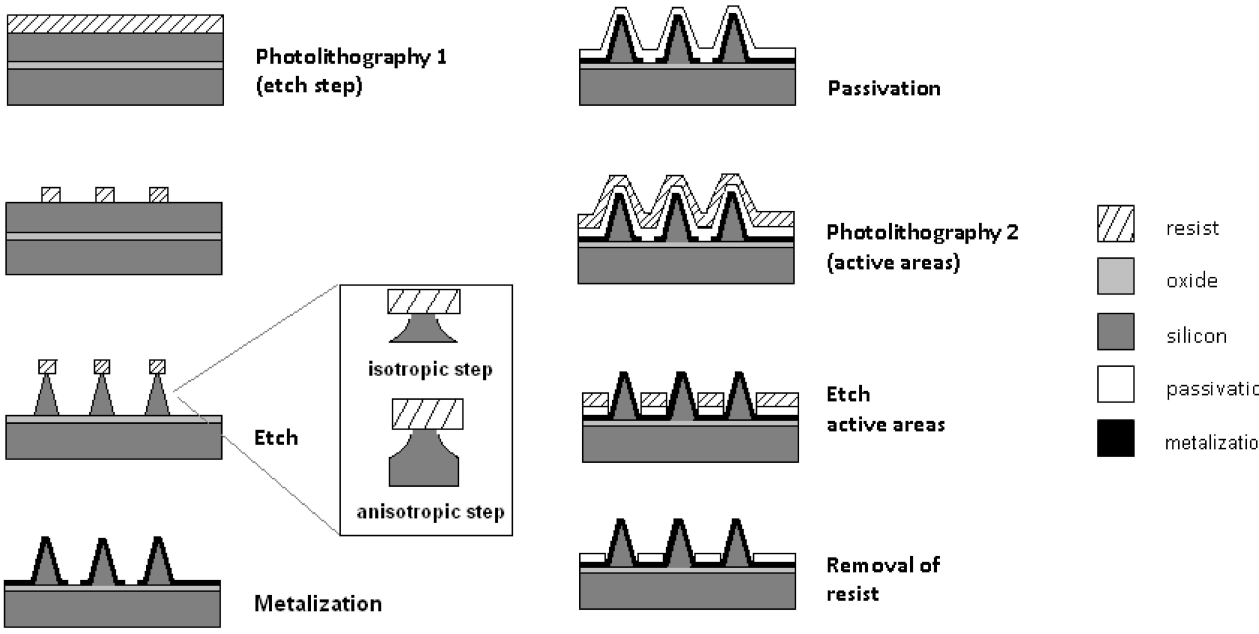

Figure 2.19: Fabrication steps for 3D scalloping electrodes. The steps consis of the same as in the case of a single wafer, except from the first passivation step, which is avoided thanks to the use of an SOI wafer

The main steps of the fabrication process are described in figure 2.19. The use of a silicon-on-insulator wafer (SOI) is key to facilitating the whole process, since the structures that will be fabricated will lie on an isolation layer, typically silicon oxide, and thus be electrically independent from each other as individually addressable electrodes. The steps followed for the fabrication are identical as those described at the beginning of this section, when using a single wafer. The only difference with those is the avoidance of a first passivation due to the advantageous use of the SOI, as just mentioned.

The etching is then performed in an inductively coupled plasma etcher (ICP), which stops automatically when it reaches the isolation layer, in this case a 0.4 μm layer of silicon oxide (a further advantage of using an SOI wafer). Pillars fabricated in this way obtained heights of 60 μm (with a diameter of 40 μm) and very sharp tips, in the order of 1 μm, if etched with recipe *cake*, which is given in table 2.4.

Table 2.4: Parameters for *cake* recipe

Parameters (units)	Anisotropic step		Isotropic step
	etch step	passivation step	
Gas flow (sccm)	SF_6, 230; O_2, 23	C_4F_8, 120	SF_6, 100; O_2, 10
Cycle time (s)	7	5	110
Pressure (mT)	94	94	94
Coil power (W)	2800	1000	600
HF Platen power (W)	13	0	0

The reader can notice that this recipe is based in the previous one obtained for high aspect-ratio structures with vertical walls. The only difference now is the introduction of an extra isotropic step, which is based in the experience acquired from the design of the anisotropic etch (it is basically a continous version of the pulse-mode process, where now the passivation phase is omitted).

Based on the recipe previously obtained for very anisotropic etching, the number of anisotropic cycles was set to 12 –that is, 6 anisotropic cycles which also consited on a sequence of etch/passivation, and 6 isotropic cycles. The sequence would start with one anisotropic cycle, and then an isotropic one, and so on –as a fix value. This step is the key to obtaining the desired high aspect ratio of the pillars, whereas the second one, the isotropic step, is used for sharpening the structures. The, experiments were run for tuning the isotropic step against this fixed anisotropic step. The isotropic etch times tested were of 70, 90, 110, 120, 130 and 140 s. Figure 2.20 shows the results obtained from these experiments.

The tendencies observed were an increase of sharpening and scalloping as the isotropic period increased. These results were expected since with the increase of the period of isotropic etch, the typical under-etch effect of this process becomes more and more apparent, further sharpening the pillars. By increasing the etching time of each step in the etching the scallops obtained become more pronounced. With time periods for the isotropic time greater than 120 s, however, the process became too aggressive, damaging the pillars

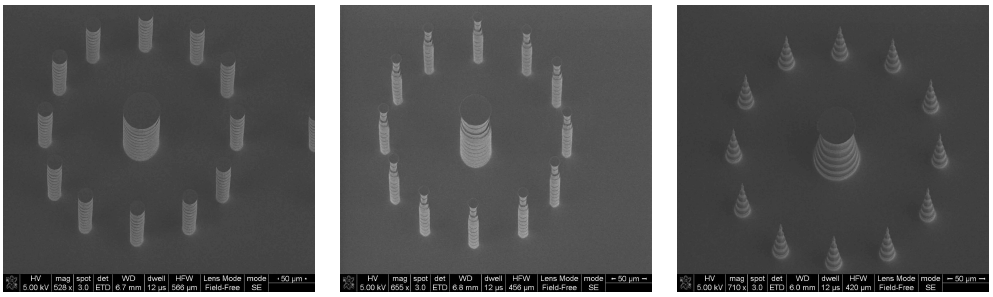

Figure 2.20: Tuning of parameters during etching of scalloping electrodes. From left to right: 70, 90 and 120 s.

or removing them completely. In conclusion, a time of 110 s was found to be the optimal one.

After running the process to achieve the desired height, the mask was removed and a last isotropic step was run. The purpose of this small additional step is to sharpen the electrodes. The sharpening was done by small steps of 20 s, after which the structures were checked, as before, in a SEM. If necessary, the step would be repeated again until obtaining very sharp tips.

The reason of this last step to be done so manually is because a great variability was found in the results, depending enormously on the batch of wafers and on the machine conditioning.

The results were exciting in that high aspect-ratio electrodes were obtain, with sharp tips for easy penetration. Figure 2.21 shows the obtained structures, at different stages of the process, first after the scalloping etch, and second, after the final sharpening step.

It should be commented that, as it can be appreciated in the images, there is a silicon layer at the base of the electrode due to the presence of the sacrificial pillars. The sacrificial structures helped to protect the main structures during the whole scalloping etch, and were eventually destroyed with the own dynamics of the process.

Moreover, the metalization became much more reliable due to the slope of the side-wall of the electrodes (figure 2.22). Nevertheless, there are still some visible gaps, although this is of no concern, since the underlying material is highly conductive silicon, and therefore the conductive path is not interrupted. This was not the case in the previous experiments, when using a single wafer as the substrate material. The reader is reminded of the fact that a passivation layer had to cover the structure of the etched electrodes, which forced the need to have pillars perfectly covered by a metal layer. In any case, this problem was also solved with the development of a novel, alternative tecnique to standard metalization procedures that guarantees conductivity even in the case of tall structures with vertical walls. This case study is explained more in detail in the next section.

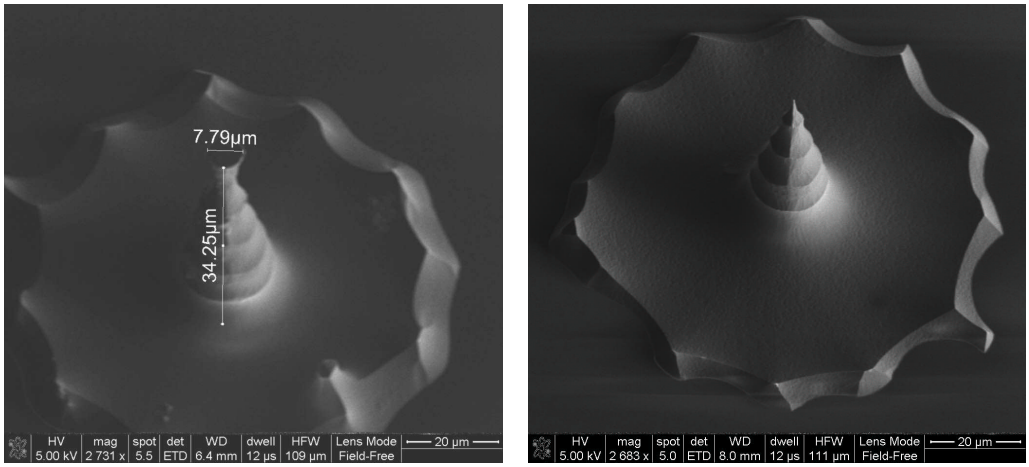

Figure 2.21: Final electrodes. Left: scalloping etch. Right: the same electrode after a sharpening, maskless etch was run for 2 min and 20 s. The platform in which the electrode lies is a consequence of the previous existence of sacrificial pillars; those are removed as the process advances in the etching (the images were taken at an angle of 30°, and therefore the vertical measurements shown should be multiplied by a correcting factor of 2).

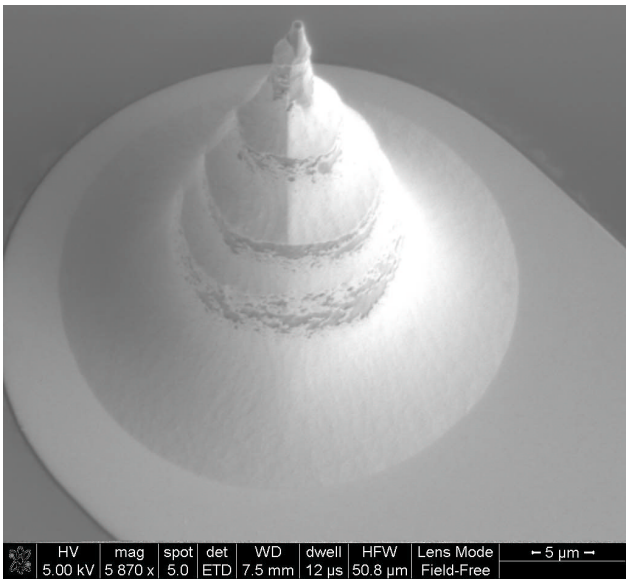

Figure 2.22: Final 3D scalloped electrode after metalization. The inclination of the side walls allowed a better step coverage than in the presence of cylindrical shapes

In conclusion, a novel type of electrodes has been fabricated, with high aspect-ratio and sharp profile, that should facilitate the obtainment of signal recordings from brain slices *in vitro*. Its profile presents a unique scalloping shape that may promote a stronger attachment of brain tissue to its surface. Although this is a hypothesis that needs to be proven, a fact is that at least these structures present a higher surface area than smooth walled pyramids, as the ones that have been reported in literature [24, 23]. This fact will be visible in the characterization of the impedance of the electrodes, in chapter 3, showing a modest but visible reduction in the overall impedance.

2.3 Experimental work: metalization

It is vital for the functionality of the electrodes to become conductive. This is usually achieved by covering the structures with a thin layer of metal or other conductive material.

The current metalization methods that are commonly used are:

- Electrodeposition
  - Electrochemical deposition
  - Electro-less deposition
- physical vapour deposition (PVD)
  - E-beam evaporation
  - Sputtering

The use of electrodeposition techniques involves a cathodic deposition of a conductive material [44]. By means of oxidation-reduction reactions, the metal is deposited on the wafer surface. This can be done either by applying a current that travels through a bath, from anode to cathode (electrochemical method), or without it (electro-less deposition). In both cases, the substrate for deposition needs to be conductive itself, or have a previously deposited conductive layer (seed layer), to allow a path for the current to transport the metalic ions.

The other options are usually carried in a clean room facility, where specialized equipment is necessary. In a PVD chamber, regardless of the type of deposition, a vapor is generated by boiling or subliming a source material; afterwards, it is transported from the source to the substrate, to be condensed to a solid film on the substrate surface [45]. In an e-beam system the metal source (target) is bombarded with an electron beam that comes from a charged tungsten filament, whereas in sputtering it is the acceleration of

ion gases that extract atoms from the metal-target. These metal atoms fly off towards the substrate, coating its surface with a thin layer.

Issues with metallization of high aspect-ratio, out of plane structures are not commonly mentioned in literature. This may be due to the fact that it is not frequent to find particular cases where high aspect ratio structures with vertical walls need to be conductive, or perhaps to a lack of a good alternative to the aforementioned methods. Although similar structures to those developed during this project have been reported in literature [24, 30, 28], they were either not metalized at all, or the structures were sharp at their tips and standard metalization procedures seemed enough to provide with conductive surfaces. It could seem confusing, at this point, to introduce this as a problem, since sharp structures have been obtained here too, and true, their metalization is feasible. Nevertheless, it should be recalled that cyclindrical structures were also created during the experiments commented eariler. It is in this case that the metalization poses a problem.

In order to test the metalization process on abrupt-shape structures, it would be adequate to use electrodes with very straight profiles. In this way, the major concern of step coverage, that is, the deposition of metal on all surfaces (even the ones with vertical profiles) would be fully examined. Therefore, cylinder structures etched with the sacrificial technique (see section 2.2) were used.

It must be remarked that electochemical techniques are not suitable for the problem of metalization of the electrode created in a single wafer. The reader is asked to remember that, in order to isolate the electrode-pillars etched on the substrate, they were coated with a thin passivation layer of silicon nitride, which renders them non-conductive. Therefore, ther requirement for a path of current (anode-cathode) in the case of these methods is not feasible. This is unfortunate, since these techniques offer better step coverage than the PVD ones. This represents a major problem, as it is explained in the following developments of the experimental work.

2.3.1 Metalization with standard methods

Metal deposition and lift-off

There are three steps necessary in the metalization of the electrodes:

1. a negative photolithography process in which wires and electrode sites are defined

2. metal deposition (by a PVD equipment

3. lift-off of remaining resist and non desired metal areas

In regard to the photolithography process, one of the main challenges presented by the particular design of three dimensional pillars is the existence of a hollow shape that forms the final chip area. This is a 2x2 cm square in whose center lies the array of electrodes.

The hole shape was included in the design to act as a stopper of the mask when performing a hard contact photolithography process. During the UV exposure that is required for photolithography, a chromium mask with the desired patterns is attached by vacuum to the surface of the wafer. If the hollow was not designed, the hard contact of the mask against the silicon wafer would systematically destroy the pillar-electrodes that stand out from the substrate.

Yet, this hollow feature hinders a good transfer of the patterns onto the substrate, since there is a factual distance in the order of at least 70 μm (the hole is etched during the same process as the pillars) from the mask to the substrate. Also, the out-of-plane structures that made the electrodes obstruct an even spun of the resist and block the light during the process of exposure.

In order to assess these issues, a mask was designed with two different distances between electrodes and sacrificial pillars, 100 and 250 μm. Also, different thicknesses (1.5, 2.2 and 4.2 μm) of resist were deposited on the wafer.

As a result, it was observed that, firstly, the different thicknesses used in the experiments didn't show any relevant improvement in the results; secondly, for an optimal resist spread, a minimum of 75 μm pitch (figure 2.23) was necessary. It was reported in [46] that the optimal resist spread was due to the distance between the main electrodes, but it is clear that these distances, of 150 and 250 μm, could not possibly interfere in the deposition of the resist. The design of the circle surrounding the main pillars, composed by smaller sacrificial pillars, is the one to blame for this issue, and after using pitch diameters of 250 μm or higher, this problem dissapeared.

In addition, the effect of the slack distance between mask and substrate may translate into poor definition of the wires on the substrate. The left image of figure 2.24 shows the consequence of poor metalization due to the fact that different places are either over or under-exposed at different locations, which provokes irregularities in the definition of the wires. By opposition, choosing a right pitch of electrodes (right side of figure) shows a well defined pattern of wires that connect to outside pads.

In order to address the problem of the gap between the surface of the electrode and mask, a thick layer of SU8 was used as an alternative to the standard resist. SU8 is a common resist material used in microfabrication. It is possible to deposit thick layers of this material and pattern them with standard photolithography, although one of the main problems for the appli-

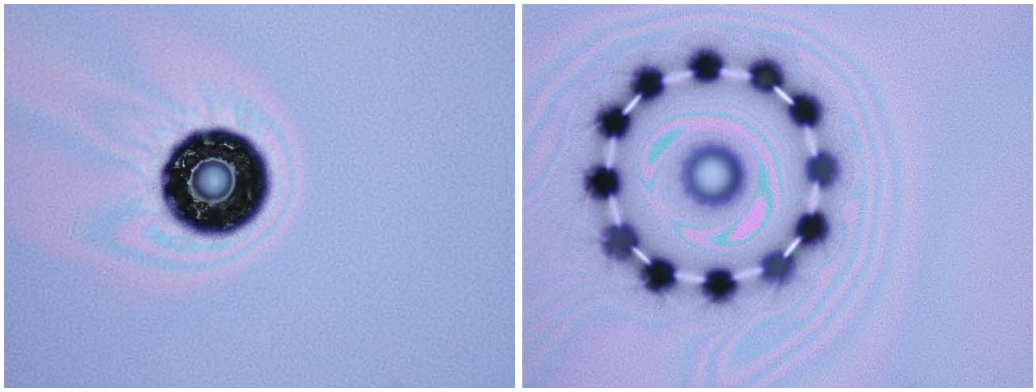

Figure 2.23: Spun resist (1.5 μm) on (left) a 30 μm electrode surrounded by sacrificial pillars with a pitch of 100 μm and (right) on an electrode of 50 μm in diameter with surrounding pillars of 250 μm pitch

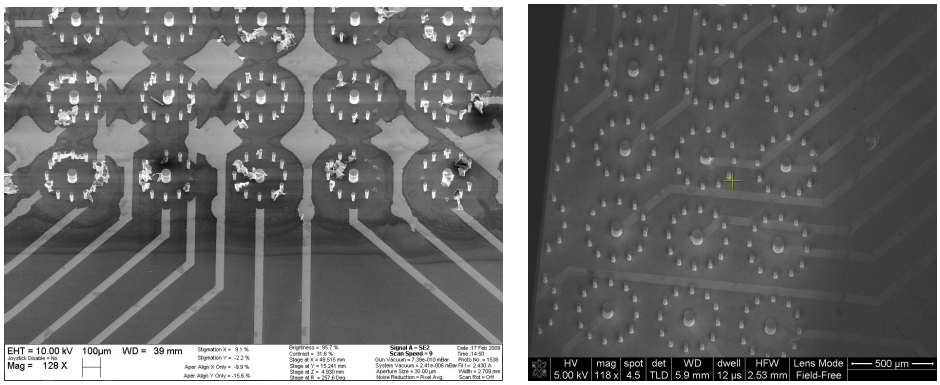

Figure 2.24: Poor lithographic results lead to bad definition of wires (left). With the right pitch between sacrificial and main pillars (right) the wires connect the electrode sites with external pads

cation at hand (metalization by lift-off) is that after development, SU8 stays on the surface of the wafer and it is difficult to get rid of it. Nevertheless, it was interesting to try this material for lift-off.

The fabrication steps are as follows: a manual spinner was used to spread a SU8 layer 20 μm thick on the wafer with cylinder structures. After this, the wafer was soft baked on a hot plate for 20 minutes (at 90° C), and exposed to UV light. Finally, a post-exposure bake was run for another 20 minutes (at 90° C).

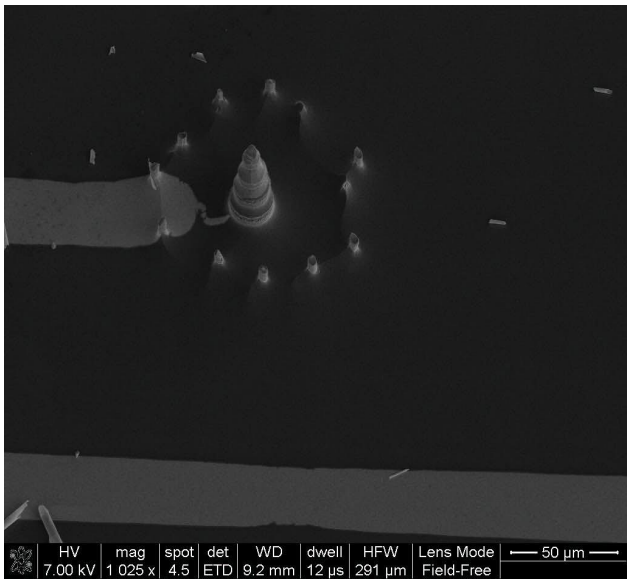

Figure 2.25: Lift-off with SU8 resist. The metalization is not optimal; the metal wires didn't reach the site of the electrodes, but lift-off was possible

Surprisingly, it was possible to do a lift-off. The wafer was introduced in an ultrasonic bath of acetone for 1 hour, aftwer which the wafer was rinsed with water. Although this line of investigation was not followed afterwards, these results proved that it is possible to realize lift-off with SU8, which could be interesting in situations where a thick layer of resist is required.

Nevertheless, the results after metalization weren't satisfactory (see figure 2.25), which proved that the main issue causing bad metalization was not likely to be the gap between the surface of the wafer and the mask. It became also obvious that SU8 wasn't a good choice of resist. As explained, the fact of choosing the right pitch of electrodes helped greatly into avoiding bad metalization; this fact is linked to the easiness of spread of the resist for the lithography. According to this, surely the use of SU8 wouldn't help in the matter, since it is even more viscous than the standard resist, and therefore will have more problems in the spinning to all areas.

Once the photolithography was successful, the next step that followed was metal deposition.For the experiments that will be commented, Pt was used, and a standard resist thickness of 1.5 μm was spun for the negative photolithography.

The metal was deposited on the wafer with a Physical Vapor Deposition (PVD) process carried out in a magnetron sputtering machine for 299 seconds. This process provides good step coverage, which is critical for reliability of electrical conductivity in the electrodes.

Figure 2.26 shows the results from metallization after the lift-off step. The picture shows some debris remaining after the lift-off process (top left comer and bottom right in the image of electrode), but it can be observed that the majority of the wall surface remains uncovered after the deposition. This result was confirmed by obtaining an x-ray spectrum in the SEM (figure 2.27).

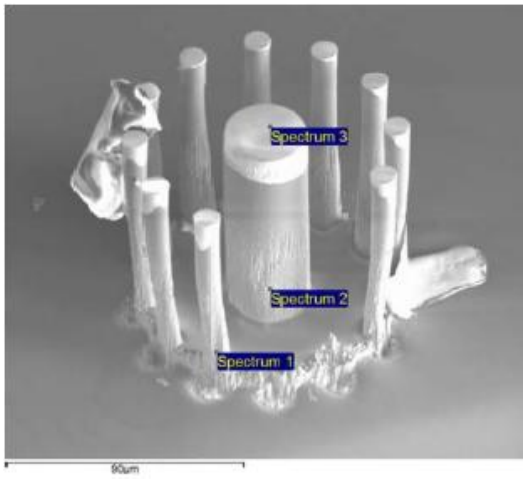

Figure 2.26: The image shows the defficiencies in coverage of the side walls of the structures.

Although spectrum 2 shows some trace of Pt, it is not enough to ensure proper conductivity, and the rest of data is in agreement to conclude the non-existence of a metal layer on the walls.

In order to obtain a better coverage at the side walls of the pillars, a custom-made holder was used to tilt the wafer inside the vacuum chamber of the sputtering system. This setting allowed for the obtainment of better results, as it can be confirmed by comparing figures 2.26 and 2.28.

As a conclusion, it was seen that several technical issues arised in the presence of different planes when it comes to photolithographic processes and metalization. The different height between the top of the electrodes and the surface of the wafer, together with the density of the electrodes, inter-

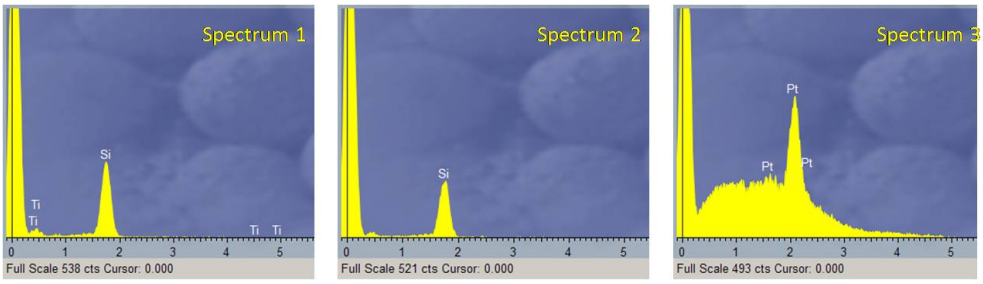

Figure 2.27: An EDX analysis in the SEM shows the spectra of the spots marked in figure 2.26, with some areas not covered well enough by the metal ions

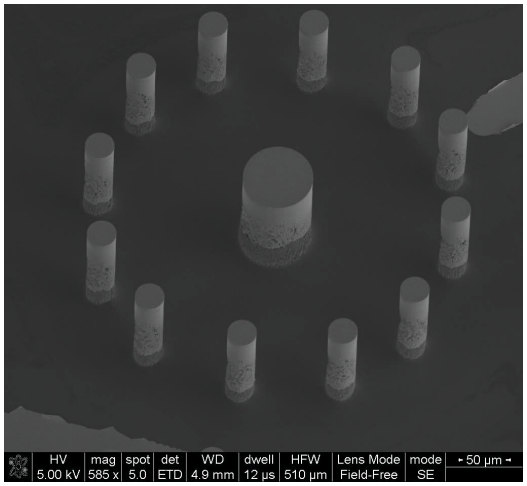

Figure 2.28: Tilting the wafer inside the metal deposition chamber favoured a better step coverage

fere with a perfect transfer of the desired pattern onto the wafer. With an adequate design of the pitch, some of the problems were resolved, mainly the photolithography of the wires to connect the electrodes to external pads in a reilable way. Nevertheles, there was still the issue of full metalization of the pillars. Although tilting the wafer inside the vacuum chamber when performing metal sputtering improved the step coverage, a complete metalization wasn't achieved.

Shadow mask

The use of a shadow mask for the metalization of the design could seem, in principle, an alternative solution to the standard metalization explained previously. With this method, the photolithography step would be avoided, which at the time was believed to represent an unsolvable problem (although later on, as it has been discussed, it was seen that by adjusting the distance between the sacrificial structures and the main electrode the photolithography step was successful).

A shadow mask is a physical mask with the desired pattern to be transferred, which is placed on top of a wafer. Its name comes from the fact that it acts as a shell in the areas where no metal is wanted, shadowing the deposition of the metal. Therefore, the presence of the shadow mask defines where the metal will be deposited, with open areas where the metal should be sputtered or evaporated.

In the particular case of this project, a shadow mask was fabricated in a wafer of 500 μm of thickness with a thick layer of oxide (16 μm). By spinning a resist layer of 4.2 μm, the metalization pattern was transferred onto this wafer with standard lithography (for details of this process, the reader is referred to section 2.2).

According to the specifications of the recipe to be used for etching the silicon wafer (*deep*), the selectivity rate between silicon and silicon oxide is 100:1. After calibration of the process, the etch rate was calculated to be of 4 μm/min. It was deducted then that it would be necessary to have a mask of oxide of at least 5 μm in thickness to stand fully the etch through the whole wafer thickness (about 2 hours). On top of that, it needs to be considered that in the last phase of the etch process, as it happens with any process that fabricates holes through a wafer in a dry etch equipment (see section 2.4), the wafer needs to be attached to a carrier wafer. This procedure worsens the efficiency of the cooling of the wafer, and slows down the etching. In fact, the real time of the etching in this case rose to 3 hours. Therefore, the thickness of oxide was chosen generously so that it would be capable to remain throughout the process without any doubt.

The oxide was then etched in the Advanced Oxide Etch (AOE) for 55 min with a standard recipe run at 0 °C. This process has a measured etch rate

of 310 nm/min, and therefore 55 min shoud be more than sufficient to etch away the oxide. The reader should notice that for these kind of processes (etching passivation materials like oxide and nitride deposited on silicon) the selectivity of the etching between materials is high and leaves the silicon almost unaffected for a long time. Therefore, it is recommendable to use etching times for longer than necessary (shorter times would involve the risk of not removing completely the oxide or nitride at areas that should stay clear of those materials).

After these steps, the etch of the wafer was carried out in the ASE. This was done with the standard recipe *deep*, commented in previous sections, with parameters as given in table 2.1.

The resulting shadow mask is shown in figure 2.29. The dark areas on the picture are open areas on the wafer. The purpose of this is to expose the underlying wafer only in these open areas for deposition of metal.

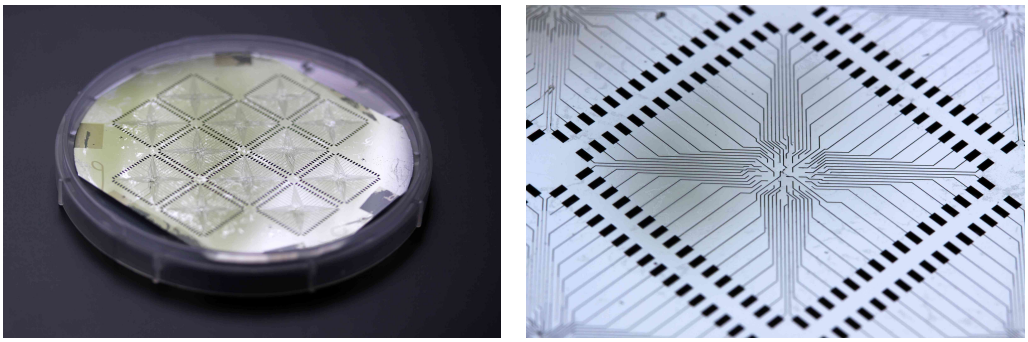

Figure 2.29: Shadow mask for metalization. Left: whole shadow mask to be placed on top of wafer for metalization. Right: detail of a single chip showing the openings for depositing the metal for the wires

For the metalization, the shadow mask was attached with cellotape to a wafer with electrodes previously etched, and in this way it was inserted in the Lesker sputtering machine. Deposition of Pt was run for 299 s, for comparison with previous experiments. Figure 2.30 shows how the pads and wires looked on the final wafer.

The results weren't completely satisfactory. Irregularities in the shapes of the pattern were obvious, and deposition of metal didn't' correspond to the expected dimensions in the wiring and pads. As an example, figure 2.30 shows some images of the obtained pads, on the left, with squares of about 0.5 mm of side. In reality, the dimensions of the pads are 1x0.5 mm. The same applies to the definition of wires. Some patterned wires are shown on the right side of the same figure, with widths not higher than 22 μm, whereas the original wires had been designed to be 50 μm wide. All these effects are most probably due to a non-uniform adhesion of the mask to the wafer.

Surely, this could have been improved with a more secure method of

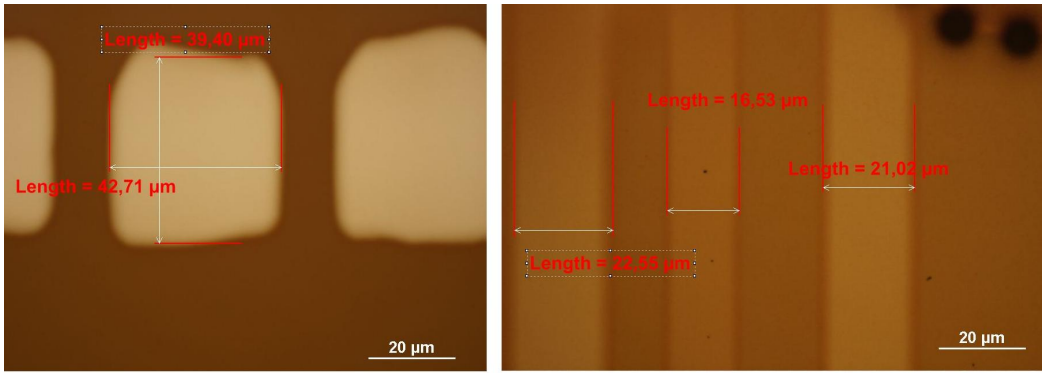

Figure 2.30: Metal deposition with shadow mask. The images show the site of pads (left) and wires (right), which came out with irregular shapes

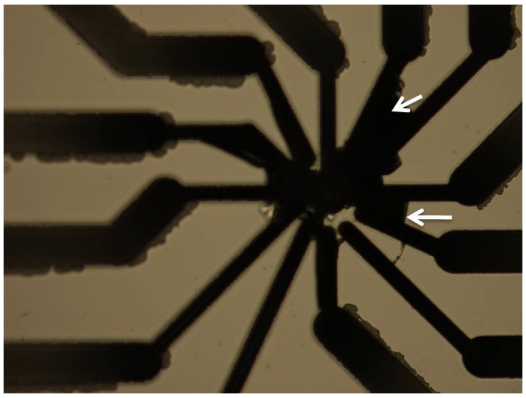

Figure 2.31: Fracture of the shadow mask at the end of the etch process (detail). The wires are too close together and the surface becomes brittle. Shorts created as a consequence of this are marked with the arrows.

attachement, but a more serious issue impeded the development in this direction. Due to the density and distribution of the wiring, the shadow mask proved to be a fragile structure, and in areas where wires laid too closely the mask came out broken after the etching process. Figure 2.31 shows clearly some sites where this effect ended up connecting two wires together.

Conclusions

Metalization of high aspect ratio structures with sharp profiles (as in the case of the fabricated cylinder pillars) by standard deposition techniques is not a viable solution. The step coverage offered by these techniques is not sufficient to reach all areas of vertical walls, and this fact renders the so fabricated pillars isolated from any electrical connection. Several issues arose with the presence of sacrificial pillars in the design, namely the spinning of resist in all areas of the electrode array. This technical difficulty was avoided by choosing a suitable distance between the already mentioned sacrificial pillars and the main structure-electrode.

As a side comment, it is worth notice that the use of SU8 for metalization and lift-off is possible, as it was experienced while trying this material as an alternative to standard resist (later on this option was dropped since SU8 spreads with even more difficulty than then normal resist, and therefore didn't help for solving the problem of a uniform spinning over the surface of the wafer). This method, though, could help in the development of fabrication processes where a very thick resist was required for the deposition of metal.

In regards to the approach taken when using a shadow mask, the results were unsatisfactory due to the bad contact of the shadow mask with the wafer lying underneath, which created irregular structures during metalization. But the most serious issues to consider with this technique is the difficulty in alignment of the mask with the underlying wafer, since the shadow mask is non-trasparent and doesn't allow to see through. Also, due to the design of the MEA, the shadow mask tended to crack, and shorts would appear often between wires on the pattern, due to the closeness of each other. Nevertheless, this technique may be useful in cases where it is required to pattern with different metals several areas of a wafer. By exposing only the ones desired with this mask, it would be possible to deposit selectively different materials.

2.3.2 Alternatives to metalization

After the reported issues with metalization of high aspect ratio pillars, a new direction was taken for obtaining conductive structures. Until now, standard techniques based in metal sputtering or evaporation weren't enough

to provide a good coverage of the side walls of the electrodes, rendering them unconnected to the outside world.

Electrode polymerization

Due to all these problems, the metallization process was replaced with a polymerization of the wafer surface with a conductive polymer. The idea behind this technique lay in the fact that the polymerization itself is done by dipping the wafer into a solution containing the polymer. Since a liquid reaches all the area of the wafer, this could solve the problem of the step coverage that until now proved difficult to overcome.

Among the potential candidate materials for the polymerization, polyaniline (PANI) and polypyrrole (PPY) were attractive options due to their biocompatibility [47] and their ability for trapping enzymes onto the surface where they are deposited [48]. Moreover, they have been widely used in different fields like microelectronics or electrochemical sensors, and nowadays their properties and synthesis methods are well known.

This technique is a combination of microfabrication methods with chemical polymerization.

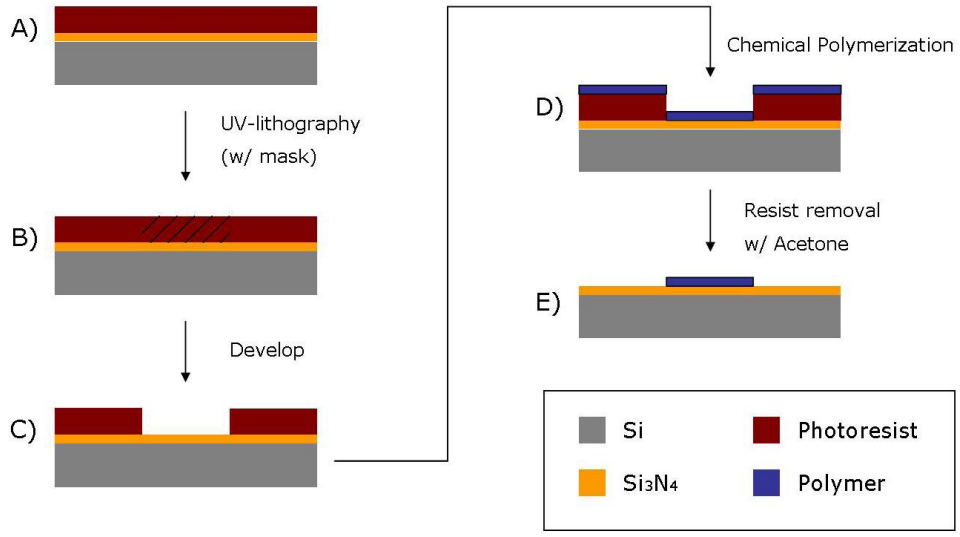

Figure 2.32: Fabrication steps of conductive polymer 3D electrodes. (A)-(C) standard lithography to define electrode areas to be polymerized. (D) chemical polymerization on the surface of the wafer and (E) lift-off of the unwanted polymerized areas [49]

The sequence of steps for the fabrication of these conductive polymer structures is depicted in figure 2.32, and involved very simple steps, with which the reader will be probably familiar by now since most have been

borrowed from standard fabrication processes and commented in previous sections:

1. Negative photolithography process in which wires and electrode sites are defined

2. Chemical polymerization

3. Lift off of remaining resist and non desired polymer areas

The novelty of the process lies in the substitution of the metalization for the chemical polymerization. Two type of solutions were used for this purpose. For the first experiments, PANI was the choice of material; these experiments served as a proof of concept for the method. In a second step, PPY substituted PANI to improve the first results obtained, as it will be explained later.

For the formation of PANI, chemical polymerization of aniline is generally carried in acid medium (pH $\backsim$ 1), and the presence of a chemical oxidizing agent such as ammonium persulfate. In the case of our experiments, this step was done in the following fashion: a solution consisting of aniline, ammonium persulfate (oxidizing agent) and HCl (acidic solution) was mixed. For the synthesis of PPY, a mixture of the monomer pyrrole and a solution of $FeCl_3$ with distilled water was prepared (for details on the concentrations, see [49]).

At this stage, the wafers had been previously processed as explained in previous sections, up to the point where the 3D structures had been passivated with a thin layer of silicon nitride of 200 nm. After this, the wafers were patterned with the electrode and wiring sites by means of a negative photolithography (identically as when a metalization process was performed).

The variation from the normal metalization starts at this point, when the wafers are dipped into the polymerizing solution (70 minutes for PANI, 10 minutes for PPY), after which they are washed in 1M HCl (PANI) or distilled water (PPY) and dried with nitrogen. The mixing of the polymerizing solution is done just before submerging the wafer in it, in order for the reaction to start at that moment. Also, the solution is left to sediment (no stirring) with the purpose of allowing the deposition of the polymer on the wafer surfaces. The thickness of the coating layer obtained in this way was 90 nm for PANI and 50 nm for PPY.

As a final step, another passivation layer was deposited in the same fashion as explained before, with the function to protect the structures from a microfluidic environment and to control the electrode areas that are to be active. These areas are patterned by photolithography and exposed open with a deep reactive ion etch process.

As methods of validation, cyclic voltammetry will be used. Therefore, a brief introduction is required to understand the consequent discussion of the

experiments. The introduction will be based on the main technique used in our experiments, that is, cyclic voltammetry.

Validation method: cyclic voltammetry

Cyclic voltammetry is one of the techiques most used in electroanalytical studies. Among other information, it provides with a rapid location of redox potentials of the electroactive species, which gives a good characterization of the system [50]. The basic procedure to perform cyclic voltammetry is to introduce a linear potential sweep in a Working Electrode (WE) with the shape of a triangular form; that is, running a linear increase from, for example, negative to positive voltages, and afterwards a reverse scan of the same linear form. The measured current passing through the WE during these sweeps is represented in a plot versus the corrensponding potential values, and it is what is called a *cyclic voltammogram* (see figure 2.33 for an example)

Without entering into too much detail, which is beyond the scope of this thesis, the main characteristics of a cyclic voltammogram are given by the position and magnitude of the reduction-oxidation peaks. These peaks are formed in the following dynamic:

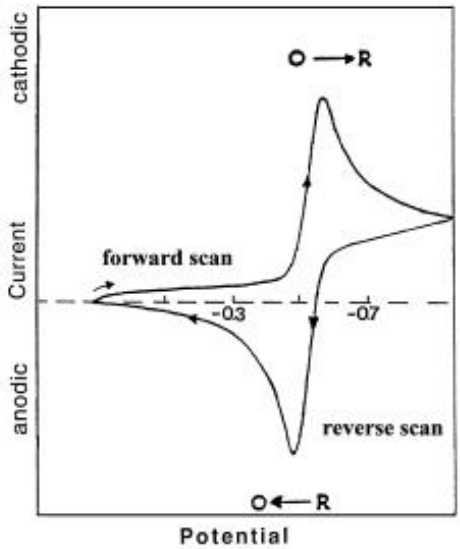

Figure 2.33: Typical voltammogram of a reversible redox process (from [50])

In the regime of the linearly increasing potential, let's imagine that only the oxidized form of the redox couple is present initially. If a negative potential is applied, at a value where no reduction occurs yet (i.e., the inital

potential applied is lower than the characteristic potential E^0 of the redox process), only a non-faradaic small current flows. In the vicinity of the potential value E^0, though, a faradaic reduction current starts flowing, and as the potential keeps increasing, the reduction process accelerates (with the consequent increase of current), until a current peak is reached. After this point, the oxidation species are depleted in the area close to the electrode surface, and therefore the current drops. If the redox reaction is reversible, then a sweep of potential in the opposite direction will give a similar response to the one described, but in this case for the oxidation of the analyte [51].

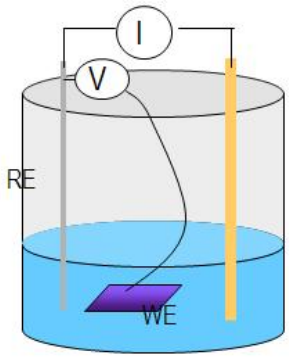

Figure 2.34: 3 electrode configuration for cyclic voltametry. The Reference Electrode (RE) sets a constant voltage during the measurements, while the Counter Electrode (CE) provides current to the Working Electrode (WE).

In a typical configuration for cyclic voltammetry, three electrodes are used. This configuration is shown in figure 2.34. The electrodes are defined as follows:

- Reference Electrode (RE): provides with a constant reference voltage for the measurements, and keeps independent from the properties of the solution
- Counter Electrode (CE): delivers current to the working electrode
- Working Electrode (WE): is the electrode where the electrochemical reactios happen and are measured

The potential is measured between RE and WE, with both electrodes positioned closed by. This measurement is done with a high input impedance device, in order to avoid leakage of current through RE. Due to this fact, the RE potential remains constant and equal to its open-circuit, known value. In all experiments carried, RE was an Ag/AgCl (3M KCl) and CE a Pt wire. As for the rest of the set up, a vial was glued to the center of the polymerized chip, containing the electrode array area. The chip was then mounted onto a

custome-made holder that had spring contacts betweent the pads of the chip and outside connections (the 3D polymerized electrodes were the WE)

Electrode polymerization with polyaniline (PANI)

The results of this experiment are shown in figure 2.35. It can be seen that all wiring, pads and electrodes seem to have been coated completely by PANI. The darker areas on the chip are caused by the presence of the polymer.

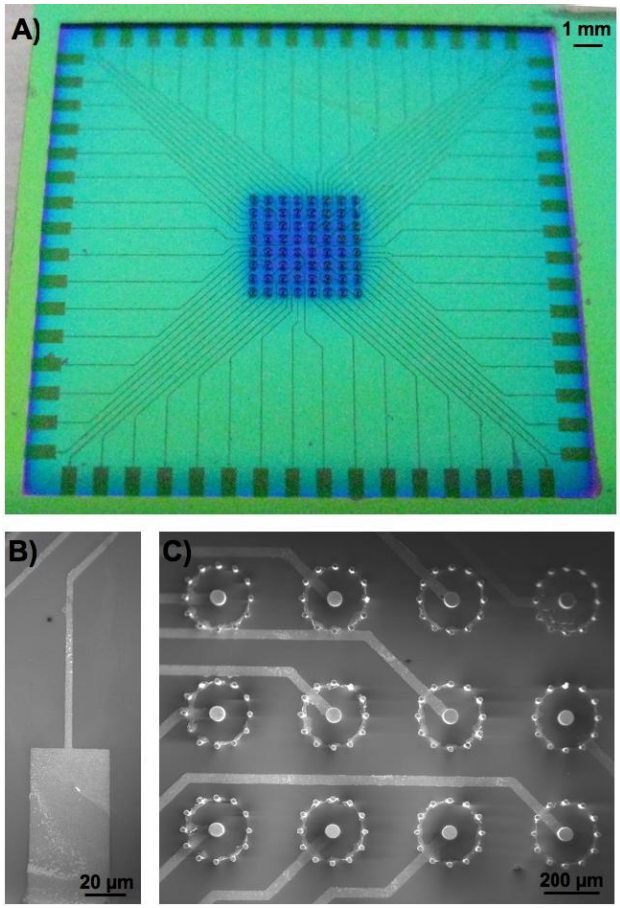

Figure 2.35: PANI 3D electrodes. (A) Oveview of PANI chip. (B) detail of a pad and (C) electrode sites with wires. The granularity of the tracks is typical from a PANI deposition

To confirm with a better validation of the polymerization, an analysis of an EDX-ray spectrum, performed in a SEM (figure 2.36), showed that, as suspected, all wanted areas were covered by the polymer. This was proved by the presence of carbon in areas that had been exposed to polymerization

(marked as "1" in the image), in contrast with the areas that had been covered with resist during the polymerization (marked as "2")

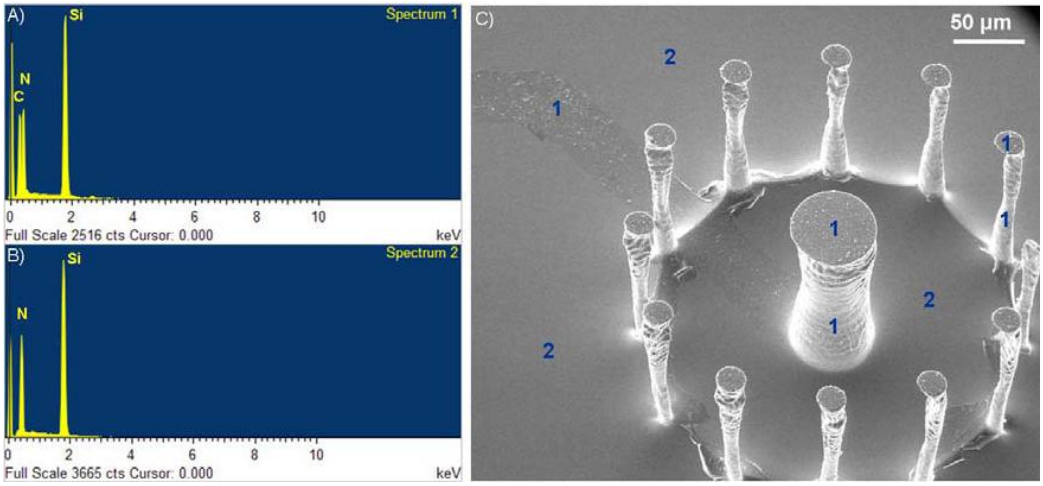

Figure 2.36: EDX-ray spectrum of PANI electrodes. The presence of nitrogen in the side walls

Despite the success in the step coverage, there were some concerns in regard to the low conductivity of PANI. This fact was confirm by running several cyclic voltammetry experiments with the electrodes as the WE in solutions of HCl with different pH: -0.2, 1, 2, 3 and 4. The currents measured were in the range of μA, so low that it was difficult to obtain meaningful results. Worse than that, due to the nature of the material, it is conductive only in an acidic environment [52, 53]. From the point of view of cell culturing, this is absolutely incompatible.

Even though we knew this fact from the starting point, the aim of these first experiments was to prove the feasibility of the method itself. As such, it proved to be a very useful substitute of normal metalization methods, and moreover, it is a very attractive technique since it can be done outside the clean room facilities, where all equipment is costly and the processes themselves are lenghty and cumbersome. In opposition, the chemical polymerization of the electrodes only requires a very simple preparation of a chemical solution and a container where to leave the wafer is submerged for the amount of time required.

Electrode polymerization with polypirrole (PPY)

In a second approach, PANI was replaced by PPY as the coating material. Figure 2.37 shows a SEM image of a pillar after the chemical deposition of PPY. The presence of the polymer is shown in the granular texture of the surfaces.

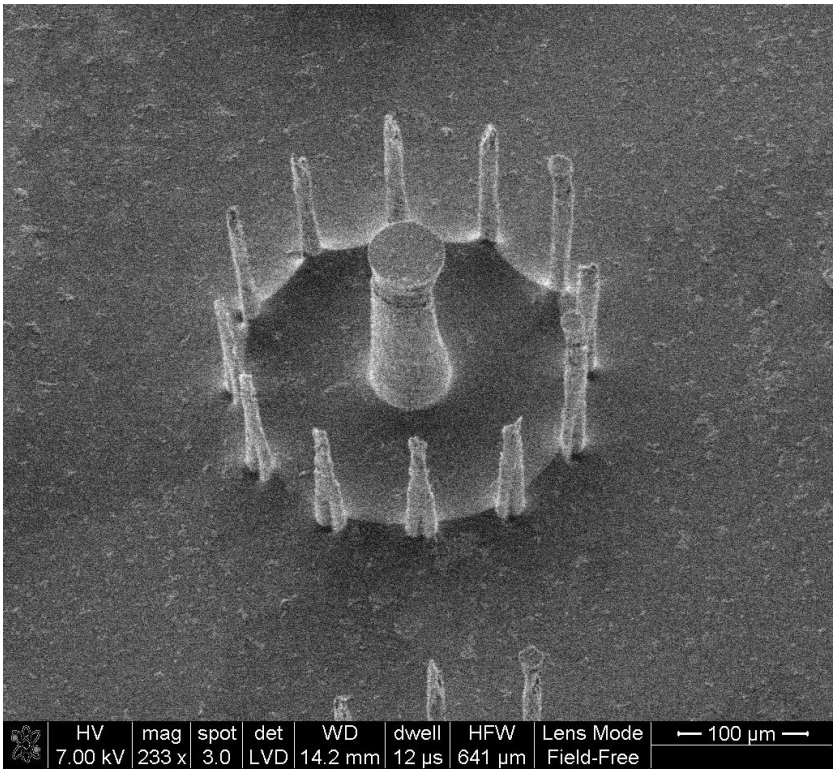

Figure 2.37: Pillar covered with PPY. The presence of the polymer is obvious with all surfaces showing a granular texture.

For comparison purposes, the polymerization was done also onto electrodes previously metalized with a thin layer of 200 nm of gold. This was done with the suspicion that the use of the polymer alone wouldn't suffice for a good conductivity (as it had happened in the experiments with PANI). As before, an EDX analysis performed on the SEM showed a profile with a presence of carbon atoms, which can only be caused by the composition of PPY. The electrodes polymerized with PPY were also characterized by cyclic voltammetry. The set up was similar to the previous CVs run for the PANI electrodes, with the difference that this time the electrolyte used was a ferrocyanide solution (10mM) in PBS (pH 7.4), with potential sweeps ranging from -0.2 to 1 V at several sweep rates in between 50-500 mV/s. The CVs obtained for a sweep rate of 250 mV/s are shown in figure 2.38. As the scale of this plot doesn't allow to appreciate the behaviour of the PPY electrodes, the measurement is shown in figure 2.39 for ease of inspection.

For comparison purposes, the CVs of Au/PPY electrodes, just gold and just PPY are represented together. The results are extraordinary if attention is paid the difference in response between the three type of electrodes. In particular, the current measured with the combination Au/PPY is 100 times largerthan a plain gold or PPY electrodes. Nevertheless, this enormous difference in current is most likely due to the fact that the presence of the polymer in the golden electrodes helps to cover the gaps of metalization that these exhibit, was shown in the previous section. If any gap in the metalization happens, it causes disruption in the conductivity of the whole connection to the outside pad, and therefore no signal would be detected. As the PPY behaves as a bridge in those critical areas, the signal is able to travel to the outside pads.

As for the behaviour of PPY by itself, it is unfortunately not conductive enough to show a strong current signal. Figure 2.39 gives evidence of this by representing currents in the nA regime.

In conclusion, this novel process guarantees the conductivity of the electrodes, even in the case of poor coverage of their surface during a subsequent metallization. The metalization is still necessary after the polymerization step if one wants good conductivity, but it becomes a non-critical step. Whereas with a normal metalization the existence of poor coverage was shown that left open gaps without metal, with this technique the polymer creates a bridge between isolated islands on the side walls, and makes a perfect connection throughout all the conductive traces. It may also be possible to use doped PPY in order to increase its conductivity, but this needs to be investigate further to draw any conclusions about it. On top if it, the method proves to be a very easy method that eludes the use of expensive equipment in a clean room, in which most processes carried are long and usually complex to handle.

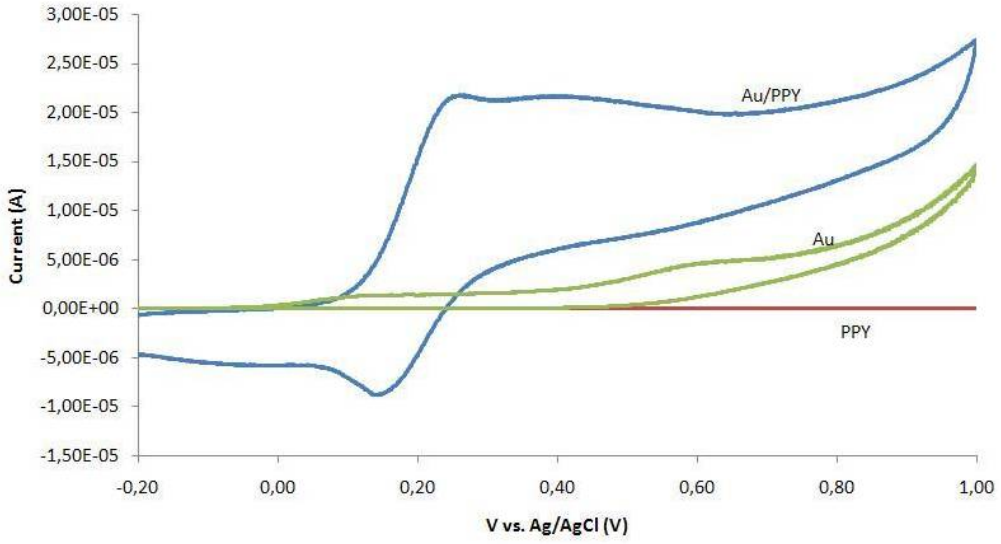

Figure 2.38: CVs of PPY electrodes, Au electrodes and Au/PPY electrodes at a sweep rate of 250 mV/s

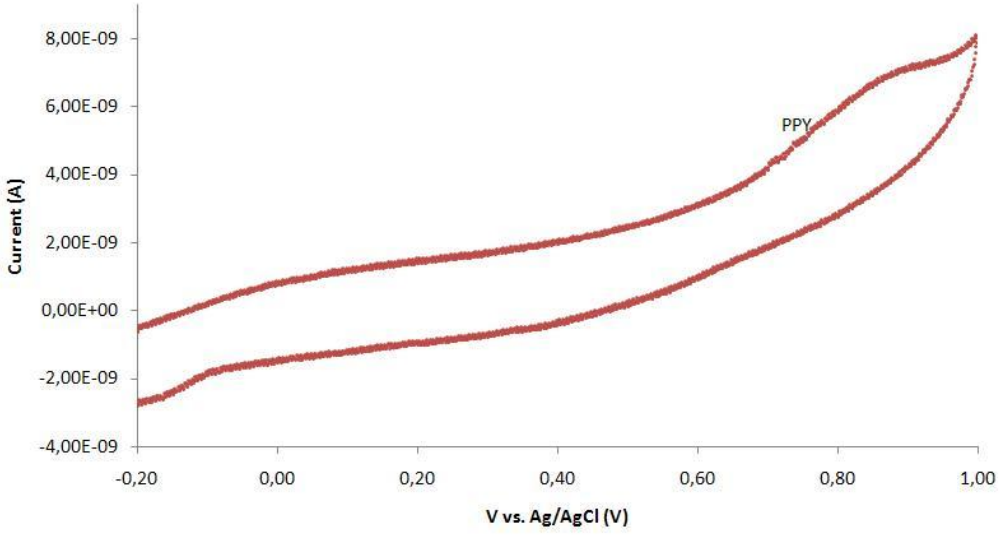

Figure 2.39: CV of PPY electrodes at 250 mV/s

Cell culture on PPY electrodes

As a last test of the newly created technique for conductive PPY-electrodes, it was considered relevant to observe the interaction of the material and strucutres with a real set up experiment, that is, in the presence of living cells. PC12 cells are widely used as neuron model system. In this study PC12 cells were cultured on the Au/PPy electrode chips in order to investigate the feasibility of using the described electrodes for cellular and tissue studies, mainly out of concern for possible toxicity effects due to desorption of left-over monomers in the polypyrrole film.

The protocol for growing PC12 was the following: untreated T25 flasks (NUNC, Thermo Scientific, Denmark) were coated with laminin (20 μg/ml, Sigma Aldrich, Denmark) in 1x Phosphate Buffered Saline (PBS) (Sigma Aldrich, Denmark) and left overnight. Later, excess laminin was removed and the flasks were washed twice with sterile water (Sigma Aldrich, Denmark).

Dulbecco's Modified Eagle medium/Ham's Nutrient Mixture F12 supplemented with 10 % fetal bovine serum, 10 % horse serum, 100 Units/ml penicillin and 100 $\mu g/ml$ streptomycin and 25 mM HEPES (referred to as DMEM/F12 from now on) was added in the flasks and placed at 37 °C in humid atmosphere containing 95 % air and 5 % CO2.

Undifferentiated PC12 cells (PC12-pheochromocytoma of rat adrenal medulla, DSMZ GmbH, Germany), approximately 4 x106 cells, were thawed and transferred to the above-mentioned flasks and placed in the incubator.

After 5 days, neuronal differentiation was initiated by replacing the media with DMEM/F-12 supplemented with 100 ng/ml NGF. The cell media was changed every 2 days. After 5 days of culturing, the cells were detached by adding 0.05 % trypsin-EDTA (Sigma Aldrich, Denmark) at 37 °C for 3 min.

The cell suspension was transferred to a 10 ml Falcon tube with fresh media and centrifuged at 1,100 rpm for 3 min. The supernatant was removed and the pellet was resuspended with media at 1x106 cells/ml. The centrifugation process and the resuspension of the cells in fresh media are done in order to remove the trypsin.

The differentiated cells were then seeded in a Petri dish containing the electrode chip and it was supplemented with DMEM/F-12 and 100 ng/ml NGF. Before seeding the cells, the electrode chips were sterilised with acetone at 70 °C for 5 min followed by three times wash in 70 % ethanol for 5 min. The chips were then washed with 1x PBS three times and then coated with laminin, as previously described.

The cultures were maintained for 5 days on the chips. SEM images indicate the typical morphological features of differentiated PC12 cells. A similar cell growth pattern could be seen on all parts of the chips (see figure 2.40).

The neuronal model cells showed a cellular morphology and adhesion on the electrode chips typical of PC12 cells. From these preliminary results, it

was concluded that the Au/PPy electrode chips could potentially be used for neurological applications.

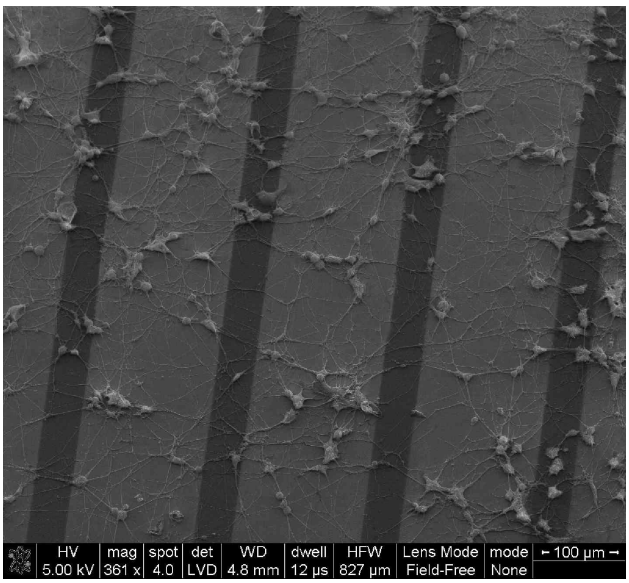

Figure 2.40: PC12 cells grow on the susbstrate with wires of Au/PPY [49]

2.4 Experimental work: vias fabrication

As it will be introduced later in chapter (culture), the integration of a culture platform for brain slices on-chip would be extremely advantageous from the point of view of long term recordings of neuronal activity. The introduction of small perforations on the substrate of the MEA chip is part of the plan for this integration. According to [23], for brain slice culture, an optimal size of these holes/vias would be 20 μm in diameter, with a total porosity of the substrate of about 13 %.

Following these indications, the design of the microelectrode array was altered to include vias. These vias were spread over the square area of the electrodes (4x4 mm), made of 20 μm in diameter and cleared off the sites where metalic tracks were laid. The porosity of the square was designed to be 13 % of the total area.

Before proceeding with the fabrication of the final distribution of holes, a previously designed mask, with patterns of circles ranging from 2 to 15 μm was used to measure up the possibility of etching through the whole wafer, and the suitability of the diameter of the holes for that purpose (one needs to bear in mind the undesired effects that have been described in section 2.1.3. The appearance of the RIE lag effect would impede the complete etch

of very narrow holes). Nevertheless, for both the test and final design, the fabrication process was the same and very straight forward in the steps to include. They can be listed as follows:

- photolithography to pattern a silicon oxide mask with holes
- etching of silicon oxide with an Advanced Oxide Etcher (AOE) (this step was necessary only in the case of using an mask of oxide)
- etching of holes in the Deep Reactive Ion Etching (DRIE)
- removal of remaining oxide in a bath of buffered hydrogen fluoride (BHF)

For the first test experiments, the mask with the pattern of holes was done with a thick layer of resist (4.2 μm). After the first runs, though, it was obvious that this material could not stand the whole length of the process, even when burned, which normally increases greatly its ability to withstand the etching process.

Due to this reason, the rest of the experiments were carried out with a mask made of silicon oxide, which is more resilient than resist. Double side polished wafer with a layer of oxide on top were used for the rest of the experiments. The oxide layer was 1.8 μm thick which was enough to withstand all the etching time.

In order to promote the adhesion of resist to the oxide layer, a treatment in an hexamethyldisilazane (HMDS) oven was necessary previous to the spinning of resist. Silicon oxide is hydrophilic, so the hydrophobic resist doesn't adhere to its surface. Therefore, it is necessary to render the oxide surface hydrophobic in order to promote the adhesion of resist to the oxide. This is done by a chemical treatment that consists of adding HMDS in a specialized oven for that purpose.

After this, a photoresist 4.2 μm thick is spun onto the wafers and processed with standard negative photolitography steps: UV exposure for 4 s, followed by an inverse bake at 90 °C and a final flood exposure for 30 s.

Once the wafers are patterned, the mask for the final etching of the holes is not ready yet. The wafers need to be placed in the AOE and the oxide on top of the wafers etched accordingly with the design patterned during lithography. Since the layer of oxide is not very thick, this step is considerably fast (just ten minutes), after which the remaining resist is removed in a bath of acetone and rinsed with water. Now the wafers are ready for the main etch process.

The fabrication of the through-holes (or vias) was done using a DRIE equipment, as was the case with the electrodes etching. Nevertheless, the machine used is a newer, advanced version of the ASE. With no previous experience with this equipment, it was advisable to follow initially the standard recipes provided by the manufacturer, as a departing point. This is advisable since the variable space of parameters is quite broad, and opti-

mization is a lengthy process (as proven with the fabrication of electrodes). The recipe used was specifically designed for etching high aspect-ratio vias, which suited very well the goal in mind. The parameters of the recipe, which will be referred from now on as "recipe A", are listed thus:

Table 2.5: parameters for standard recipe A

Parameters (units)	*etch step*	*passivation step*
Gas flow (sccm)	SF_6, 550	C_4F_8, 200
Cycle time (s)	7	4
Pressure (mT)	150	25
Coil power (W)	2800	2000
HF Platen power (W)	45	0

This recipe worked quite well up to depths of 100 μm. Despite this, a disastrous effect appears systematically after 15 min of etch: the side walls of the vias start degrading, and if the process continues this effect leads to a total destruction of the walls, connecting neighbour holes and making the substrate collapse. Figure 2.41 shows this problem; on the left side, a 10 minute etch shows almost vertical walls (notice the slight deviation in width at the bottom of the vias), with no under etch.

This profile would be perfect for the seeked purpose; the fact of not having any under etch would allow to obtain very high aspect-ratio holes with the desired diameter. Unfortunately, if the etch keeps running, the process degrades into what the image shows on its right, and if the process is left to continue the damaged part of the walls open onto the neighbor area, thus destroying the array of holes.

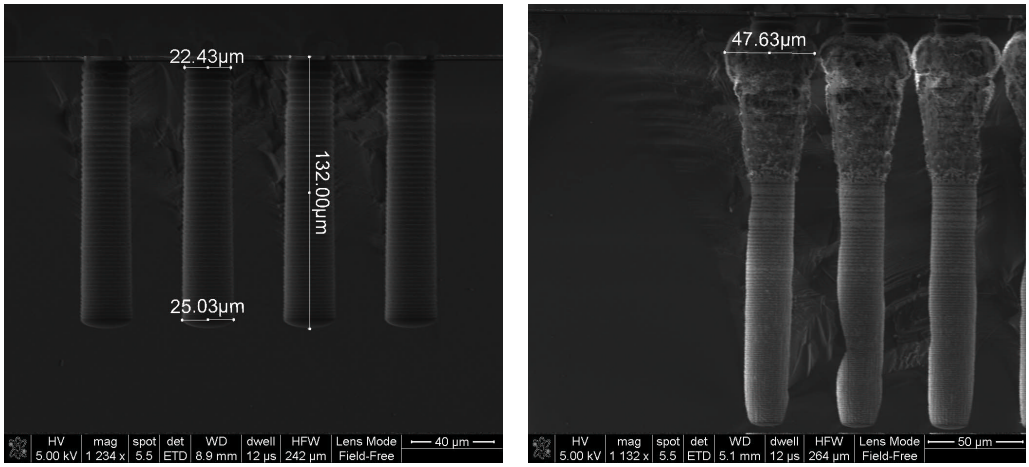

Figure 2.41: Vias etching with standard recipe. The profile obtained after 10 minutes etch (left) is quite straight, but as the process continues (30 minutes, right), the sidewalls become irreversible damaged)

In figure 2.42, holes of 3 μm in diameter show the consequence of the continuous degradation at the side walls. They end up opening up a gap and contacting with the neighbour vias. This very same effect appeared in the final design with holes of 20 μm in diameter, and it became one of the main problems to tackle.

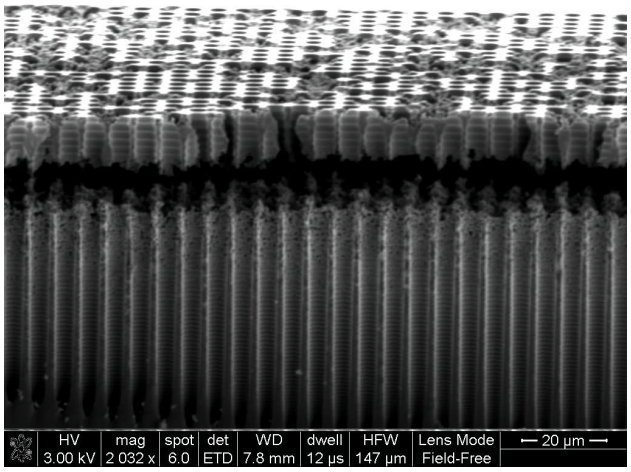

Figure 2.42: Side walls are destroyed after 30 min etching

Alternatively, another recipe, previously developed by another user of the Pegassus DRIE (Thomas Pedersen, at DTU Nanotech) for the fabrication of high aspect ratio pillars, was investigated and later modified, accordingly to the obtained results.

Although the parameters of this recipe are different than the standard recipe A, it was very useful to introduce the same changes in both recipes to extract more meaninful conclusions about the general effect of a particular parameter in the etch process. This recipe will be referred to as "recipe B", and its parameters are as follows:

Table 2.6: parameters for recipe B

Parameters (units)	*etch step*	*passivation step*
Gas flow (sccm)	SF_6, 275	C_4F_8, 150
Cycle time (s)	3	2
Pressure (mT)	26	20
Coil power (W)	2500	0
HF Platen power (W)	35	0

First results with these settings are shown in figure 2.43. This etching was run for 10 min; the walls of the vias etched are very smooth and the profile seems to be quite straight, but in comparison with recipe A, the etch rate is much slower (during the first 10 min, recipe A had an etch rate of 13 $\mu m/min$, in stark contrast with recipe B, with just 5 $\mu m/min$. Not only that, if the process continues (see figure 2.44), the profile narrows at the bottom, up to a point where the etching cannot reach further due to the occlussion of line of impact of the etching species. On top of that, there is some under etch at the top of the holes, which can become problematic if the process is left to run long enough for the holes entering in contact one with another.

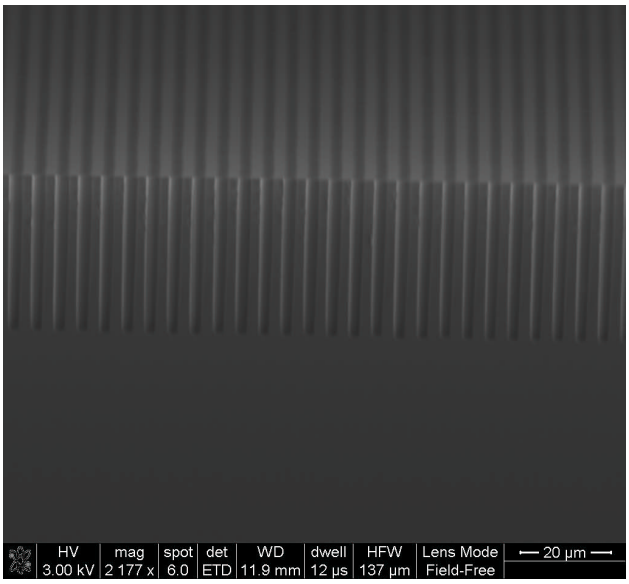

Figure 2.43: Recipe B, 10 min. Vias shown in the picture are 2.5 μm in diameter, with an etched depth of about 26 μm

The main differences between both recipes are the etching times. The modification of shorter etch/passivation times reduces the ripples on the side wall, and also decreases the efficiency of the etching process. This is the reason why the etch rates are much slowlier.

2.4.1 Optimization of etch recipe

After the first contacts with the etch recipe and their results, it was deemed necessary to play with the basic etching parameters in order to optimize the processess. The variation of the parameters was done with an "educated guess"; that is, based in the experience acquired during the development of the electrodes, there were few parameters, like gas percentage and

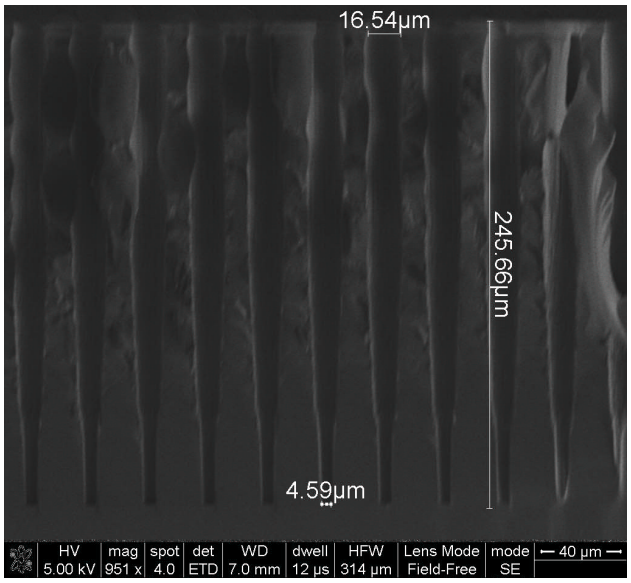

Figure 2.44: Recipe B, 80 min. The holes have the tendency to narrow their profile, which appears clearly as the etch time lengthens. There is also a slight under etch at the top of the structures (the pattern was of circles of 15 μm in diameter, which in the picture show an expansion to 16.5 μm

temperature, that seemed to have a major impact in the profile of the etched structures, and therefore those were some of the first variations studied.

Gases

The addition of oxygen to the composition of the plasma should help in the protection of the side walls (section 2.1.3). In practice, though, the introduction of O_2 was not efficient in stopping the damage on the side walls (see figure 2.45). It could be observed, though, that it had the effect of minimizing the ripple profile and most importantly, decrease the etch rate (see figure 2.46). Therefore, any further modification of this gas was discarded.

The pair of gases SF_6 and C_4F_8 were studied together as their effect is related to each other. The reader should remember that the etch process consist of a basic Bosch sequence of active and passivation steps that are mainly due to the switching between these two gases (SF_6 for the etching, C_4F_8 for the passivation). Therefore, it is expected that, for example, the increase of SF_6 or the decrease of C_4F_8 will speed up the etching process. This happened to be true, yet with additional effects. The increase of C_4F_8 decreases the etch rate. This is reasonable, since by adding up this gas during the passivation phase the thickness of the protective layer is increased, and thus the active etching process is less effective.

Nevertheless, this fact comes also with the advantage of the extra protec-

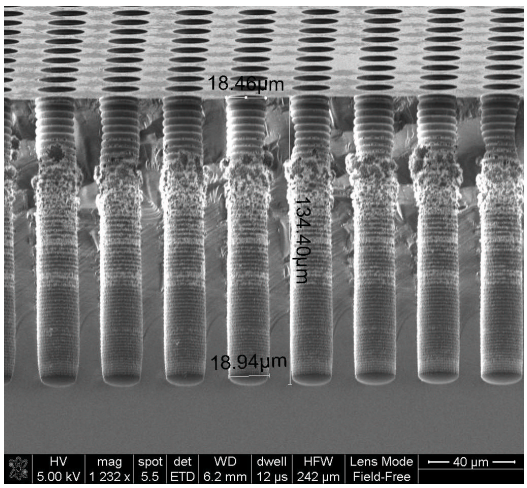

Figure 2.45: O_2 effect in vias etching doesn't stop damage on side walls. The results shown correspond to a process run for 10 minutes with an oxygen concentration of 50 standard cubic centimeters per minute (sccm); the rest of the parameters were fixed to the standard values of recipe A.

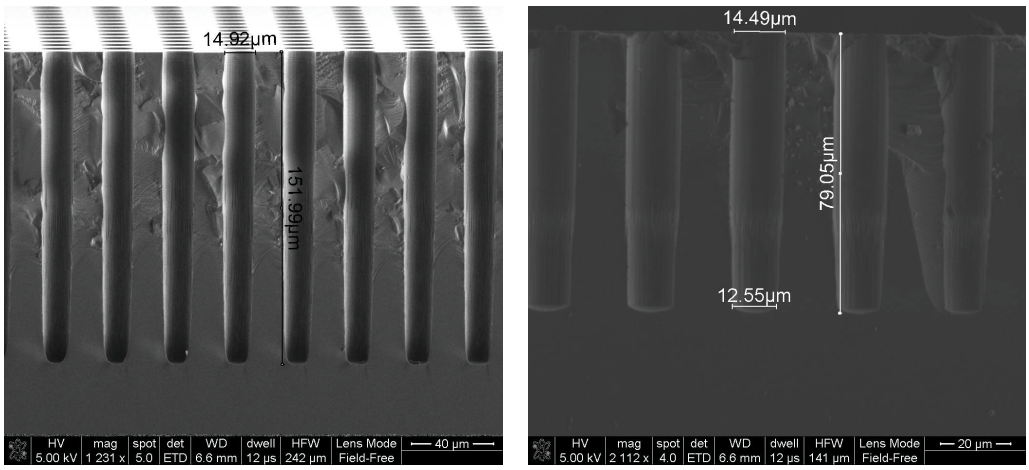

Figure 2.46: The introduction of O_2 slows down the etch rate. Both images shown correspond to processes run for 45 minutes with recipe B, with the only difference being that the right hand side introduces an O_2 content of 20 sccm.

tion of the side walls. This was reflected in a visible decreas in the damage on the walls (see figure 2.47).

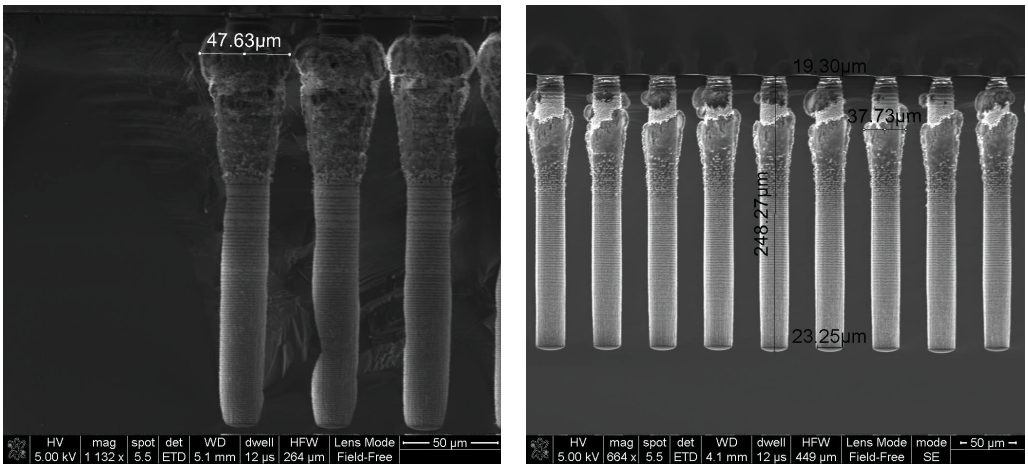

Figure 2.47: The increase of gas C_4F_8 (200, left; 300, right) helps in reducing the damage on the side walls, at the cost of a slower etch.

Temperature

Two different temperatures were tested, 0 °C and 10 °C (see figure 2.48). The temperature seems not to affect greatly the etch rate or the under etch of the mask. The main difference in between the two processes ran was the profile, straighter for the higher temperature, and the quality of the walls, that are more damaged when the process is done at 0 °C. These facts are in accordance with what was discussed during section 2.1.3.

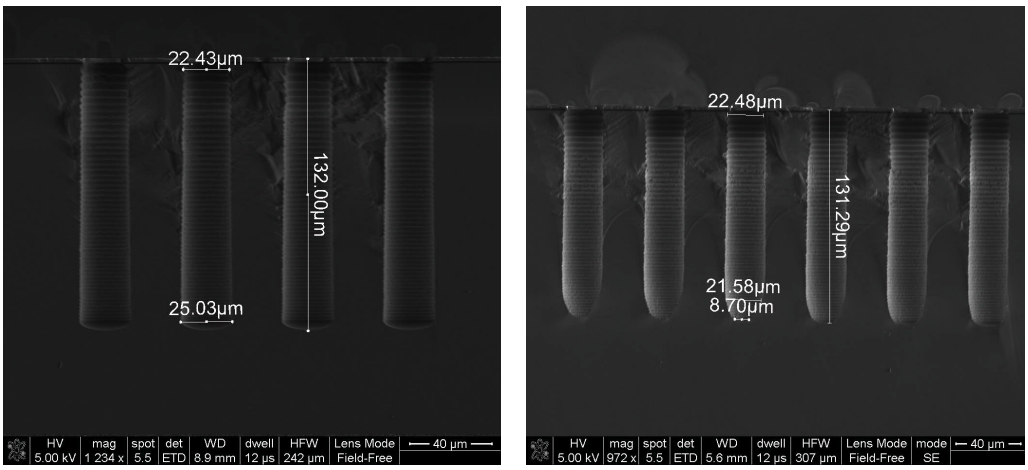

Figure 2.48: Effect of temperature on the etch of vias. On the left, standard A process at 10 °C. On the right, same process ran at 0 °C

Therefore, the temperature was set at 10 °C for the final recipe.

Pressure

It was while reading the work by Ayon *et al.* [37] that the idea of modifying the pressure parameter as to avoid the damage on the side walls came up. This would at the same time achieve good aspect ratios for the holes. The very same damage on the walls was reported to be most likely due to the redeposition of the masking material on these sites, which provokes this irregularity in the etching profile.

When using a pressure value of 30 mT it was the first time that holes came out with very straight profile, and with barely damaged walls. The results were very encouraging, and the rest of the investigation addressed this direction.

Despite the step forward that this finding was to the creation of the vias, by applying lower pressures than in the original recipe (150 mT) there was also a significant reduction in the etching rate.

One could be tempted to think that this fact shouldn't matter, as far as there is patience and time to ran the process long enough. Nevertheless, it is important to reduce this time as much as possible, since the mask used on top of the wafer, although resilient to the etching, keeps being eroded by the process, and may end up dissapearing. In fact, this is what happened in many occasions when the processes were run for longer than 1 hour. In order to avoid this effect, a pressure value of 50 mT was found to be the optimal one to avoid significant damage on the walls and at the same time obtain a reasonable etch rate.

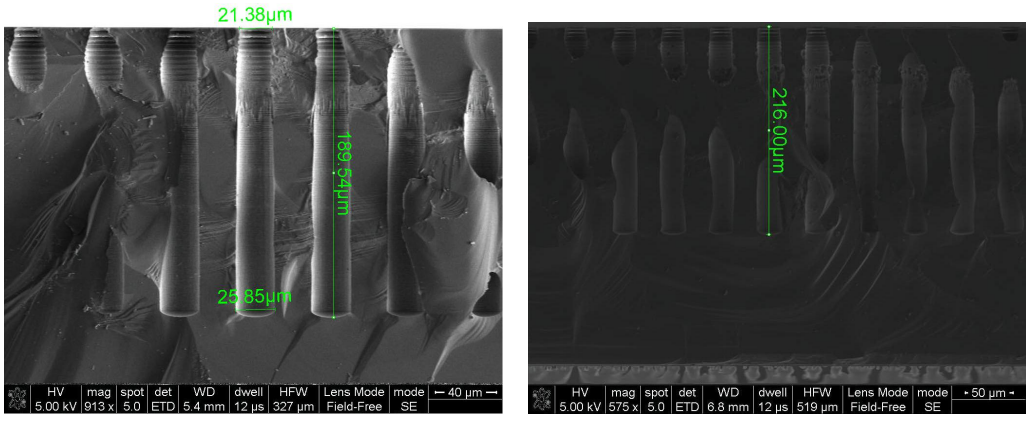

Figure 2.49: Effect of pressure on the etch of vias. A recipe ran for 30 minutes with (left) a pressure of 30 mT and (right) 50 mT. Damage on the walls is more obvious at higher pressure, while the etch rate is also higher.

2.4.2 Final vias

After the previously explained investigation, it was decided to drop recipe B in favour of recipe A. Recipe B presented the problem of occlussion of the holes at the bottom, which proved more stubborn to changes in parameters than the mishaps caused by recipe A. The worst defect developed during recipe B, though, was the under etch, which ended up destroying the structures when they merged with one another after a long process. The modified recipe A, used for the fabrication of vias of 315 μm height and 20μm in diameter, was as follows:

Table 2.7: parameters for modified recipe A

Parameters (units)	*etch step*	*passivation step*
Gas flow (sccm)	SF_6, 550	C_4F_8, 200
Cycle time (s)	7	4
Pressure (mT)	50	25
Coil power (W)	2800	2000
HF Platen power (W)	45	0

The process was run for 75 min at a temperature of 10 °C. It must be noted, though, that the whole etching time had to be divided in two steps. The reason for that is that the machine doesn't tolerate the presence of holes on the wafer, because it cannot establish a good pressure on the backside of the wafer to clamp it securely to the supporting plate. In the case of this design, holes appeared first on the sites of the alignment marks at the sides of the wafer (they etched faster than the rest of the patterned holes on the wafer due to their larger dimensions). The reader is referred to 2.1.4 (RIE lag), to go into detail about this effect.

Therefore, a first step etches the holes for about 1 hour. Afther this, the wafer is attached with a thin layer of resist (1.5 μm) onto a carrier wafer, and put back on the Pegassus DRIE to complete the etching. It is recommened to keep this second step as short as possible, since the presence of two wafers in the chamber of the DRIE equipment doesn't allow for a proper cooling, and the etching will slow down and may change the profile slightly.

After 75 min, the process was stopped, since the oxide mask seemed not to be able to withstand for much longer. The wafer was then cleaned of the remains of oxide by dipping it in a BHF bath for 10 min, after which it was turned around and etched in the ASE to thin it down until reaching the holes from the opposite side. In this way, the final results showed holes of 315 μm, with a very straight profile.

Figure 2.50 shows an image of the obtained vias. Despite the fact that the damage on the side walls is not completely avoided, the structure of the

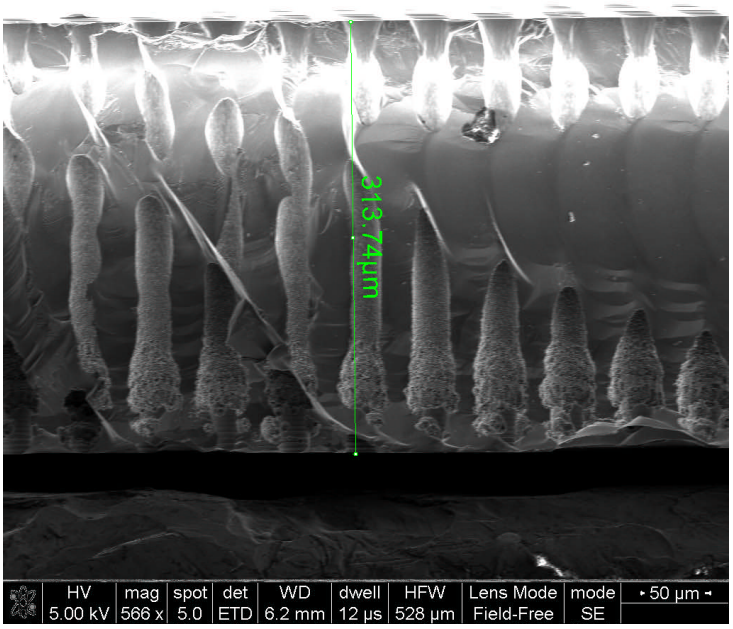

Figure 2.50: Final vias going through the wafer. The holes have a depth of 315 μm. The discontinuities in the holes are due to the trasnvesal cut done to the wafer to take the image on profile.

vias keeps being intact and functional for the purpose of perfusing liquid through, as it will be demonstrated in chapter 4.

A very interesting observation was also made: it seems that there is a logaritmic behaviour in the relationship between the diameter of the holes and the depth reached with the etch. Figure 2.51 shows this effect, by plotting the depth measured against the respective diameter of the holes, for several times of etching. The image shows also the logaritmic fittings to the data plots.

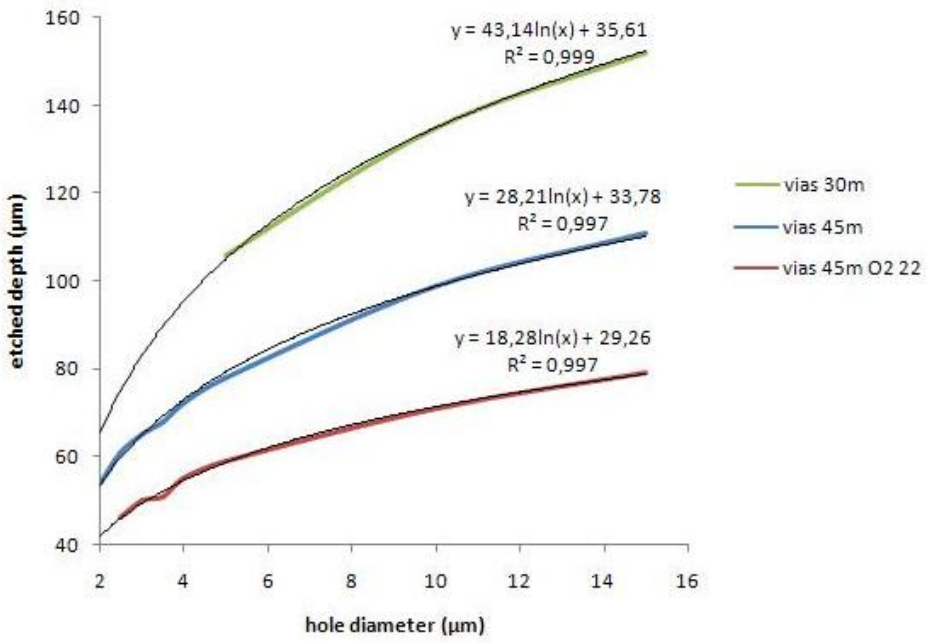

Figure 2.51: Relationship between hole diameter with etched depth

It seems as if the etching equipment could be characterized with these equated trend:

$$D = A{\cdot}t{\cdot}ln(d) + B$$

where D and d are the depth and diameter of the holes, respectively; t is the etching time, and A and B are constants of the system (in the processes shown, A = 0.95 and B = 35). These constants are the same for a process run in the same conditions (just notice that A and B are multiplied by the factor t, which represents the etching time).

It may be useful to take this behaviour into account for future predictions of depth when etching structures under the same conditions.

2.5 Summary and conclusions

Novel electrodes

In this chapter, the main focus of attention of the project was presented. The outcome of this research produced high aspect-ratio, sharp electrodes, with a novel profile made of scallops. The method followed for their fabrication is easy to optimize and it offers a good control of the slope on the side walls.

The profile obtained has many advantages. First of all, it increases the surface area of the strucutres, with a consequent improvement of the signal-to-noise-ratio of the system. It implies a good discrimination between the real signal and noise, which is crucial for the range of signals that this system will be dealing with, that is, neuronal signals of about 500 μV. This will be further supported by the results of the charaterization of the electrodes impedance, in chapter 3.

On top of that, this type of structure could favour the adhesion of brain slices onto them, with the benefit of giving more stable recordings and a better anchoring of the brain tissue to a surface, which is necessary for a healthy growth of brain slices when cultured *in vitro*.

Despite all this, an unexpected issue arose in the last period of the project where it was seen that many of the fabricated electrodes ended up broken rather often without ever being used. Figure 2.52 shows the typical sight of a broken electrode. They always appear broken at the base, as if cleaved by some external force.

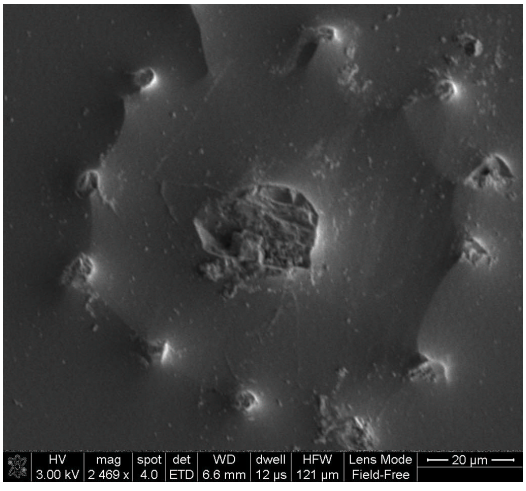

Figure 2.52: Image of a broken electrode

This was blamed first on mistreatment of the finished wafers. However, it was later observed repeatedly on electrodes for which any mechanical contact

had been avoided. It is hypothesized that it is most likely due to the fact that the electrodes lie on a surface of silicon oxide, and this may cause a weak attachement of the structures to the substrate. It could also be due to a thermal stress caused by the difference in thermal coefficients between the substrate layer of oxide and the passivation layer of silicon nitride. But as stated, these are just hypotheses that need to be investigated further to obtain a solid conclusion

Integration with holes

Although the idea of integrating holes in the substrate of the wafer with the fabrication of electrodes is not new [23], the fact of having this system facilitates the integration of a culture method on chip that is not common to find in the MEA area. Such system which would allow a continous monitoring of the brain activity during culture has not yet being achieved (for further explanation on this, see chapter 4). And even though Thiebaud *et al.* integrated holes in their chip, the results that were obtained back then didn't take full benefit from an integrated culture system that aimed for long term cultures. This will all be addressed with the design of such a system that will couple with the MEA chip.

Alternatives to metalization

From the difficulties risen during the fabrication of the electrodes, a novel method for "metalization" of high aspect-ratio structures with sharp edges was presented. This method uses a conductive polymer, PPY, as a material to coat the structures and make them electrically active. This technique is extremely interesting from the point of view of a clean room user. The simplicity of the process, added to the fact of the avoidance of the work environment of a clean room facility is appealing, and cheaper than standard metalization processes like e-beam evaporation or sputtering. Moreover, PPY has been reported to be biocompatible [54]. This fact was also proved in this work by culturing PC12 cells on the fabricated electrodes.

Chapter 3

Characterization

3.1 Impedance

It is important to characterize the electrodes from an electrical point of view, since their main purpose is to obtain electrical recordings from cells. In order to ensure a good quality of such measurements, it is necessary for the system to have a good signal to noise ratio. As explained previously, the idea of using three dimensional electrodes revolves around the target of improving this factor. The higher surface area of the three dimensional electrodes in comparison with planar ones should translate into a reduction in the electrical impedance, which would allow for the reduction in the recorded noise that accompanies the real signals.

Therefore, it is necessary to characterize the impedance of the electrodes. This characterization gives valuable information in regard to the behaviour of the electrodes at a particular range of frequencies. In the scope of this work, it is particularly important to have a minimum resistance, which can be seen intuitively as an opposition of the signal going through the electrode. It is also desirable that the electrodes exhibit a high capacitive value, as the higher the value, the higher the current values that can be used for stimulation of the neuronal tissue. This is due to the fact that the electrodes present a limit of safety in regards to the charge that they can accept before starting processes that may introduce harmful chemical species in the solution where they are placed [27].

In this work, the electrodes are placed in the media of the brain slice culture in order to record signals. This is a particular set up that needs to be characterized as the reaction of a metal in the presence of a conductive liquid, and a model that tries to fit this system should consider the chemical-electrical interactions that occur in this environment.

3.1.1 Electrical model of the electrode-electrolyte interface

The behaviour of a metal object in an electrolyte (a solution with free ions dissoved on it) presents special characteristics that affect the electrical response of the system. When a metal is submerged in the solution, it behaves as an electrochemical transducer. Although this interface is not well understood yet, it is known that two type of mechanisms happen on it: the ones where no electron transfer occurs (mostly capacitive effects) and the ones where an oxidation-reduction process takes place and forces an exchange of electrons (faradaic effects). These two mechanisms need to be studied in order to understand their influence in the final impedance model of the system.

The presence of faradaic processes causes electron transfer reactions (electrochemical oxidation-reduction reactions) at the interface between the metal surface and the electrolyte. This rearrangement of charges creates an electric field between the metal surface and the electrolyte, which itself provokes:

- water dipoles in the electrolyte to be oriented by the field into a layer, on the surface of the metal, called *hydration sheat*
- solvated ions (products from the red-ox activity mentioned earlier) to arrange into a layer by the hydration sheat; this layer is the *outer Helmholtz plane* (OHP)
- adsorption of ions at the metal surface, which creates the so-called *inner Helmholtz plane*

The outcome of this organization of ions and electrons results into an electrical interface that is defined as the *electrical double layer*. This interface will have a high impact over both processes mentioned before, both the faradaic and non-faradaic.

Non faradaic effects: double layer capacitance

The electrical double layer can be seen, in terms of electrical modeling, as a capacitance, which according to the Stern model [55] is formed of a serial combination of two capacitances that have special characteristics. The interfacial capacitance, C_I, is given by

$$\frac{1}{C_I} = \frac{1}{C_H} + \frac{1}{C_G} \tag{3.1.1}$$

where C_H is the Helmholtz capacitance and C_G the Gouy-Chapman capacitance. The Helmholtz capacitance represents a traditional pure capacitor that is confined between the metal interface and the hydration sheat layer.

Its value is given by

$$C_H = \frac{\epsilon_0 \epsilon_r A}{d_{OHP}}$$

with ϵ_0 being the permitivity of free space, ϵ_r the relative permitivity of the electrolyte, A the area of the interface and d_{OHP} the distance of the OHP.

This model doesn't take into account the dependency of the interfacial capacitance on the applied potential, as it is seen experimentally (see Figure 3.1). But the Gouy-Chapman capacitance does, as it is shown in the following calculations. The mentioned dependency is due to the solvated ions diffusing

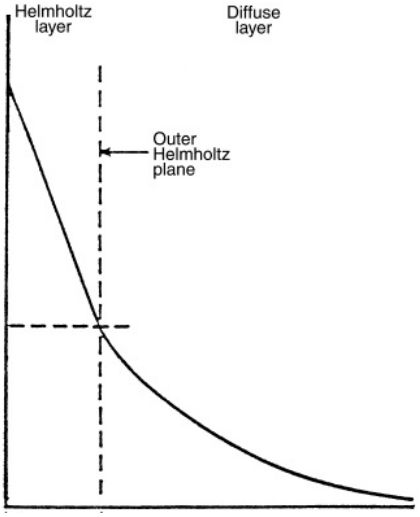

Figure 3.1: Potential at the metal-electrolyte interface. Between the Helmoltz layer and the OHP it shows a linear behaviour. At the bulk of the electrolyte, the potential decays almost exponentially (from [50])

through the bulk of the electrolyte instead of being located on a rigid plane (as the Helmholzt capacitance assumes). The drop of potential at the interface for small signals (< 50mV) that is caused by the diffusion is described as follows [56]:

$$V(x) = V_0 e^{(\frac{x}{L_D})}$$

where V_0 is the potential at the metal interface, x is the distance from the metal layer and L_D is the Debye length. L_D can be viewed as the characteristic thickness of the diffusive layer:

$$L_D = \sqrt{\frac{\epsilon_0 \epsilon_r V_t}{2 n^0 z^2 q}}$$

with V_t being the thermal voltage (kT/q), n^0 the bulk number concentration of ions in the electrolyte, z the valence of the ions and q the the electron

charge. Although it is not shown here, it is possible to deduce that the contribution to the capacitance by the drop of potential V(x) is given by [55]

$$C_G = \frac{\epsilon_0 \epsilon r A}{L_D} cosh(\frac{zV_0}{2V_t})$$

The phenomena described above are purely non-faradaic; that is, only non red-ox reactions have been considered. In other words, the polarized interface can be seen as the combination in series of two classical capacitances of values C_H and C_G.

The following parts that will be included in the final model of the impedance describe the effects related to the faradaic behavior of the interface. They will account for the charge transfer through the interface capacitance. Two main mechanisms are the most predominant ones in the movement of charges between the metal layer and the OHP: charge transfer and diffusion. These effects are particularly relevant when high currents are applied.

Charge transfer resistance

Charge transfer results from oxidation-reduction reactions that occur at the interface. At equilibrium, there is a net exchange of current equal to zero as the oxidation current balances the reduction current. In the final model of the impedance, a resistive term R_t will appear due to the path where this currrent goes through the double layer capacitance. R_t can be derived from the Butler-Volmer equation:

$$I_F = I_0(e^{(1-\alpha)\frac{nF\eta}{RT}} + e^{-\alpha\frac{nF\eta}{RT}})$$

I_F is the faradaic current, I_0 is the exchange current, n the number of electrons per molecule oxidized/reduced, α the transfer coefficient, and η the transfer overpotential. For small applied signal amplitudes (< 50 mV peak),

$$R_t = \frac{RT}{nFI_0}$$

Warburg impedance

The phenomenon of diffusion of ions from the electrolyte to the metal can cause a current to go through the metal-electrolyte interface. The ions are driven by an applied electrical field and follow it towards the interface in a sinusoidal manner, according to the frequency of the excitation. This effect tends to disappear as the frequency of the AC signal increases, since the ions are not able to follow the field. This effect is included in the model of the impedance of the metal-electrolyte interface with the Warburg model [57]:

$$Z_W = \frac{10^3 V_t}{2Az^2 q n^0 \sqrt{\pi f D}}(1-i)$$

where f is the frequency of the applied voltage, ,D the diffusion coefficient of the ions and $i = \sqrt{-1}$. This impedance has a phase angle of 45 degrees and is proportional in magnitude to $\sqrt{f}$.

By analyzing equation 3.1.1, it is clear that the presence of this new element on the impedance is frequency dependent. It may be easier to the impact of this element in the behaviour of the impedance by looking at figure 3.2. At very low frequencies, the Warburg impedance value increases to very high values, forcing the current through the interface capacitance In the opposite way, at high frequencies the Warburg impedance is almost non-existent, and therefore gives a free path to the ions, like a wire.

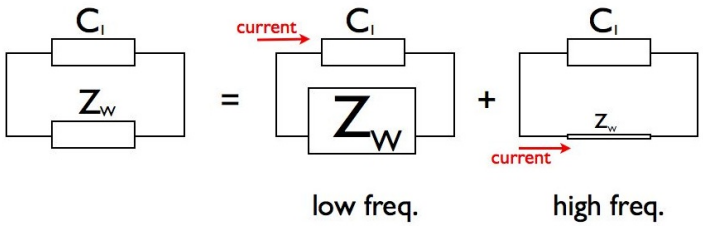

Figure 3.2: Impedance circuit with elements C_I and Z_W. The placement of these elements in parallel couples well with the real behaviour of the interface: at low frequencies, C_I will dominate, while at high frequencies Z_W disappears, offering free way to the passing of current through the wire.

That means that at the low frequencies of range, the double layer capacitance should influence the response of the system, and thus if the magnitude of the impedance is represented as a function of the frequency, it should show a negative slope with a value lower than 1 dB/dec. $1dB/dec$ is the slope of a pure capacitance, but as it will be explained later, C_I presents a typical characterisitc of a slope with less inclination than pure capacitors.

From the above commented, the fact that the Warbug impedance is only relevant for high frequencies means that, for the application at hand, that is, low to medium frequencies of the spectrum, it is safe to assume negligible its effect on the total impedance. In conclusion, only the double layer capacitance will be taken into account for the modelization of the impedance.

Empirical model: constant phase element

Although the previously discussed model works well in simple electrode systems in pure electrolytes (with no complex molecules like proteins), the reality is that for most situations, empirical methods are necessary for the extraction of meaningful electrode parameters [56]. This is a very relevant observation in the case of this work, since the culture environment of the brain

tissue will probably generate the presence of proteins in the surroundings of the electrodes. Therefore, an empirical model seems more suitable for obtaining an accurate characterization of the impedance. This is usually done by approximating the double layer capacitance to the following expression [58]:

$$Z_{CPE} = \frac{1}{AQ_0(i2\pi f)^n}; \qquad (0 \leq n \leq 1) \qquad (3.1.2)$$

where A, as before, is the active area of the electrode, and Q_0 and n parameters that are empirically calculated. The phase angle of this impedance is independent of the frequency, with a value of (-90*n)°, and this is the reason why this impedance expression is usually referred to as the Constant Phase Element (CPE).

Final impedance model

So far, the modeling has not taken into account the solution in which the system is submerged. This solution is conductive, and when an AC signal travels through this medium towards an electrode, a resistance opposes the transport of current. This effect is added to the final impedance model of the system in the form of a resistance called spread resistance R_s. The value of this resitance is given by equation 3.1.3:

$$R_s = \frac{\rho L}{A_S} \qquad (3.1.3)$$

where ρ is the resistivity of the liquid; L is the distance the current covers through the solution, and A_S is the cross-section area of the electrode.

On top of this, a last additional member is considered in the impedance model. Parasitic capacitances are ubiquitous in all electrical measurements, and this is not an exception.

Considering all the above, the final model of the impedance is given by a circuit of the CPE capacitance (double layer) in series with the spread resistance. These two components are placed in parallel with the parasitic capacitance C_p, and therefore the total impedance Z equals to:

$$\frac{1}{Z} = \frac{1}{Z_s + Z_I} + \frac{1}{Z_p} \qquad (3.1.4)$$

If the expressions of the capacitances and resistances are substituted in equation 3.1.4, Z can also be expressed as:

$$Z = \frac{1}{jwC_p + \frac{1}{R_s + Z_{CPE}}} \qquad (3.1.5)$$

Figure 3.3 shows the diagram of the final impedance model that will be adapted in this work. From now on, all calculations will be done in reference to this model.

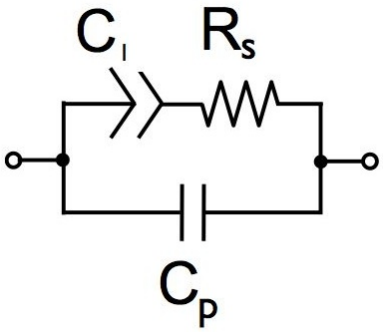

Figure 3.3: The circuit shown in the image is the equivalent circuit model of the impedance at the electrode-electrolyte interface. On it, a spread resistance R_s is connected in series with the double layer capacitance (modelled as Z_{CPE}, and a final C_p in parallel accounts for the parasitic capacitance due to wiring and leakage through the isolation layers

3.1.2 Impedance measurements

3D electrode impedance

Before showing any of the empirical measurements of the impedance of the electrodes, it must be stated that during these experiments the fabrication of the electrodes hadn't been optimized yet, and the profile wasn't perfectly sharp, as has been shown in chapter 2. For the sake of accuracy in the calculations shown here, it is therefore necessary to consider the geometry shown in figure 3.4. Such geometry corresponds to a truncated cone, of radius r_1 for the base and r_2 for the top, and a height h.

The surface area of a truncated cone is given by equation 3.1.6:

$$A_T = \pi[s(r_1 + r_2) + r_2^2] \tag{3.1.6}$$

where s is the slant height, given by

$$s = \sqrt{h^2 + (r_1 - r_2)^2}$$

For the electrodes used, $r_1 = 20\ \mu m$ and $r_2 = 5\ \mu m$, for an h = 60 μm. Substituting in the equations these values, the surface area $A_T = 4640\ \mu m^2$.

This value allows to calculate the expected double layer capacitance at the electrode-electrolyte interface, since it is known that for the solution of

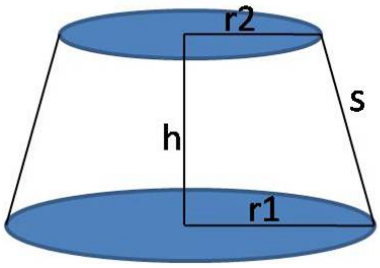

Figure 3.4: The drawing shows the geometry of the electrodes characterized during the impedance measurements

PBS used, the specific double layer capacitance is 0.1-0.2 pF/μm^2, giving a expected capacitance of about 464 - 928 pF.

For the experimental characterization of the electrical impedance of the electrodes, the configuration used for the measurements is shown in figure 3.5. The measurements were done by Marco Carminati, at Politecnico di Milano.

The configuration of the setup is as follows: a spring contact is placed on top of one pad of the chip. This pad is connected to an electrode of the array, for which the impedance will be measured. This is therefore the working electrodes that is to be characterized. A vial is also attached to the chip in order to be able to submerge the MEA in a solution of known conductivity (for these experiments, Dulbecco PBS, conductivity 1.5 S/m was used). Finally, a counter electrode of Pt was also immersed in the solution, and grounded.

As the measuring equipment, a LCR meter was used. This device is able to measure the impedance of common elements of an electrical circuit: inductances (L), capacitances (C) and resistances (R). The counter and working electrode were connected to the LCR meter (Agilent E4980A), and a range of frequencies from 20 Hz to 2 MHz was measured in order to obtain the spectrum of response of the system to the stimulus AC signal of 50 mV.

The response in magnitude of the electrode is shown in figure 3.6, where measurements from ten different electrodes were taken. It can be extracted from it that the slope of the magnitude at low frequencies is smaller than 1 dB/dec, which doesn't correspond to a pure capacitance. It is, in fact, a characteristic of the presence of a double layer capacitance element, as it was commented during the introduction, and it represents an indication of the electrodes being in contact with the solution. Moreover, the behaviour of the magnitude plot at high frequencies shows the resistance of the liquid. This is so because, as seen in the model inserted in the lower left corner of the plot, the resistance is in series with the double layer capacitance. Since

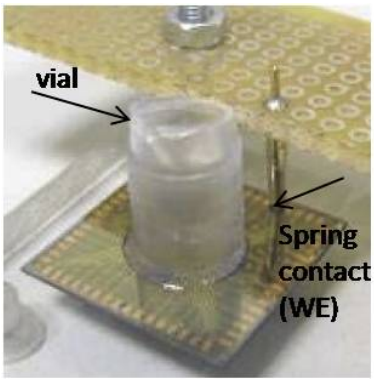

Figure 3.5: The picture shows the connections used for the impedance measurement of the 3D electrodes. A spring contact establishes connection with the external pad of the chip. The pad is wired to one of the electrodes in the array. The vial attached to the chip is filled with a solution of known conductivity.

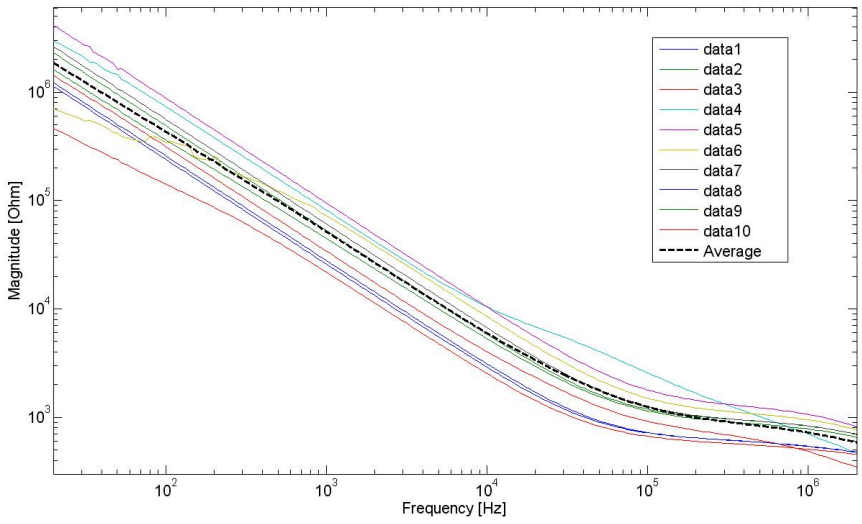

Figure 3.6: Measured impedance for 10 electrodes.

the capacitance gets shunted at high frequencies, the main component of the impedance in that range is the resistance.

As explained during the introduction, the double layer capacitance can be characterized experimentally by the CPE, which is the factor that makes the slope smaller than 1 dB/dec. The expression that relates the impedance with this experimental model was given in eq. 3.1.2.

According to this model, the constant phase element n can be calculated with the now known value of the phase and frequency. These values are extracted from the plot shown on the right side of figure 3.7. With an approximate phase value of -83 ° at 1 kHz, the constant phase element is therefore n = 0.92.

On top of that, from the values collected on the left hand side of the same figure, it is extracted that the value of the double layer capacitance is 3.87 nF. Nevertheless, the spread of this value is of ± 50 %, and therefore the variability is too great to take it as a definite value.

As for the resistance values extracted from the magnitude response (figure 3.8), an average of 833 Ω was obtained at high frequencies (500 kHz), as it is shown in figure 3.8. In theory, this resistance should correspond to the R_s of the solution. The theoretical calculations of this resitance aren't trivial for the three dimensional structrure of the electrodes. Nevertheless, for a planar disk electrode of an equivalent radius, it is calculated from 3.1.3 that R_s = 4.2 kΩ.

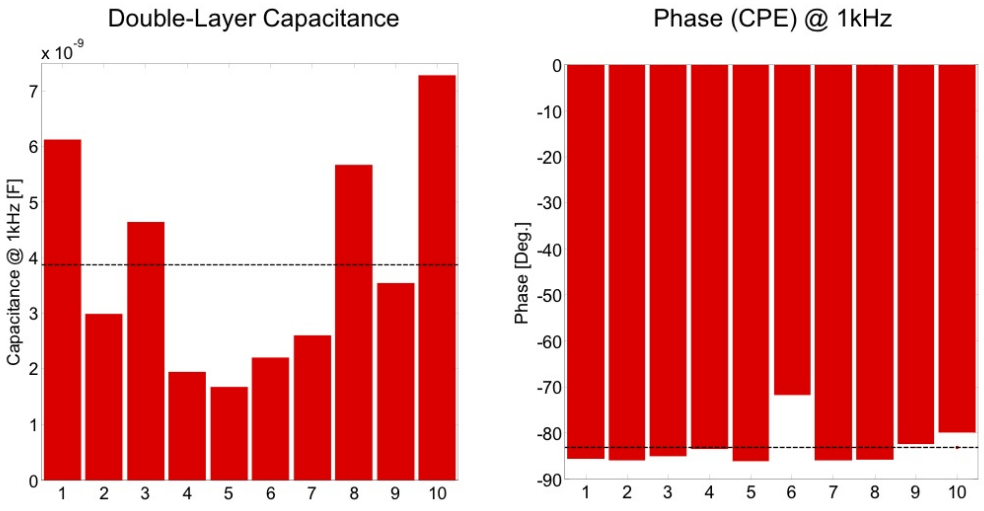

Figure 3.7: Extracted capacitance value according to model X

The discussion of these results will be postponed until the end of this section, when all the experiments performed in regard to impedance characterization are explained.

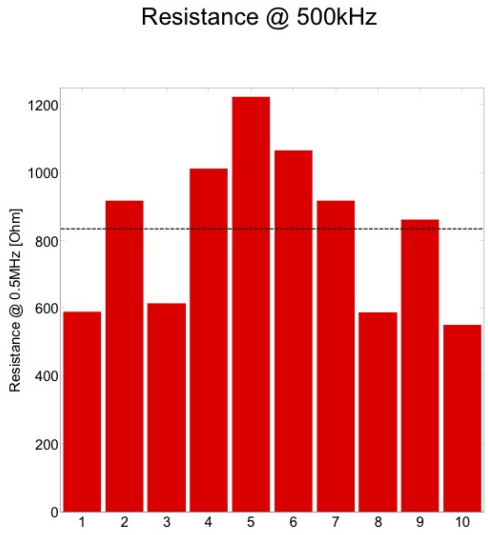

Figure 3.8: Extracted resistance value according to model X

3D versus 2D impedance

In a second set of experiments, the electrical impedance of 3D electrodes was compared to identical measurements taken for planar electrodes, in order to observe the expected decrease in impedance when using three dimensional structures that present a higher surface area.

Expected impedance decrease

The area of a disk-electrode of 20 μm of radius is 1256 μm^2. By comparing this value with the surface area A_T of the three dimensional electrodes, calculated previously, a decrease in the overall impedance of about 5 should be seen between the 2D and 3D electrodes.

Similarly to the previous experiments, the electrical impedance of the electrodes was measured with a HP4294A impedance analyzer, which can measure impedance in the range of 40 Hz to 110 MHz In the experiments performed, a bandwidth between 40Hz and 1 MHz was chosen to characterize the electrodes. The setup of the experiment is illustrated in figure 3.9.

The array of electrodes was immersed in a solution of 1 % NaCl (similar to biological culturing conditions) and a sinusoidal voltage signal with 250 mV of amplitude ran between one electrode on the array and a Pt wire that was grounded. The impedance analyzer measures the current coming out of the system, extracting the final impedance values.

These measurements were realized in both a three dimensional array and a planar one. The planar array had been fabricated with the same design as the 3D one, and using the same materias in order to perform a meaningful comparison between the two type of electrodes.

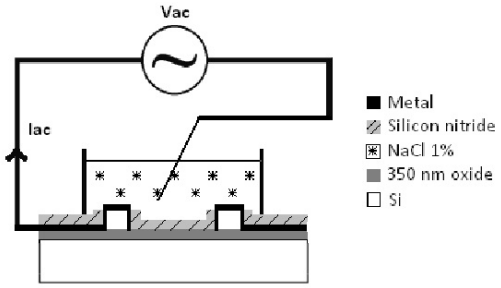

Figure 3.9: The picture shows the connections used for the impedance measurement of 2D and 3D electrodes.

Also, a stimulus signal of 100 mV was used on the same set up configuration to test comparable signals to that of the real measurements on cells. Nevertheless, the results were identical to the ones obtained with the stimulus signal of 250 mV except at the start of the frequency spectrum, where more noise was added to the response. Therefore, all the measurements shown here correspond to the 250 mV stimulus

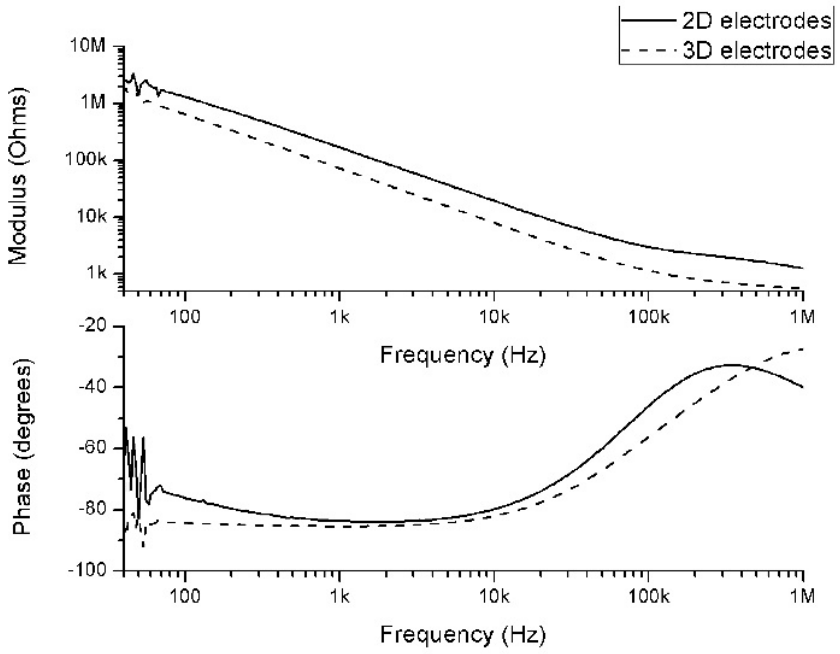

Figure 3.10: Impedance measurement with an impedance analyzer. The plot shows the response of one electrode to a stimulus of a V_{AC} signal of 250 mV.

The results, shown in 3.10, reveal an impedance gain of 1.5 for electrodes

of 20 μm in diameter. There are several reasons that could have caused this divergence with the theoretical results, as it will be discussed.

3.1.3 Results and conclusions

From the electrical impedance measurements taken for the three dimensional electrodes, the following parameters were obtained:

Table 3.1: Impedance measurements

value	*C(nF)*	*R (Ω)*	*ratio 3D/2D*
theoretical	0.47 - 0.93	4200	3.7
experimental	3.7	833	1.5

The double layer capacitance measured showed a value between 3 and 7 times larger than expected. There is also a considerable increase in the spread resistance value when compared with the theoretical value. Despite the variation of the values obtained during the measurements (figure 3.8), R_s shows a consistent trend around the average value taken.

The fact that the values of the capacitance and resistance diverge from the theoretical model in that trend is not a negative result in itself, if the effect of this parameters is considered. As it has been mentioned during this work, it is desirable to obtain a low impedance of the electrodes in order to optimize the recording of electrical signals. In the particular case of the resistance, the fact of obtaining a low value tranlates also into a low impedance. As for the case of the higher capacitance seen, it is also considered positive to have large values of this parameter, as it gives a higher margin of currents that can be applied for stimulation without initiating faradaic effects at the metal interface.

The divergences in the impedance values could be due to the fact that the top passivation layer of silicon nitride in the electrode has an opening in the form of a disk. This opening is intended to allow the electrodes be in contact with the solution, in order to record electrical signals from it. As it happens, the radius of this disk is of 70 μm in diameter, which exposes more are of the metal wire than the one used for the theoretical calculations (40 μm). Therefore, the theoretical calculations should be considered only as an approximate expectation of the real impedance.

Despite this, both experiments (measurements with the LCR meter and comparison between 3D and 2D impedances with the analyzer) showed a range of magnitude for the impedance that held coherently, in the order of 2MΩ at the electrophysiological range of frequencies. In comparison with other similar electrodes [24], this value is a positive result (it seems to improve by a factor of 2 the 3D electrode impedance) that may improve the recording

quality of the electrodes in regard to the available solutions by an important reduction in the value of the impedance.

In regard to the comparison between 2D and 3D values, it is clear from figure 3.10 that the use of the conical elecrodes shows a decrease in the magnitude response, as expected. The impedance factor gain of 1.5 seems low in comparison with the expected value, but this could be due to the following: the planar electrodes are made of 200 nm of gold, whereas the three dimensional ones are made of highly doped silicon. It is true that the latter ones have also a deposited layer of gold of the same thickness, but as shown during chapter 2 the metalization of these strucutres presented gaps due to a poor step coverage. Therefore the conductivity of the materials won't be the same.

It could also be due to the difficulties in obtaining accurate measurements with the current set up; it was seen that the results varied greatly in relation to the quality of contact with the external pad of the chip that connected with the electrode under analysis. In the experiments where the impedance was measured for both the 3D and 2D electrodes, the external pads were put in contact with a micro needle that sent the signal measured to the impedance analyzer, and it may be that the small area of the probe could introduce noise and irregularities.

Nevertheless, these results are comparable with [24] in regards to the order of magnitude of the impedance obtained, even improving the given values slightly.

3.2 Penetration

Probe insertion is an important factor to take into account for minimization of damage in tissue. An electrode array penetrating neuronal tissue needs to go through neurons and their processes, glia cells, capillaries, etc. Fibrous structures like microtubules and neurofilaments may catch on the electrode and thus propagate the insertion force within the adjacent tissue. This would cause tear, which is one of the most damaging effects upon neurons and may also rupture some blood vessels. Bleeding inside the brain provokes displacement of active neuronal tissue from the surface of the electrode and even death of cells. Another effect to avoid is the streching or compression of the tissue, since it could disrupt the cells membranes.

Brain matter, like other biological tissues, responds like a viscoelastic material to mechanical forces. This means that its response presents a complex dependency on mechanical parameters such as the magnitude of the penetration force or the speed of insertion. Geometrical parameters like probe size and geometry influence the force exerted during penetration, and therefore the viability of the tissue can be compromised by the choice of these features.

3.2.1 Penetration mechanisms in soft solids

The main reason that motivates this and previous works [24, 30] to go through relatively complicated fabrication processess for obtaining conically shaped electrodes is the intuitive notion that a sharp tip would ease the penetration of the tissue and reduce the tear and distortion, if compared to a cylindrical rod. Tall cylinders could be a suitable candidate for electrodes fabricated in silicon, since their fabrication would relax the conditions of the fabrication process (at least in regards to the etching part).

Previous studies favour the idea of sharp tips for penetration of soft tissue [59, 60]. Shergold *et al.* showed the difference in the puncture mechanisms between a cylindrical punch and a sharp tipped punch. While the cylinder

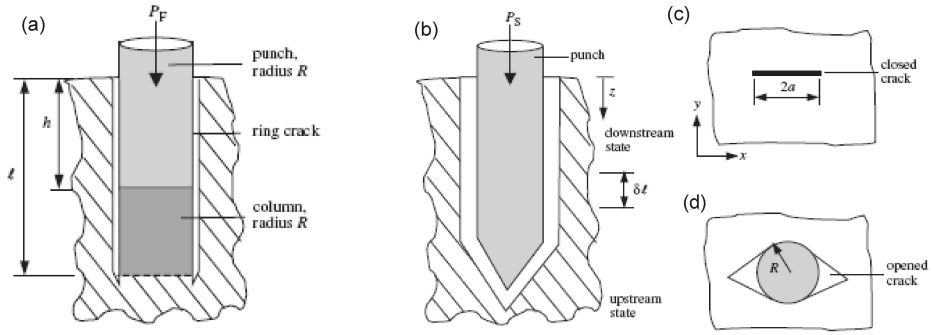

Figure 3.11: Crack formation in soft tissue due to penetration of a rod. Mode II crack (a) and mode I crack (b). (c) and (d) show the two steps that occur during mode I crack (from [60])

produces a mode II ring crack, the sharp tip forms a mode I crack (see Figure 3.11). In mode II crack the opening takes the shape of a circumference that propagates ahead of the object and forms a column. As the punch keeps pushing, this column is compressed and its radius increased to the size of the foreign cylinder (due to the incompressibility of the tissue). On the other hand, the dynamics of mode I crack are sequenced in two steps. First, a slide tears the tissue at the contact point with the tip. Then, as the sharp tipped cylinder keeps pushing, the crack widens to engulf the rest of the cylinder. It is easy to conclude that the crack produced by a cylinder will be bigger than that of a sharp tip cylinder (the cylinder making its way through a ring size opening, whereas the sharp tip does only produces a slide).

As for the penetration force itself, for a flat bottomed cylinder it is two to three times higher than that for a tip sharp cylinder [60].

According to [61], using an energy balance equation, the work exerted by the electrode for a first indention is equal to

$$Fdx = d\Delta \tag{3.2.1}$$

where F is the insertion force and x the distance travelled by the electrode. $d\Delta$ is the change in the stored internal strain energy.

By calling W_p the work necessary to create the puncture and W_c the one to create a crack, it follows from 3.2.1 that

$$W_p = \int Fdx = W_c A \tag{3.2.2}$$

which represents the balance of energy between the moment before puncture of the tissue (left side of equation) and after (right side). The force involved in 3.2.2 is the force required to do the insertion in the tissue.

Davis et al. [62] fitted empirically this force to an exponential form like

$$F = \alpha e^{\beta x} \tag{3.2.3}$$

where A and β are constants.

Substituting this form into 3.2.2, one can come to the following expression of the force:

$$F = \beta W_p A + \alpha \tag{3.2.4}$$

Therefore, the insertion force is linearly proportional to the tip area, and it can be concluded that a cone with a sharp tip and the same diameter in its base as an equally tall cylinder will penetrate with less force, which will produce less tear in the tissue.

Alternatively, if cylinders of very small diameters were to be used instead of sharp cones, the structures would be very brittle due to the great heights required for the recording of active sites in the brain slices.

3.2.2 Experiments on penetration of electrodes

In order to investigate the penetration mechanisms of the scalloped electrodes, as well as their wear and tear, a simple experiment was realized: with a microcontroller driving an arm in the x, y and z directions, a thick piece of PDMS was moved in micro steps towards the array of electrodes.

A single wafer with scalloping electrodes was fabricated as described previously (chapter 2). No passivation layers or metalization was used this time, though, since the purpose of the test was to study the structrue of the electrodes itself, and therefore those steps were omitted for the sake of simplicity in the fabrication.

The array was cleaved in a way that at least some electrode stayed close to the border of the cut. This was done for easiness of observation, as it will become clear after the explanation of the set up. This piece of the array

was stuck to a holder that allowed to place the surface perpendicularly under the lens of a microscope. In this way, the cut area of the array was shown in profile to the microscope, therefore allowing the focus onto the electrode structures.

PDMS was chosen as an insertion reference material for the experiment since its Young's modulus is much higher than that of mouse brain tissue. In the case of the PDMS used for the experiment, made with a mixing ratio of 1:10 between polymer and its curing agent, the Young's modulus is about $7.5 \cdot 10^5$ Pa [63] . By contrast, brain tissue of mice has been defined to be about 3.2 Pa [59]. Therefore, testing the electrodes by trying to penetrate this layer of PDMS will give an idea of the behaviour of the system: if the electrodes don't present any buckling, they will endure the penetration of brain tissue without any problem.

The piece of PDMS was inserted into a chip that fits into a robotic hand, as mentioned at the start. The microcontroller that drives the arm was operated manually in micro steps that moved the sample of PDMS towards the electrode surface, and the experiment was recorded with a camera embedded in the microscope for further analysis. Figure 3.12 shows the sequence of one of the electrodes (left) penetrating the PDMS layer (right). The movement was carried out until the chip with the array of electrodes touched the surface of the PDMS layer. Then, the polymer was retracted in the same fashion. The mechanics of the insertion could be divided into 3 steps:

1. The PDMS layer deformes around the electrode tip
2. Puncture of the polymer by the tip. The insertion force of the electrode tip overcomes the energy barrier to perforate the PDMS.
3. Continuation of the perforation until both surfaces come into contact

Upon removal, the electrodes were inspected under the microscope and showed no signs of damage. Robustness was further tested by lateral displacement of the PDMS once the electrode had been inserted. After removal of the PDMS, the electrode remained intact.

3.3 Summary and conclusions

Three dimensional-scalloped electrodes described in the previous chapters have been characterized by measuring their electrical impedance. It is important for the ensurance of good quality recordings of signals to calculate the impedance values of the electrodes, since it dictates the behaviour of the system that depends on the frequency of the input signal.

The results obtained showed the benefits of using three dimensional electrodes in comparison with planar electrodes. This is due to the fact of having

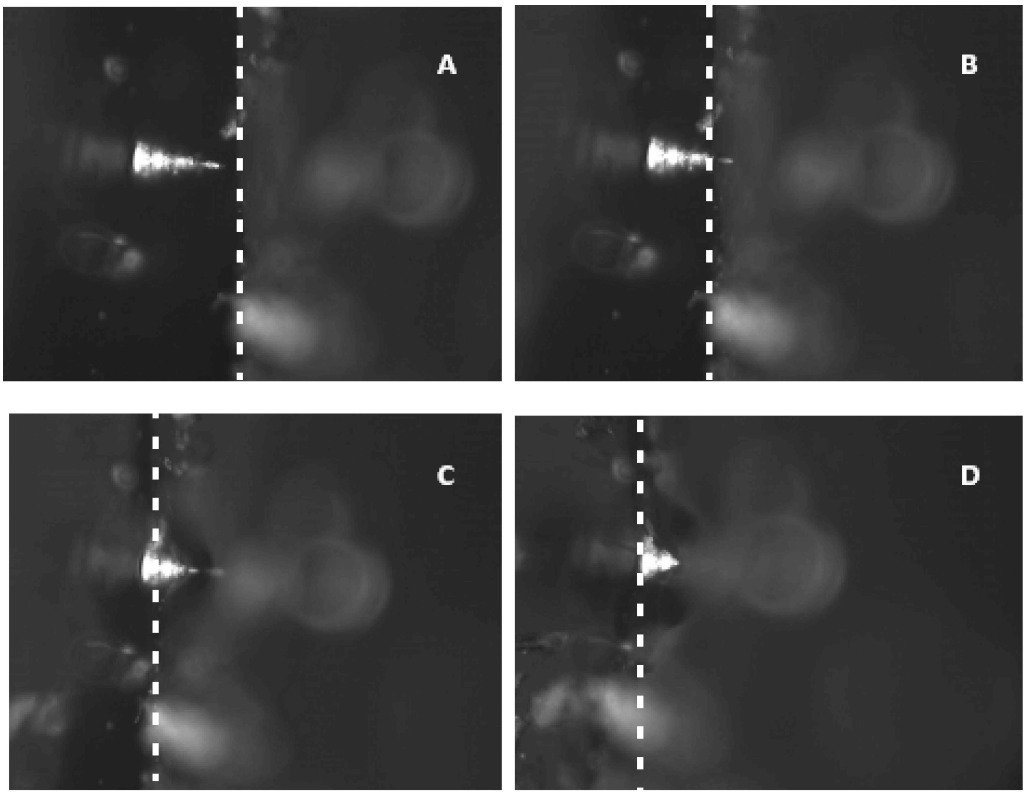

Figure 3.12: Penetration of a thick layer of PDMS by one scallop-shaped electrode. The discontinuous line shows the border of the PDMS slice. (A) Before indentation; (B) penetration of the PDMS layer (right hand side) with the tip of the electrode; (C) continuation of the movement with deeper penetration of the PDMS layer; (D) the surface of the chip with the electrodes gets in contact with the PDMS layer

a higher surface area then their counterpart, which reduces the resistance of the system and thus the total impedance. The measurements showed an improvement factor of 1.5 against planar electrodes, which will contribute in the reduction of the noise picked up by the electrodes during recording sessions. Moreover, different experiments showed a consistent value in the magnitude of the impedance, which is a good indication of the reliability of the results.

The range of the impedance measured shows also an excellent performance in view of the state of the art in regard to three dimensional electrodes, which characterizes the system as a very suitable tool for electroneuronal recordings.

As for the tear and wear test, it was a positive outcome to see that the fabricated structures were able to stand the penetration of a thick layer of PDMS without any damage. If they are able to stand the penetration of such material, it guarantees their integrity in the presence of brain tissue, as the nature of the tissue is much softer than the PDMS used for the experiment.

Nevertheless, a discussion about the durability of the electrodes needs to addressed here. The issue of breaking of the electrodes that was mentioned in chapter 2 doesn't seem to agree with the results shown, and in retrospective it seems that a reasonable cause of this problem is the attachment of the silicon electrodes to the layer of silicon oxide where they sit.

The penetration test showed without doubt that the structures themselves are solid and stable, and therefore they should not break. But since the test was done with silicon electrodes that are part of the silicon wafer where they lay, the stablility of the electrodes fabricated on top of a silicon oxide layer is unknown. The test should be repeated for the structures fabricated on SOI wafers, which couldn't be done at the time that this thesis was written, due to time constrictions.

Chapter 4

Brain slice culture

4.1 Brain slice culture *in vitro*

In vitro studies of brain slices offer several advantages over *in vivo* settings. As an artificial environment, the tissue is cultured with well controlled parameters. Key factors like pH, temperature and gas concentration are not left in the hands of nature but driven for the purpose of the experiment [64, 65]. This fact can also bring light to parameters that may affect the brain but that wouldn't be so easy to differentiate in a living surrounding [8]. Chemicals can be added to provoke different reactions in the tissue, and accesibility becomes easier than *in vivo*, for visualization purposes or to manipulate the slice for different kind of measurements.

The downside is that this type of culture is short-lived: brain slices die after 1 day in vitro (DIV) if not kept under special conditions [11, 66]. The electrophysiological survey of long term period culture has been elusive, limited in most cases to recording periods of 6 to 10 hours [18, 67]. Long term tissue properties (connectivity, apoptosis, development, response to injuries, etc) are yet not well known, and although many efforts have been targeted towards this problem, there is not yet a definite solution. Few methods, which will be discussed later, are used broadly in the labs, and are only able to produce thin organotypic slices that contain a maximum of 3 or 4 layers of cells, flattening out to about 150 μm after few weeks of culture [64]. It is important to consider carefully all the conditions necessary for a successful culture of brain slice. For a safe environment where the brain slice would survive, it is critical to ensure the following parameters:

- Sterility of the system

  The materials used in the integration of the culture environment need to be considered in regards of biocompatibility and easiness of sterilization. In culture labs, the common methods of sterilization are, in order of preference [68]: autoclaving (high pressure and saturated steam at 121°C

or more); UV exposure; soaking in chemical sterilants, such as ethanol or NaOH.

Autoclaving is the most efficient and easy method, but due to the high temperatures required, common polymers used in microfabrication of lab-on-a-chip systems, like polycarbonate (PC) or PolyMethyl Methacrylate (PMMA) cannot stand the process and therefore chemical detergents need to be used (details about the choice of materials will be commented later on).

UV exposure is a good method for sterilization, but it could leave some areas of inner channels or structures unexposed and thus not sterilized completely. Since polymers are the most common material in micro fabrication, the sterilization process most commonly found in this area is chemical soaking.

- Stable temperature above 30°C

  Brain tissue is extremely sensitive to temperature. Although a range of 32 to 37°C is considered adequate , the tissue is most sensitive to excitation at the body temperature, 37°C [65].

  Most experiments with brain tissue are carried at lower temperatures than the physiological one, with the purpose of slowing down its metabolic rate, and thus reducing the demands of nutrient and waste exchange [69]

- Tissue attached to a firm substrate

  Brain tissue needs a mechanical support to avoid deformations and develop a stationary placement during the culture time. This is even more critical in systems with perfusion flow, in which case the tissue could be damaged if not well attached to the substrate that holds it. The earliest reports on brain tissue cultures mention a nylon mesh as support of the slices [70]; curiously, it was made out of a simple cutting from a piece of a normal nylon stocking, and held with a ring shape (made of glass or plastic) [65]. Things have improved with time, and nowadays, although laboratories still use nylon nets to hold the slices, they are commercially available. Nevertheless, the most common substrate used currently is a teflon membrane [66]. Despite the good support offered by these materials, there is a serious shortcome: after few hours, the slices tend to conform and adhere to these supports, making it impossible to detach them once the experiment is finished [65], which is desirable for further analysis like histology or maybe different experiments like electrophysiology itself.

- Oxygenation

  The normally accepted levels of gases are 95 % O_2 and 5 % CO_2. Submerged slices may require about 10 ml/min of oxygen flow rate, whereas slices placed in contact with air may need as little as 1 ml/min or less

[65]. To avoid necrosis at the center of the brain slice (as observed by some colegues in our lab), the tissue needs to be well oxigenated [11].

- Bubble-free media

  In cell culture systems that are dynamically perfused, a common problem that needs to be avoided at all costs is the formation of bubbles. Air bubbles are a well known issue in microfluidic cell culture system. They are harmful in proximity to cells as they cause rupture of their membranes when they burst [71, 72, 73]. Moreover, their presence in microchannels is a hazard for the flow of liquid. If big enough, they are even able to dry out a section of the culture region by obstructing the reach of media to those areas. Getting rid of bubbles is not an easy task if one wants to obtain a closed culture system for brain slice culturing; such platform needs to be delivered as an open system to allow the placement of the tissue in the chamber, and be closed afterwards. Having the open system in contact with air and then closing it promotes the formation of bubbles, and although it seems like a simple problem, it is one that impedes the progress of good design ideas for brain culture.

Nevertheless, the most important problems to address when considering the design of a culture system for maintaining explants of nervous systems is the attachement of the tissue to the substrate and the proper exchange of media and gases. Different procedures have been tested, with higher or lesser degree of complexity and success, but to day there are mainly three that have become well established techniques. These will be described in section 4.1.

In regard to the development of this project, it is also essential to consider the integration of the culture system with the microlectrode array that has been extensively explained in this work. This integration is imperative since the goal of the system under development is the monitoring of long term cultured brain slices. Surely, this can be done by fluorescent methods that show the presence of live or dead cells within the tissue. Nevertheless, these methods miss essential information of what is happening in the culture during the transition time that leads to cell death. It is here where the microelectrode array plays an important role, since the recordings of the action potentials sent out by the cells would give valuable cues about the decay of the tissue, its survival, what kind of activity is typical at what state, etc.

The possibility of culturing explants of brain tissue on chip would also minimize the damage caused by the penetration of the array into the tissue at punctual experiments as it should be done every time that a measurement need be taken. Cultured on top of the electrode structures, the tissue could mold itself to the shapes of the electrodes and close the gap in between, improving the quality of the recorded signals.

First of all, let's have a brief overview of what are the standard culturing methods, what alternatives are given by the state of the art in microflu-

idics, and what is the progress in the integration of the microlectrode array with a culture system. This will give an idea of the possibilities available and a background to explain the driving force behind the system ultimately designed.

Standard culture methods

The first and most straight forward method is the culture in a simple petri dish. Slices are placed in a petri dish with a gas-permeable bottom, embedded in a collagen matrix and submerged in medium. This method of culture is not used very often, since the tissue only lasts for few days. The main cause of death of the tissue, in this case, is provoked by the fact that this technique doesn't take special care in providing oxygenation during the culture. It is, however, worth mentioning as it highlights the relevance of the oxygenation during the culture.

The other two main methods are the ones currently used at laboratories: the roller-tube (introduced first by Hogue [74] but currently used with the modifications introduced by [75] and the interface culture (Stopinni *et al.*[76]). These techniques are depicted in Figure 4.1.

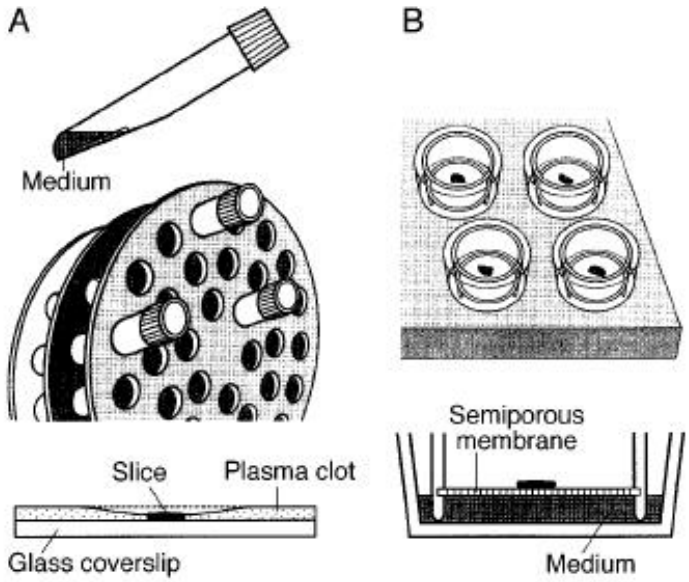

Figure 4.1: Techniques for preparation of brain slice cultures. (A) roller-tube method. (B) interface method (modified from [11])

The concept behind the roller-tube method is to alternate between a phase of liquid submertion (feeding) with another one in contact with air

(oxygenation). The tissue is fixed on a glass coverslip with a plasma clot or collagen matrix, and then introduced in a plastic culture tube with a small amount of culture medium. The tube is continuously rotated at a very slow speed (ten revolutions per hour), in which the tissue is covered by the medium half the time. This leads to an alternation of feeding and aeration of the tissue that ensures its proper oxygenation. With time, the layer in which the tissue was embedded is lysed and the culture is accesible for electrophysiology. The roller-tube method is suitable for applications where good visibility of individual neurons is necessary. After few weeks, the tissue goes from the original 400 μm to a mere 50 μm, flattening into a monolayer structure where individual neuronal cells can be easily identified with a phase contrast or fluorescent microscope.

The interface method is also referred to as a membrane culture, as the slice is placed onto a porous membrane that is slightly off the floor of a petri dish. The media reaches the tissue from underneath the mebrane by capillary forces, whereas the oxygen comes from the air above the interface. In contrast with the roller-tube technique, after a few weeks *in vitro* the slices cultured on a membrane keep a thickness around 150 μm ([11]).

Although these two techniques are commonly used for brain culture, they are both impaired by the limitation of transport of gas and nutrients by diffussion to the inner layers of the tissue. Whereas diffussion would suffice in monolayer structures, in thick brain slices the exchange of nutrients and gas doesn't reach all the areas of the tissue, often provoking central necrosis ([68]).

The roller-tube technique and the interface method constitute a great advance in the area of neurology, since now organotypic cultures are able to survive for culture periods of about 4 weeks [76]. Despite this fact, one cannot but wonder what information we might be losing, since it seems that it is only after the 4th week of culture that mature slice cultures show closest anatomy to those of the living model [67].

4.2 Microfluidics and brain slice culturing

The standard techniques (the interface method and the roller-tube ones) are fully accepted and yield good results. Nowadays, they are able to keep healthy brain slices for up to months. Nevertheless, the application of microfluidic techniques can improve the perfusion of medium and oxygen to the culture, which could bring the advantage of longer periods of culture time, and automatization of the process, which is lengthy and laborious.

Berdichevsky *et al.* [77] adapted the interface method into a platform where no porous substrate was needed. Instead, the medium was delivered by a main channel that connected a petri dish with the main chamber (see

figure 4.2).

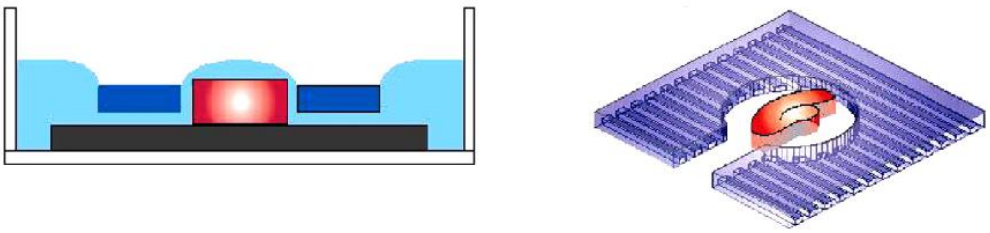

Figure 4.2: PDMS well for brain slices culture. Left: sketch of side view of PDMS culture system; right: top view showing the multiple microchannels pattering the surrounding surface of the culture site [77]

This chamber was also provided with multiple microchannels as cues of orientation paths for axonal sprouting. The material used to fabricate this system is a common one found in microfabrication: PolyDimethilSiloxane (PDMS). Its versatility has made it a very popular material for rapid prototyping of micro devices. Usually, and as it is the case of the work in focus, PDMS is molded by "soft lithography"; that is, a pattern is transferred to this material by using a hard mold with the desired features. PDMS is then cast by pouring it in liquid state and allowing to cure. Microchannels of 5 μm height, 50-100 μm in width and a distace of 100-200 μm between channels were fabricated in this fashion. They were embedded in a PDMS layer of 150 μm that was later cut with holes of 2 mm in diameter to give shape to the main body of the chamber. The PDMS membrane thus fabricated needs to lie on a rigid support, mainly a glass slide, and by simple contact the surfaces seal against each other.

Interestingly, the hydrophobicity of PDMS, combined with the surface tension of the liquid held inside the chamber, was a control to limit the culture to be just barely covered by medium, comparable to the interface technique. These settings were sufficient to keep hippocampal slices 350 μm thick alive for up to 4 weeks. But maybe the most curious detail of this design is that the anchoring of the slice was done by its own axon spreading through the microchannels surrounding the chamber (figure 4.3). Without applying any coating, the brain slice survived comparably to those where coating was used, but with the advantage of a weaker attachement to the surface of the chamber, which makes easier to remove the tissue once the culture time is up for further analysis.

An interesting feature introduced by Blake *et al.* [78] is the use of microposts as support for the brain preparation. The dimensions and distance in the network of microposts is designed with the purpose of allowing to hold the brain slice in place without causing damage, and at the same time ensure an optimal perfusion throughout the tissue. The design included six

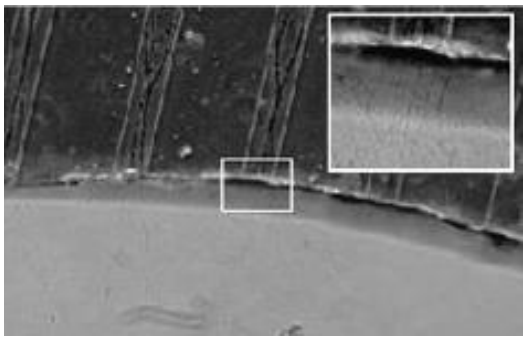

Figure 4.3: The spread of axons through microchannels of the chamber promoted the anchoring of the brain slice. Insert: detail with axons spreading towards the input of a microchannel (modified from [77])

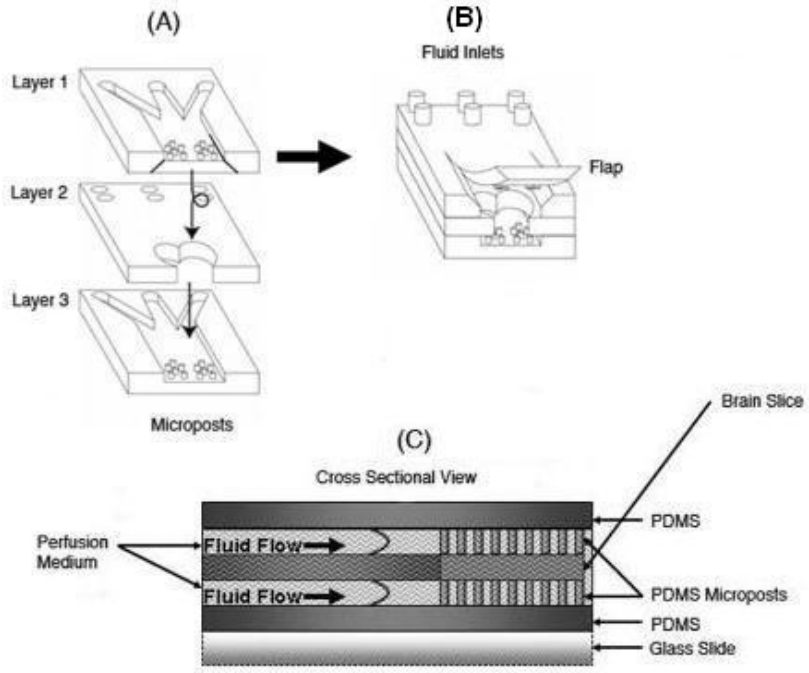

Figure 4.4: PDMS multilayer chamber for brain slices. (A) shows the three different layers that form the chamber, with three concurrent inlets at the top and bottom layers. (B) final integration of the chamber, with flap open for insertion of brain slice. (C) Transversal view of the system, showing the flow from the inlets and reaching the microposts area, where the brain slice is sandwiched in between [78]

inlets, three for the top part and the other three for the bottom, to allow the introduction of different chemical compounds in the culture. By having this distribution, it is possible to perfuse independently top and bottom of the chamber, and even expose locally particular areas of the slice to an input chemical. This is done by taking advantage of the laminar flow regime in which the chamber works: the flows from the three inlets on each level of the chamber don't mix up and address a particular area of the culture. It also allows to focus the main inlet flow by adjusting the flow rates at the inlets (the flow width coming from the central inlet will be fixed according to these values). Simulations were run in order to avoid dead volume areas in the flow and keep it stable in the micropost area. Measuring experiments were run for a maximum time of 60 minutes. But the main purpose of the design was to show that it is possible to introduce different chemicals in selected parts of the brain slice in a controlled manner. This could be useful for studing the effect of drugs on the tissue. The brain slice is placed inside the chamber through an open flap at the top, which according to the report seals itself again afterwards. There is no comment in regard to possible bubble formation, which is very prone to happen if an opening like this is used for the placement of the slice and closed afterwards. This should be avoided at all cost, since it would damage the tissue.

Forced convection provides food for thought

Despite the blooming progress in brain slice culture, there seems to be an empty space with regard to culturing thick brain slices. And it is surely not due to lack of relevance. Large preparations of brain present better preserved network connectivity than thin samples, which may be related to the fact that it is only in slices thicker than 500 μm that spontaneous neuronal rythmic activity can be seen consistently [79].

It is most likely that the main cause for the short life of brain slice cultures is due to a deficiency in the supply of oxygen and nutrients [76]. The fact that the brain doesn't possess any circulatory system makes mass transport inside the tissue completely dependent on the external flow. This factor is exacerbated in the presence of thick cultures, where diffusion-limited mass transport is not able to reach deeper layers of the tissue.

This fact is clearly relflected in figure 4.5, where Wu *et al.* measured the oxygen percentage inside brain slices of different thicknesses, a 1 mm thick one and a second sample of 500 μm. The U profile of the plots follows the intuitive notion that surface levels of the slice are closer to the superfusion flow, thus receiving higher content of oxygen, whereas the middle part shows the lowest percentage of oxygenation. It is also worth noticing how the progression of oxygen within the tissue decreases much more abruptly in the thicker slice than in the 500 μm one.

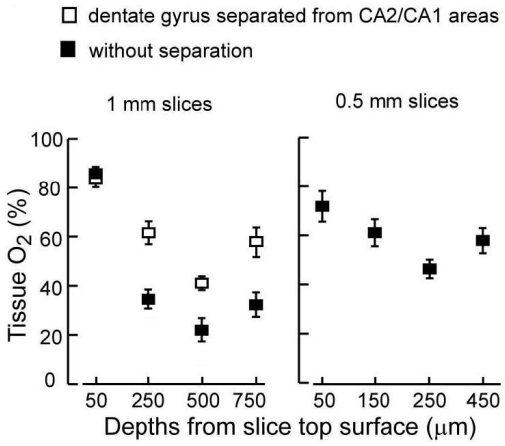

Figure 4.5: oxygenation levels within the brain slice. The graphs show a comparison between a standard brain slice of 500 μm and a thick one of 1 mm. The oxygen levels have an U profile that reflets the fact that the most inner layers of the tissue are deprived of oxygen, due to lack of mass transport in the tissue. It also reveals how thick cultures of brain are more affected by this phenomenon (extracted from [79]).

Forced convection can provide a more efficient delivery of oxygen and nutrients to those unaccessible tissue layers in large explants by pushing mass transport through all the thickness of the culture.

Choi and McClain were the first to apply a similar concept to brain slice culture. They devised an array of hollow microneedles that could penetrate the tissue, and while the tissue kept growing around the needles, these hollow structures would deliver the nutrients to all layers. Figure 4.6 shows a schematic of the concept and an image of the fabricated needles.

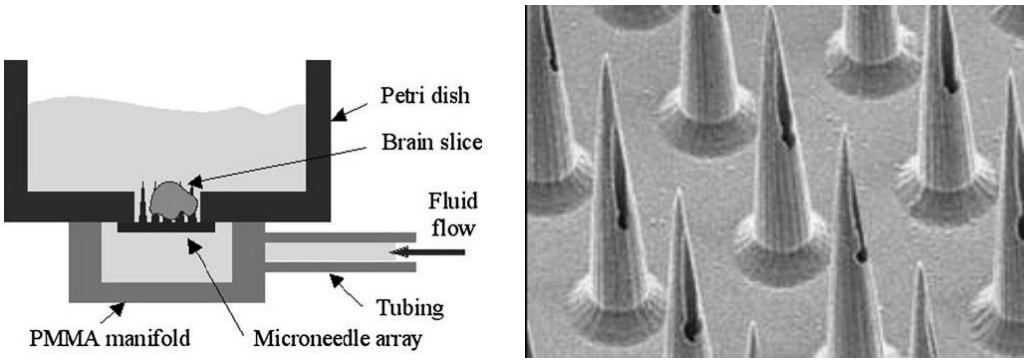

Figure 4.6: Culture chamber with SU8 perfusion microneedles (from [69]). Left: concept of the design. The perfusion comes from the tubing at the bottom of the chamber and accessess the tissue through the hollow needles that are piercing the brain slice. Right: SEM image of the SU8 needles

Microneedles of about 500 μm were fabricated in SU8 (see figure 4.6, left image), an epoxy-based photoresist that can be patterned to obtain high aspect ratio structures. The microneedles were perforated on the side to create a channel that connected to a recipient attached on the back side of the chip. As shown on the left of figure 4.6, the liquid is delivered through a channel that is connected to a main pool. The medium passes through the needle ports and is delivered inside the brain slice, which at the same time is submerged in medium itself.

Although the idea of this design is innovative and interesting, the experiments lasted just four hours, which cannot prove the concept of long term culture of thick slices. Moreover, it is reported that original brain slices of 400 μm in thickness clumped into a mere 150 μm at the end of the experiment.

Rambani *et al.* [64] implemented a forced convection system for brain slice culture *in vitro* with great success, by designing a chamber that perfused media through a golden grid in which the brain slice lied. The outlet was divided into a ring of small interstitial channels that disposed of the liquid by channeling it into a withdrawal chamber surrounding the main chamber (see figure 4.7.

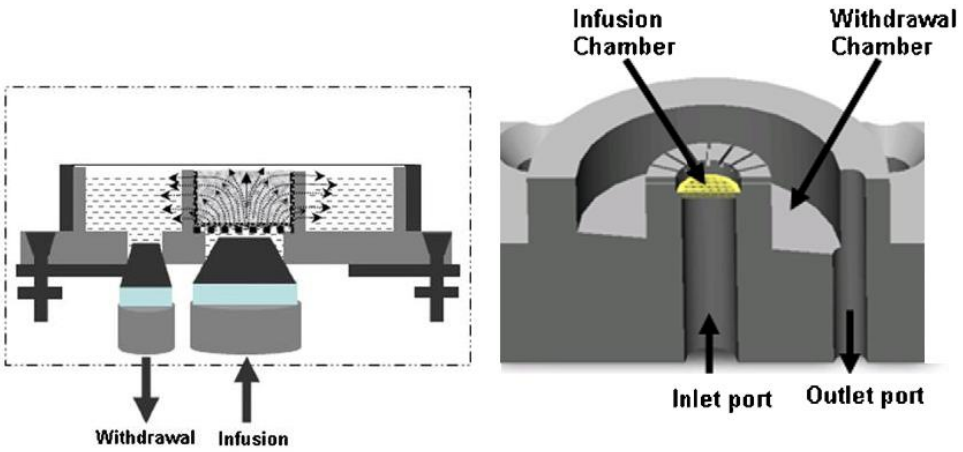

Figure 4.7: Interstitial chamber for brain slice culture [64]

The dimensions of the chamber were coupled to the size of the cut of tissue in order to make it fit snuggly. The main purpose of this is not to leave any gap in between the slice and the grid that forms the base of the chamber. It is essential to obtain a good adhesion of the brain sample with the walls of the chamber; the creation of gaps would cause a non uniform availability of nutrients to all the areas on the tissue.

The results of this work showed a significant improvement in the viability of the cells in the tissue when compared with the interface method, achieving

culture of brain slice with an impressive thickness 700 μm, and maintained. Nevertheless, this work failed also (as the previouly commented work by Choi and McClain) in to running experiments for a satisfactory lenght of time to extract rigurous conclusions about long term culture. The main point of the report was to prove that forced convection feeding makes an improvement in the viability of the tissue if compared with standard methods. Therefore, the experiments weren't continued after 5 DIV.

Despite this, the thickness of the brain slices increased from a 450 μm for a standard interface culture to a 600 μm for the interstitial chamber, which shows already the potential benefits of using this technique. Their study of different flow rates gives also a helpful hint into how important it is to find the right balance between a forced flow through the tissue without damage caused by excessive pressure. Rambani *et al.* showed this by finding the optimal flow rate to be 20 μlh. For higher values, the tissue started presenting significant damage in its structure, and for lower values the viability of the culture wasn't as good.

In conclusion, microfluidics solutions seem a good alternative to standard culture methods, where the change of media is done by a technician and needs unnecessary transport of the culture from the incubator to the laminar flow bench (for the change of media). On top of that, the use of forced convection feeding in the design seems to open possiblitites for the optimization of thick brain slice cultures that is otherwise impossible to keep in healthy conditions for long term periods, due to insufficient oxygenation.

Therefore, it seemed a good approach to try to apply force convection-based perfusion in a system that aims for a long term culture of brain slices. The way that it was done will be described in the following section.

4.3 Integration of a microelectrode array with a culture system

The possibility of monitoring the electrical activity of neuronal tissue in long term experiments could provide with new information in the dynamics of neuronal damage [10], information processing and storage [67], neuronal plasticity [19], development and degenaration of the central nervous system, etc. Ideally, brain slices should be grown on the MEAs, as this would promote a good seal between the electrodes and the tissue. This is so because the brain slice would attach more firmly to the profile of the surface where it is cultured. Moreover, the possibility of culturing explants of brain tissue on chip would also minimize the damage caused by the penetration of three dimensional electrodes into the tissue at repeated short experiments.

Nevertheless, since brain slices have a very short life-span if not cultured

under special conditions (as explained in the previous sections), electrophysiology has been hampered in the past to recording periods of few hours at maximum [19]. Thanks to the development of the roller-tube and interface techniques, now slice preparations are available for long term experiments, ranging from days to up to four weeks [11, 76], and the field is evolving in the direction of integrating these techniques with microelectrode arrays. It definitely shows a huge improvement in the results of the length in the recordings, proven with works by [67, 80, 10, 81, 82], to give some examples. The approaches taken in this area have been quite simple, in comparison with the developments carried in the microfluidic community. Nevertheless, in all the cited works, organotypic brain slices were cultured on chip for lengths of about 4 weeks. This in itself is a most desired achievement as a starting situation to obtain optimal recordings, since it has been shown that mature slice cultures grown for that amount of time have very similar anatomical features to those found *in vivo* [67] .

Figure 4.8: Tliting table for the integration of the roller-tube tecnhinque with a MEA. A drummer inside the incubator space keeps rolling to switch the culture in a submerged state in medium and breathing in contact with air [82]

Integration of roller-tube technique with MEAs

Some of the aforementioned reports [67, 80, 82, 81] opted for the integration of the roller-tube technique in a MEA system, and despite showing encouraging results (Beggs and Plentz managed to make LFPs (local field potentials) meaninful recordings for up to 10 hours), it is obvioulsy not a realistic solution as a final integration that could be used in a lab. The main cause of the impracticality of this set up is the requirement of a tilting table, shown in Figure 4.8, that has the function of keeping the rotation that is

necessary for having the culture submerged in medium and in contact with air at equal times. The equipment is bulky, expensive, and worst of all, doesn't allow to perform the electrical measurements, which implies that the user needs to remove the MEA with the brain slice from the tilting table and place it in a suitable platform to make the electrical recordings. This means that: a) the experiment will be finished after a single measurement, or b) the measurements will need to be done in sterile conditions, e.g. under a laminar flow bench, which lends the process awkward and introducing risk of contammination during the change of settings.

It is also worth noting that the amplitude of the recorded signals wasn't particularly good: with a spontaneous spike of a maximum of 400 μV, it could be that the seal between the electrodes and the tissue leaks a good part of the signal. This may be because, due to the use of a motion-set up, the tissue needs to be ensured and firmly attached to the surface of the chips; this was done by applying a thick layer of chicken plasma. It is also noted by Egert that during the first days of culture a considerable percentage of cells die, and although this condition stabilizes afterwards, it may affect the quality of the final recordings. The measured LFP waveformes were more variable and smaller in amplitude than those obtained from acute brain slices.

Integration of interface technique with MEAs

The incorporation of the interface culture technique to MEAs seems an easier approach than the roller-tube set up, and also yields better results as for the thickness of the culture. For a start, the application of the method is very straight forward and doesn't require any extra equipment. All that is needed is the confinement of the electrode area with a ring shape. An example of this is given in Figure 4.9. The area inside the ring will be the culturing site, and as such, care has to be taken when deciding what kind of material is used for the ring and the method used to adhere this ring to the surface of the chip. Only materials that are biocompatible should be used; rings are usually made of glass or plastic, and attached to the chip by gluing them. For the culturing itself, a very small amount of medium needs to be applied, enough to keep the brain slice half way submerged and at the same time in contact with the upper air. This is done by hand, which means that the MEA needs to be removed from the incubator, where it lays during the culturing time, to a laminar flow bench, in order to preserve the sterility and avoid contamination.

Thiébaud *et al.* [23, 84] showed how the integration of the interface method with MEAs technology is possible. They added to their design a pattern of holes (vias) to go through the full thickness of the silicon where they had previously fabricated micro electrode needles. The purpose of these holes is to mimic the set up of the interface culture method, where the slice

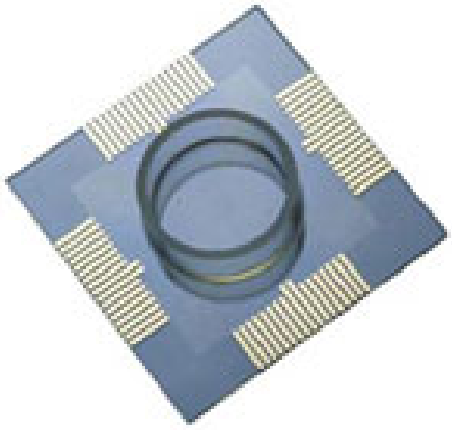

Figure 4.9: A commercial MEA chip with attached ring for interface culture. The area inside the ring will be the site for the culture of the brain slice by the interface method (image taken from [83])

is perfused from underneath through a porous membrane. In the case of the reported work, the membrane is substituted by the MEA chip itself, and the perfusion is done through the holes perforated in the silicon. Jahnsen and coworkers[85] studied the effect of culturing brain slices on this chip by standard methods (microscope pictures, histology analysis and electrophysiological recordings with a glass microelectrode), concluding that the use of the MEA chip as the substrate for the culture didn't interfere with the viability of the tissue.

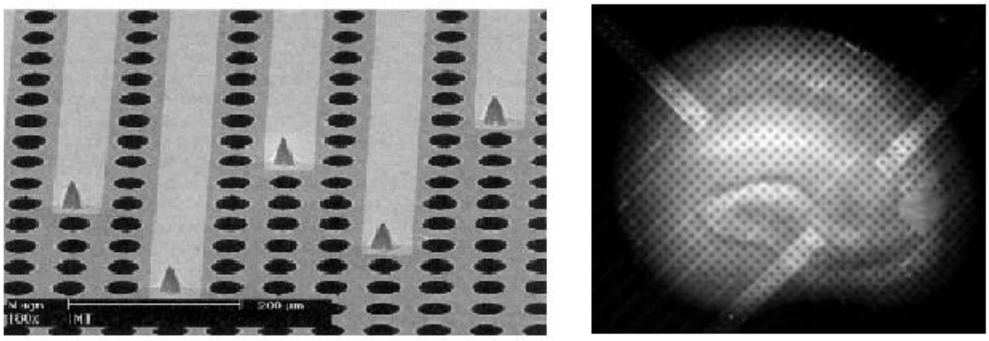

Figure 4.10: Integration of MEA with porous substrate for interface method. Left image shows the MEA chip with neddle electrodes and holes in the substrate. Right image: culture of hippocampus on top [85]

Despite the first encouraging results, the investigations didn't address the

integration of a more developed idea for the culture side of the project, and the longest set of electrical measurements done outside the incubator lasted for three days, after which the brain slice started drying out.

Shimono *et al.* applied the interface method to culture hippocampus slices on a commercially available MEA system [83]. The results shown were related to 20 DIV cultures. The downside of this method, as with all the previous ones, is that the system needs to be removed from the incubator chamber for the measurements, and there onwards either preserve the necessary conditions to keep sterility, temperature and gas at the optimal level, or discard the culture afterwards. In the case of Shimono *et al.*, the measurements were performed in a special incubator that was connected to the stimulation/recording component of the MEA system, for the special purpose of doing the measurements. The amplitudes recorded were stable during the whole period of measurement, in the range of 600 μV. In stark contrast with the results offered by the roller-tube method, this amplitudes seem an improvement towards the obtaintment of clear signals from the tissue. This could be due to the use of different coatings depending on the culturing method, the electrodes used, or maybe the thickness of the tissue (which is always 3-4 layers thick with the interface method, in comparison with a meagre monolayer from the roller-tube technique)

4.4 Culture chamber system 1: lemon shape chamber

The prototype presented here has the aim at minimizing the dead volumes inside the culture chamber, in order to provide a homogeneous distribution of the nutrients to the brain slice.

The basic idea behind the design proposed is to place in opposite corners both inlet and outlet, so that the path for the fluid, marked by the drop of pressure would be evened out in the whole chamber. Also, the shape of the body, like that of a lemon, follows the intuitive idea of designing round borders in order to minimize the dead volume inside the chamber. This idea can be justified by the fact that the velocity of the fluid is driven by the derivative of the pressure. At sharp cornes, the derivative vector of the pressure cancels out, which doesn't happen in round corners. As a final addition to the structure of the design, a porous membrane is incorporated to separate an upper part for a lower part of the chamber. This idea applies the concept of the interface culture method, in which the brain slice lies on a membrane support and is fed from underneath. Nevertheless, as it was proved by [64], the use of forced perfusion through the membrane should improve the yield of the culture, as it increases the reach of nutrients inside

the tissue of the brain slice.

With these concepts in mind, a chamber made of two parts was designed. These two parts are symmetric, and separated by a teflon membrane with pores of 0.4 μm in diameter. Such membrane is a standard support used for brain tissue culture, and this is the main reason for integrating it in the design. The chamber has a total volume of 32 μm^3, which is equally divided in between the upper and lower part. The inlet is situated at the bottom of the chamber, connected from the side, while the outlet is placed at the top, leaving the chamber from the opposite corner as where the inlet is. For a clearer perspective of the system, an image of a first version is shown in figure 4.11.

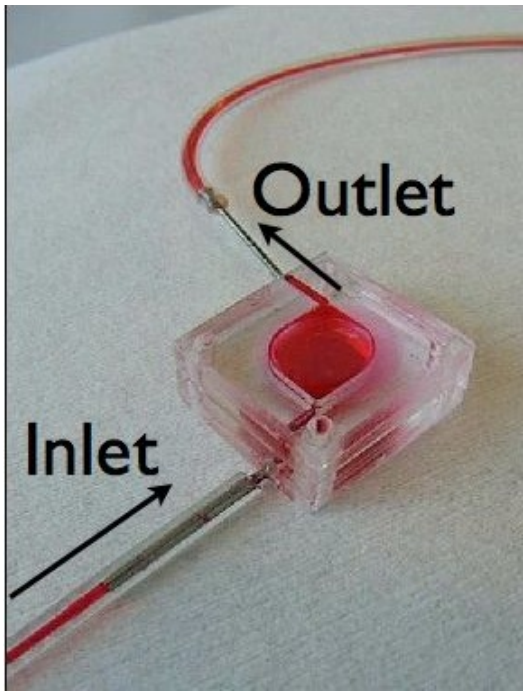

Figure 4.11: Lemon-shape culture chamber. The inlet and outlet stay at opposite corners in order to optimize the flow of liquid. The round corners help also to obtain a homogeneous distribution of the liquid inside the body of the system.

In order to ensure the coherence of the design, simulations were run for analysis of the flow of a liquid within the chamber. For the simulations, the Navier-Stokes equation for incompressible liquids was applied in a three dimensional model of the chamber. The Navier-Stokes equation describes laminar flow in viscous fluids, and it is applied for solving transient and steady-state models of incompressible fluid dynamics. Its expression is as follows:

$$\rho\left(\frac{\partial V}{\partial t} + V\nabla(V)\right) = -\nabla(P) + \mu\nabla^2(v) + F$$
$$\nabla(v) = 0 \tag{4.4.1}$$

where ρ is the density of the liquid and v its flow velocity. P stands for pressure and F for force (all parameters in international system units). The first equation is derived from Newton's second law, or conservation of momentum. Equation 4.4.1 reflets that by showing on the left hand side a term related to the inertia of the flow movement. At the other side of the equality, momenta due to external factors such as pressure, shear stress and other forces are included. The second equation is the application of mass continuity to an incompressible liquid (which means, with ρ constant).

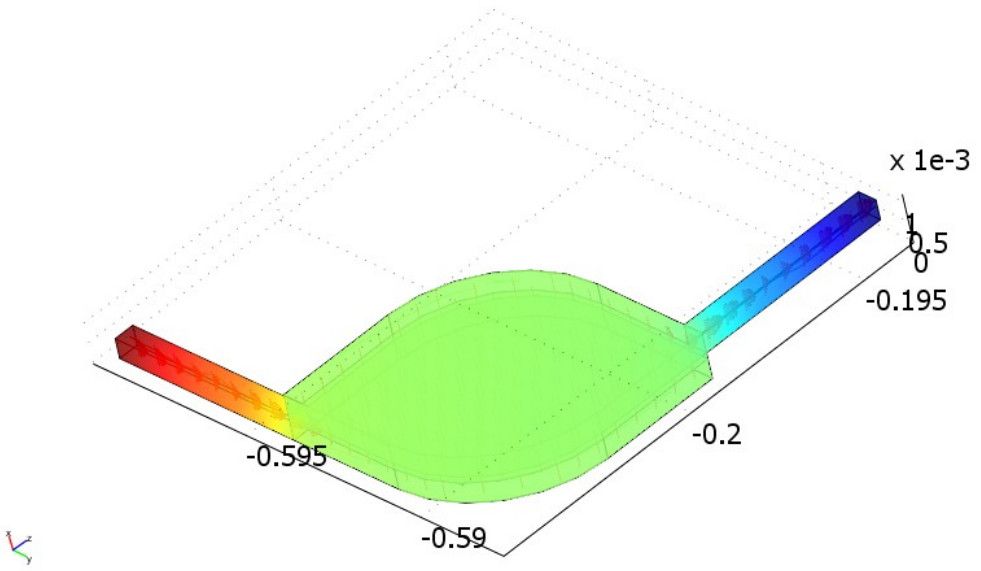

Figure 4.12: Flow simulation of lemon-shape chamber. The design avoids dead volumes inside, optimizing the distribution of media in the chamber. On top of that, the perfusion through the membrane pushes the nutrients within the tissue. The red color shows the maximum flow rate, green medium values and blue the lowest ones. The flow shows being uniform inside the body of the chamber

Figure 4.12 shows that the chamber is completely filled and the flow uniformly distributed within the volume. The fabrication was done with a

design in CAD of the different parts of the chamber. The drawings obtained were milled in pieces of PMMA at a micromilling machine, and bonded in a bonding press (with the surfaces previously activated with a 2 min exposure to UV light), at a temperature of 90 °C and a pressure of 15 KN for 30 minutes.

Figure 4.13 shows an image of the final device. Inlet and outlet were connected through nanoports that fit fused silica tubing.

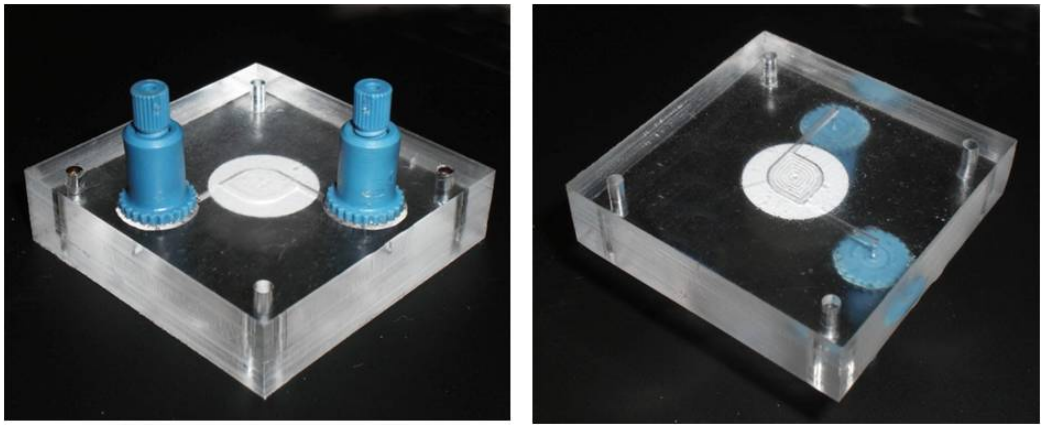

Figure 4.13: Prototype of lemon-shape chamber, showing the inlet and outlet ports, which are placed at the bottom of the device in order to clear out the top surface for easy handling and visualization. The outlet is connected to the top part of the chamber, whereas the inlet goes to the lower part. The perfusion goes bottom up, through a teflon membrane with pores of 0.4 μm diameter

4.4.1 Test of lemon-shape chamber

As a first test, a leakage test was performed. A pump was connected to the inlet of the system. Leakage and the system functionality was tested by perfusing liquid at different flow rates (from 0.5 $\mu m/min$ to 50 $\mu m/min$), without presenting any problems.

After this first trial, two different tests were done that showed the performance of the device for different purposes.

Bain slice culture

For a first application, the lemon-shape chamber was used as a closed system (sealed) by Emanuel Weber, at the Analytical Biotechnology Group from Delft University of Technology. The aim of this project was to use a cell trapping mechanism that would immobilize cells, and once trapped, they should be kept alive and stimulated to secrete peptides. The final goal is to

measure the concentration of the secreted peptides in a Matrix-assisted laser desorption/ionization (MALDI). Figure 4.14 illustrates the sequence of steps required for the experiment.

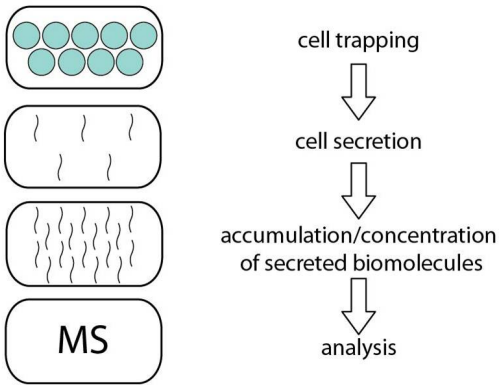

Figure 4.14: Sequence of experiment for MALDI [86]

Without entering into details that are out of the scope of this work, it suffices to mention that this equipment uses mass spectrometry as a technique to analyze the composition of a sample. The experimental set up is mounted as in figure 4.15, but it is only shown here for the clarity of the use given to the chamber.

The chamber is connected at the inlet with a syringe that introduces the cells first (haploid yeast cells). Once they are sedimented, media is continuously flown in order to keep the culture alive. The idea of using the chamber for this project is to trap the cells in the lower chamber, while allowing the flow of the secreted peptides through the teflon membrane.

The results of the test in this set up proved the functionality of the prototype. A continuous flow was run for 16 hours without disruption, and mass spectrometry analysis showed that no absorbance of peptides had happened in the chamber, which is desirable for the application in mind. The chamber was also tested under high presssure conditions (at least a pressure of 7 bar is necessary for the experiments with MALDI), and this caused the appearance of leakage.

These experiments showed the potential of this model to behave as a cell trap for measurement of chemical released by the culture. The system was reliable as a perfusion flow system.

Despite tha the report on this project decided eventually to drop this model for its purpose (the MALDI experiment), it was due to the need of using high pressures in the aforementioned set up. This pressures caused, eventually, a leakage in the system. Nevertheless, for more standard conditions of pressure, the lemon-shape prototype is functional.

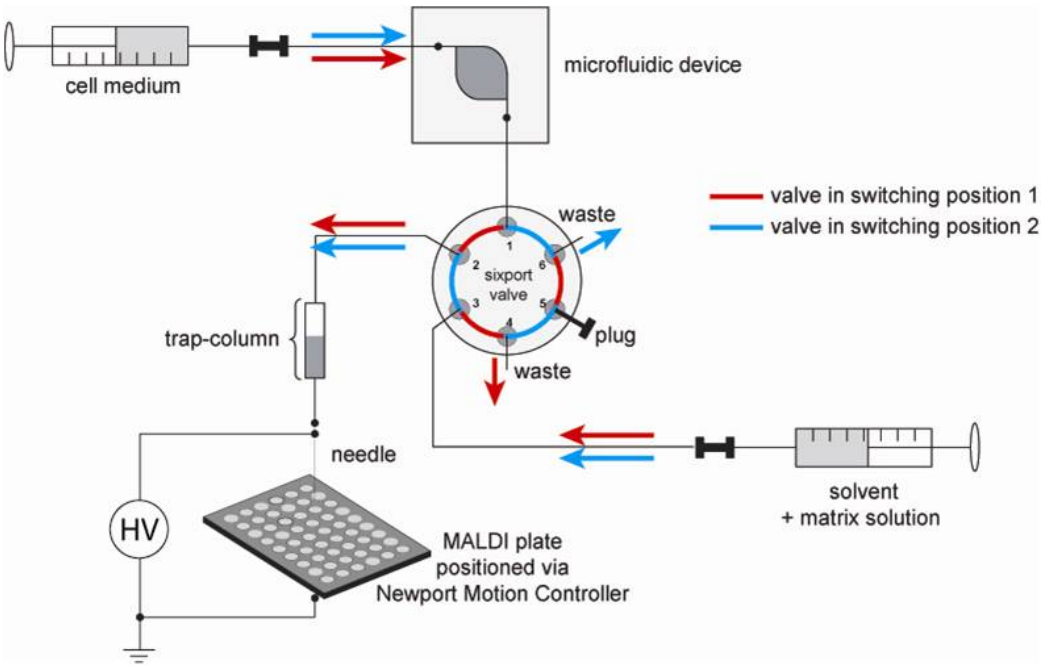

Figure 4.15: Setup for MALDI [86]. The lemon-shape chamber is connected at at the inlet with a syringe with cell media, and the outlet to a valve that leads to the MALDI system.

Bain slice culture

The same design of the chamber was used to culture brain slices, as it was its original purpose. Nevertheless, the system needed to be able to open in order to place the brain slice inside, and then close tightly, whithout allowing any leakage. This details is important for this design, since the upper body of the chamber is filled with liquid, and if the device is not well sealed, leakage will occur.

In order to tackle this problem, the prototype was modified slightly with the final top chamber being covered by a lid. This lid was made of a plane piece of PMMA and a silicon tape as means of sealing mechanism. The silicon tape was given a cut with the same shape as the body of the upper chamber. The purpose of this was to close the system when required. This was done by aligning the silicon tape with the chamber, and then placing on top the flat PMMA lid to close the whole device.

Unfortunately, this model proved not practical for a realistic manipulation of the brain slices. The alignment of the silicon tape with the chamber was far too tedious and awkward to operate, with very poor results. As result of this, the brain slices were left outside for too long, and worse than that, the full experiment couldn't be run any further due to leakage in the system.

4.4.2 Results and conclusions

The design of a lemon-shape culture chamber is not well suited for a realistic set up for brain slice cultures. Although the system provides a very uniform flow distribution inside its body, there are major issues in relation to the mechanism to seal the device. This is due to the fact that it needs to be open for the placement of the brain slice, and then close perfectly in order to avoid any leakage.

But these are not the only problems: the fact of having an open system and closing it after the insertion of the brain slice creates a bubble of considerable size in the top part. This should be avoided at all costs, since the presence of the bubble damages the tissue (due to irregularities in the nutrients delivery).

Last, but not least, the integration with an MEA chip is not trivial, and therefore it defeats the purpose of this project. One of the main goals is to obtain a full MEA system with an integrated culture platform.

Nevertheless, this device has proven very useful in cell trapping and culturing, and in the future the benefits of this design could be exploited in this direction.

4.5 Culture chamber system 2: suction chamber

So far, the most prominent effors for obtaining a reliable platform for electrophysiological recordings while culturing on site have been described. There is a clear tendency towards the adaptation of the interface method for this task. This seems an appropriate approach, since it results in the thickest tissue for long periods of time, and appears to ease the process of culturing.

Nevertheless, all previous works found in literature provide a perfusion bottom-up; that is, the media flows from underneath the brain slice and goes up with the idea of forcing the liquid through the tissue. As mentioned earlier, perfusion through the tissue is critical for delivering oxygen and nutrients to all the cell layers inside as even as possible.

But what would happen if the perfusion were done top-down? The media would enter an upper part of the chamber, where the brain slice lay, and would leave through the substrate membrane to be collected in a lower chamber that would provide an exit to the discarded media. This concept seems appealing if the typical perfusion were replaced by suction as the mechanism to drive the flow. In that case, on top of obtaining a force-convection feeding of the tissue, the anchoring of the slice would be done automatically by the pressure exerted from the suction outlet. This would be quite desirable, since it would avoid the inclusion of extra parts like nets to fix the tissue to the

substrate. Anything that gets in contact with the brain slice in culture is a potential risk to the viability of the tissue, or in the best of cases deforms it.

This is exactly what the model presented here tries to achieve. The media fills the upper chamber where the brain slice lies, on top of the multielectrode array chip already developed, and it is forced through the tissue and down to a lower chamber by suction through the holes present in the chip. An overview of the system is shown in Figure 4.16

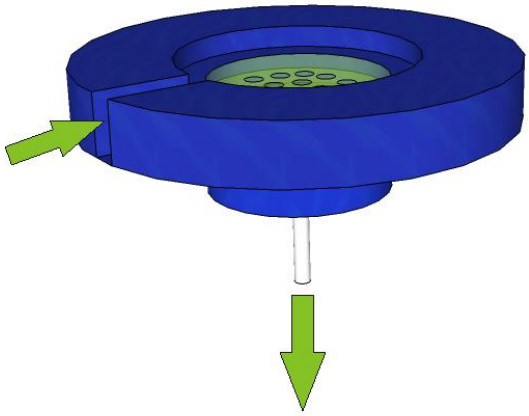

Figure 4.16: Culture chamber with forced-convection system. The arrows show the direction of the flow. It enters from a side channel (left side of image) and leaves by the outlet, placed at the bottom of the chamber. The flow is done by suction from the bottom, forcing in this way the attachement of the brain slice to the membrane substrate and feeding the media trhougout the tissue as it goes to the lower part of the chamber.

Special care needs to be taken in filling the body of the chamber only enough to provide media to the tissue, but not overwhelmingly so. If the brain slice were completely submerged in the media, the exchange of gases in the culture would be hindered (as in the culturing method of the petri-dish explained earlier). Therefore, it is necessary to design a mechanism that ensures a minimum level of liquid in the main body of the chamber. This is done by including in the design of the upper chamber a hollow ring surrounding the main body (see detail in Figure 4.17).

The ring behaves like a dam restraining the waters of a river, only allowing the flow to enter the chamber after filling the entire body of the ring. This ring has a also an extra function: it ensures an even input of the liquid in the chamber, without any privileged direction. If this occurred, the brain slice would be fed in isolated areas, which needs to be avoided at all cost. The volume of the ring is carefully calculated in order to allocate the desired amount of liquid to enter the main chamber.

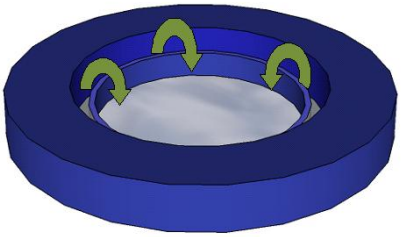

Figure 4.17: Detail of ring in the upper chamber controlling the flow. It has a twofold function: it allows the flow in the main body of the chamber evenly and controls the volume that floods into the chamber

The volume of the body of the upper chamber is given by

$$V_{ch} = \pi r^2 h \tag{4.5.1}$$

where r is the radius of the chamber and h the height.

A side view of the design of the chamber is shown in figure 4.18.

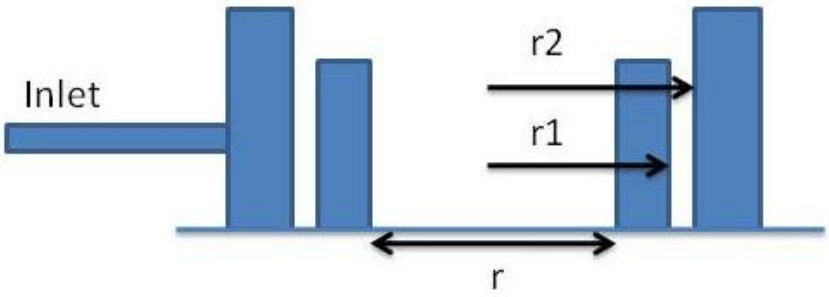

Figure 4.18: Side view of the chamber design. The inner body of the chamber is defined by the wall of the outer ring. The ring is confined between radii r_1 and r_2 , and its main function is to restrict the volume ofliquid that enters the inner body of the chamber.

Ideally, the chamber should be filled just enough to cover the brain slice (as discussed previously). Typically, brain slices are about 500 μm, and this should be the height reference to reach with liquid. As for the dimensions of the chamber, it would be convenient to make it of the same dimensions of the brain slice to make this one sit tightly inside, since that may preserve the compactness of the tissue, forbiding it to spread out. The close contact with

the walls of the chamber would also promote the adhesion of the tissue to them. It would also force the tissue to be present all over the substrate area, thus making the forced convection more efficient than if there were empty areas where the flow could go through easier.

Having these considerations in mind, it was decided to take a radius of 2.5 mm, since the length of the cut slices is about 5 mm. The ring space surrounding the main body of the chamber is designed to contain just the amount of liquid necessary to cover the main body of the chamber up to 0.5 mm of height. This should ensure that the brain tissue is not completely submerged in media. The calculations to fit the ring for this purpose are done by equalling the volume of the inner chamber (equation 4.5.1) to the volume of this ring (equation4.5.2),

$$V_{ring} = \pi(r_2^2 - r_1^2)h \tag{4.5.2}$$

Therefore,

$$r^2 = r_2^2 - r_1^2 \tag{4.5.3}$$

By choosing $r_1 = 3mm$, equation 4.5.3 determines the value $r_2 = 3.5mm$

In conclusion, it was calculated that the dimensions of the system should be:

- Main body of 5 mm in diameter and 0.5 mm in height
- Ring with diameters of 7 and 6 mm. A height of 1 mm was chosen; The higher external wall ensures the avoidance of spillage towards the outside of the chamber, since the inner walls of the chamber are shorter (0.5 mm)

Another consideration to take into account when designing the system is that inspection of the culture should be done from the top. This is due to the fact that the membrane-substrate that holds the tissue is the microelectrode array, impeding the observation of the tissue with an inverted microscope. Therefore, tubing, ports and any other element stay clear from the top side of the chamber, to allow the use of an upright microscope.

4.5.1 Fabrication of chamber prototype

The chamber was fabricated in PMMA by designing the parts in a CAD software and milling them in a micromilling machine. After this, the parts obtained were thoroughly wiped with a tissue that had barely some ethanol (this step needs to be done carefully in order not to damage the material) and rinsed in distilled water. Then, they were bonded in a bonding press (with the surfaces previously activated with a 2 min exposure to UV light), at a temperature of 90 °C and a pressure of 15 KN for 30 minutes. In between the layers laid the microarray chip with holes of 20 μm of diameter (for fabrication details, see chapter 2). It must be noted that, for the first

test of this system, a bare chip with only holes was used. There were several problems arising during bonding, but the most severe one was caused by the cracking of the vias chip under the pressure set at the bonding machine. There is a very fine balance between obtaining a good bonding of the device and avoiding the breaking of the chip. Despite optimizing the pressure value to 15 KN, the yield of chambers fabricated wasn't high.

As for the connections, the tubing was fully biocompatible, as its main application is for infusion catheters (provided by BD Connecta). The outside diameter of the tubing is 2 mm, with an inner diameter of 1 mm. They are provided with luer lock connectors, which fit easily into a standard syringe. Nevertheless, in order to avoid unnecessary dead volumes, these connectors were fit directly onto the inlet/outlet of the system, as shown in figure 4.19. First, they were attached to the main device by using a PDMS layer as means of glue. It was soon realized that this mechanism wasn't reliable, since the PDMS ended deattaching from the surface of the chamber after a while. As a final solution, the outlet was modified to fit perfectly with the dimensions of the nozzle of the connector, and just by simply fitting it into the hole made for the outlet, the connection proved to be reliably firm and stable throughout all the experiments done. In the same image the positioning of the chips with the holes can also be appreciated. The chip needs to be aligned with the hole that goes to the outlet. This hole is of the same dimensions as the connector, and it should be placed directly underneath the area of the holes in the chip. this is achieved by defining a square shape on the chamber system, which has the same dimensions as the chip.

4.5.2 Flow rate test

In order to test the design, the inlet and outlet of the chamber were connected to two different pumps. This is done in order to ensure the pumping in of liquid at the same time as the suction happens. An image of the set up is shown in figure 4.20. The chamber needs to be held at a heigth, since the outlet is positioned at the bottom of the chamber.

In theory, it should be possible to run the experiment by using just one single pump. This pump is necessary for the suction of the media from the outlet. At the inlet, the chamber could be provided with incoming media by using the effect of gravity to fill the main body of the chamber. Nevertheless, during the first experiments it was not possible to proceed in this way. This was so because the use of the gravity pump, as it will be called, needs to be calibrated in regard to the height at which to place the container with media. The height dictates the difference in pressure between the container and the chamber, thus filling the chamber when that pressure decreases (as a consequence of evacuation of liquid in the chamber). Due to the time constrictions for testing the device, this feature was not incorporated to the

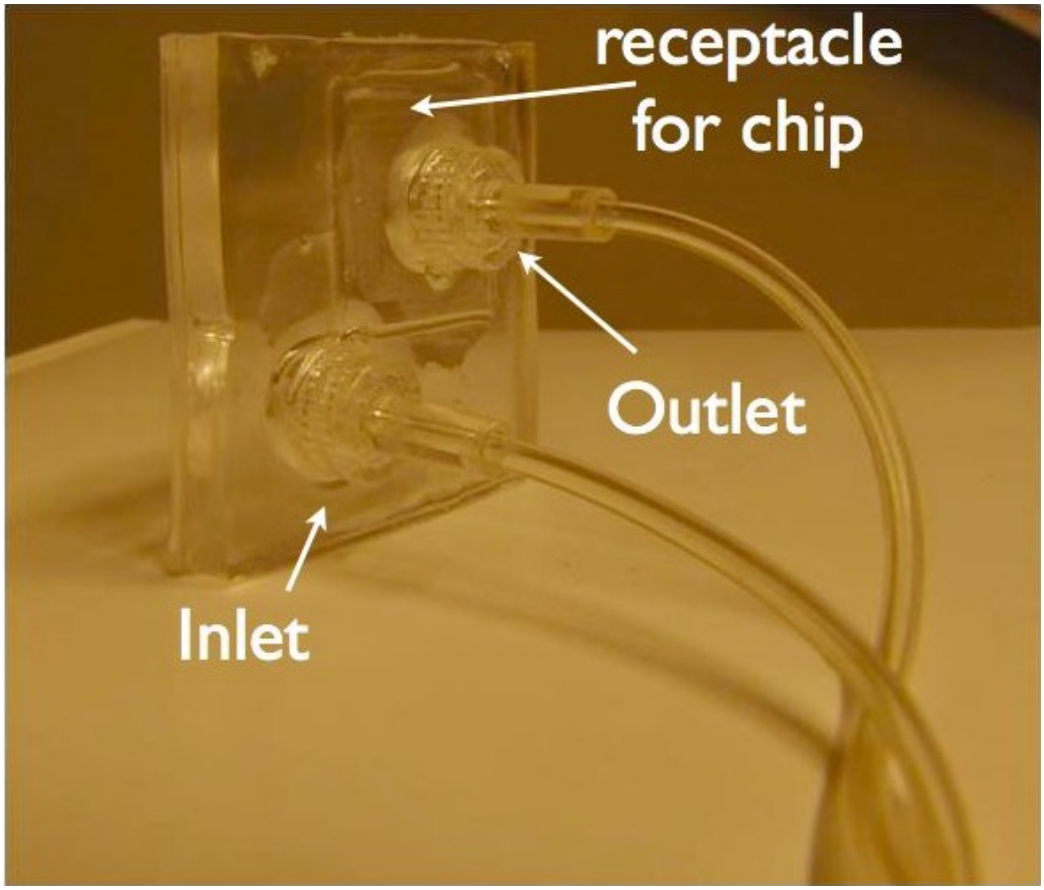

Figure 4.19: Suction-chamber prototype. The image shows the bottom part of the chamber, with the connections already attached. The chip is positioned in alignment with the outlet by a defined rectangle shape of the same dimensions as the chip, which can be seen on the top right corner of the surface

test, and an extra pump was used instead. This pump was connected to the inlet in order to provide incoming fluid, while at the same time it was withrawn by suction at the outlet, with the help of the second pump.

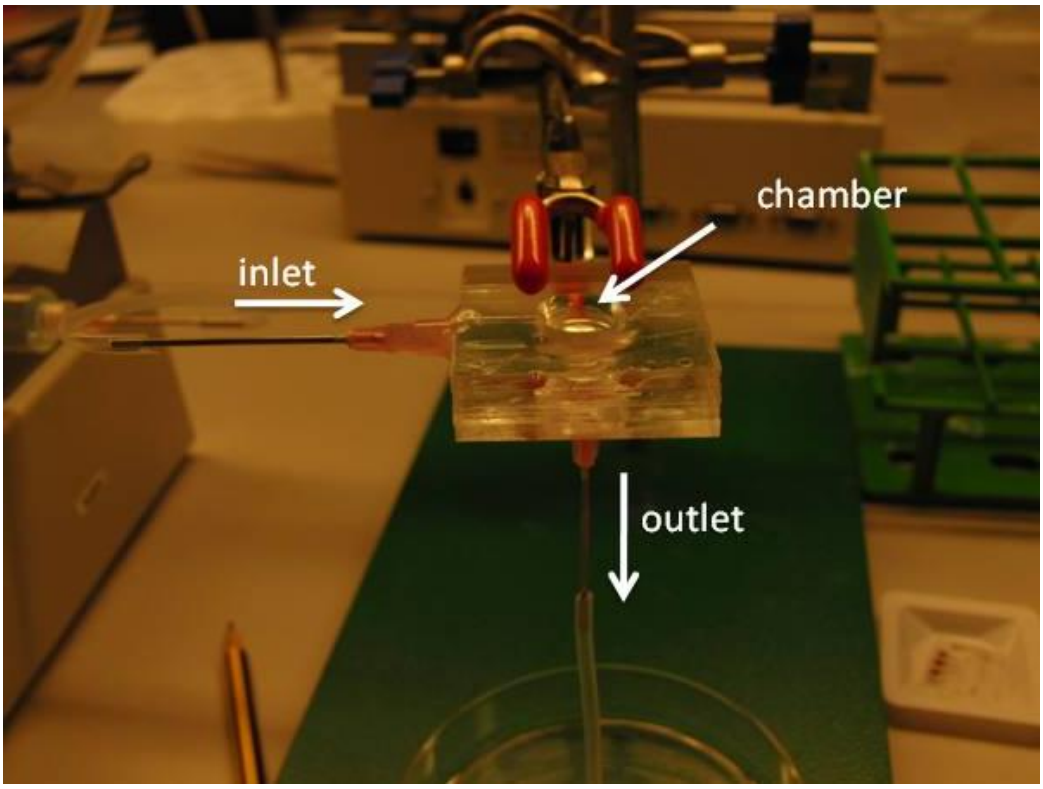

Figure 4.20: Set up for testing the chamber prototype. The inlet and outlets in the image were connected to two different pumps that had the same flow rate.

The purpose of the experiment was to ensure that the device was tightly sealed, so that no leakage would happen. It was also important to test different flow rates in order to check that the concept of the system (suction mechanism) worked without any issues such as clogging or overfilling of the chamber.

In order to do the test, different flow rates were tried, ranging from 3 $\mu l/min$ to 20 $\mu l/min$. This last value is too high for any real set up in which a brain slice should be cultured. The pressure exerted by this rate would be too strong for the tissue, but it serves very well for the purpose of testing the capabilities of the system, since it puts under strain the strength of the bond between the different surfaces of the chamber, and it gives an idea of the pressures that the chamber can stand.

For all the flow rates tried the system responded positively, with no leakage or clogging. The suction of the liquid worked, which proved the functionality of the chips fabricated with holes. To push the test towards a more

realistic situation, a piece of tissue was also placed inside the chamber, as a simulation of the presence of a brain slice, and the chamber did work in the same way as previously.

It was also observed that the hydrophobicity of the PMMA builds up a torus-shaped body of water from the outer ring of the upper chamber. This torus starts by filling the volume of the ring, and continues building itself up the wall of the chamber, until it gets to a point where it collapses and falls into the main body of the chamber. The filling occurred, as predicted, evenly around the volume of the chamber.

Therefore, the system showed its functionality and was ready for the next step, which involved an experiment with a real brain slice.

4.5.3 Culture of brain slice

The test of the culture chamber prototype was carried out in collaboration with Jan Bert Gramsbergen, at the Neurobiology Research Institute of Molecular Medicine University of Southern Denmark. Cultures were prepared as described in Bonde *et al.* [87]: animals were handled according to ethical rules set by international guidelines. Eight day old rat puppies (Sprague Dawley) were decapitated and the hippocampal region isolated under aseptic conditions. The hippocampi were sliced into 350 μm thick, transversal sections by a McIlwain tissue chopper, and afterwards transferred onto a Gey's balanced salt solution (100 ml GBSS, Gibco, Paisley, Scotland) with 1 ml 50 % D-glucose (Merck, Darmstadt, Germany) for separation and trimming of the tissue slices. The slices were kept in a fridge for 1 hour, after which they were placed in the incubator for 4 hours before handling them onto the culture chambers.

Preparation of setup

In any experiment involved in culturing brain slices, it is extremely important to ensure that all equipment is completely sterilized, and the brain sliced manipulated under a laminar flow bench. Otherwise there is a high risk of contamination that would most likely lead to the death of the tissue. As for the sterilization protocol in the particular case of the chamber in study, the material used in its fabrication imposed some restrictions in the method of use. Since PMMA doesn't tolerate temperatures higher than 60 °C, nor the use of ethanol, the sterilization procedure was done by soaking all materials in a 0.1M NaOH for 2h, all of this performed under a laminar flow bench in order to preserve the sterility of the environment.

After this, all the tubing and inside structures of the chamber were flushed with distilled sterile water for 30 min, in order to get rid of the chemical, and filled afterwards with media. The step of filling the tubing with media

needed to make sure that no bubbles were introduced in the system. It was already mentioned that bubbles are an issue in any kind of cell culture that needs to be avoided. Otherwise, it is almost certain that the culture won't survive.

After these preparations, the already prepared brain slices were put in the chamber reservoir, and closed with a thin film of parafin in order to avoid the evaporation of the media during the culturing time.

At this point, the system was ready to be put in a standard incubator, with a temperature set at 36.5 °C in an atmosphere of 5% CO_2. The pumps were left outside the incubator, and the flow rates for the perfusion and the suction, were set to the same value of 0.5 $\mu l/min$.

4.5.4 Results and conclusions

The culture was left inside the incubator without disturbance for three days, after which it was taken outside and looked under an optical microscope.

The results were unmistakable: the typical morphology of the hippocampus was completely lost and the tissue appeared dead.

Despite that, the flow of medium through the chamber with the microholes had worked throughout the whole experiment, as there was medium in the flow-chamber and also in the pulling syringe. Nevertheless, the presence of air was noticed in the tubing, which may have caused the flow rate to be very variable.

Issues that may have affected the survival of the culture

The potential reasons that may have been the cause of death of the brain slice are the following:

- The design under test doesn't work. This is very unlikely, since the previous flow tests show a good functionality. Moreover, the idea is based in concepts described in previous works, such as perfusion through a silicon chip with holes (which were of the same size, [23])
- Bubbles in the tubing obstructed a constant flow. This factor is an important threat to the survival of the culture, since it doesn't only affect the culture when the bubbles enter in contact with the tissue. It is also a cause of disruption of a constant flow of media in the tubing, changing the flow rate of the system.
- The brain slices were kept in a petri dish in the incubator for maybe too long. The preparations of the system before the placement of the brain slice on it took longer than planned (due to bubble-issues and sterilization).

- Lack of attachement to the silicon surface of the micro-hole chip. No coating was applied to the chip in order to promote its adhesion. This is a normal step when preparing a system for neuronal culture. It was hypothesized that this step may not be required due to the suction mechanism, but it could be that in the end it is absolutely necessary.

Nevertheless, the prototype showed a very positive outcome in regards to the use of a silicon support with holes that can be integrated with electrode arrays. This could facilitate greatly the culture of brain slices on chip. The fact that the flow went through the array of holes was in itself a success. The use of an insert membrane for culture as it is currently done is not compatible with the integration of MEAs, and the solution of the holes on chip provides a more suitable way of culturing the tissue.

With regard to the culture system, this model offers a good prospect for improving the culture of brain slices on chip, but further experiments should be done in order to validate the model.

4.5.5 Future improvements

Flow rate not balanced between inlet and outlet

One of the disadvantages of the system is the need to have equal perfusion and suction rates. If there is a misbalanace, it could result in an overflow or drying out the culture chamber. Both ends would be dissastrous: the former would asfixiate the tissue, while the latter would impede a proper feeding and moisturizing environment.

One potential solution to this unbalance is to connect both rates in a way that would be activated by the same mechanism, instead of using two separate pumps.

Tubing

Although at first not very much thought of, the consideration of the integration of the tubing and fittings in the design are key to avoid potential catastrophes. Too long and wide tubing causes endless problems with formation of bubbles (as already commented), and lack of control of the process of pumping. The perfusion/suction is not easily observable if the tubing diameter is too big. In the case of the experiment with the brain silce, the tubing proved too wide and thus cumbersome to get prepared, that is, bubble free, and it creates a huge unnecessary "dead volume". In a future test, a smaller tubing should be used to avoid all these issues.

Sealing of chamber

It is important to seal the culture system in order to avoid evaporation of the media, which leads to changes in osmolality of the solution that is detrimental for the culture [71]. The sealing mechanism should allow to access the interior of the chamber in order to place the brain slice, and close it tightly afterwards. Also, it is desirable that the sealing material be breathable to gas, which would allow the culture to receive enough O_2 gas and exchange it for CO_2. Finally, it would be convenient that the material sealing the chamber allowed to inspect the slice cultures under a microscope, without contaminating the medium and the cultured tissue. Therefore, it would be ideal that the flow-chamber had a transparent, gas-permeable window which could be opened (to put the slice in the chamber) and closed (to avoid contamination and to allow inspection under the microscope).

4.6 Conclusions

The lack of a system that integrates a reliable solution for brain slice culture on-chip has been one of the main motivations of this project. After a careful analysis of the state of the art in the field, it was concluded that for the culture of thick brain slices (which is a desirable condition for the recording of neuronal networks activity) the best approach was to adapt the well established interface method.

One of the approaches taken was to optimize the shape of a chamber in order to avoid dead volumes and incorporate the interface method with a microfluidic system. This idea caused the origin of a lemon-shape system with a membrane embedded in its body. The system works similarly to the interface technique, in that it uses the membrane as the substrate to grow a brain slice, but it brings the technique a bit further by using forced convection to push the nutrients inside the tissue. By doing this, the inner layers of the brain slice would survive as long as the rest of the tissue.

This prototype was useful for advancing the most common issues that may threaten the integration of a microfluidic platform for brain slice culture. Sealing of the device and the presence of bubbles are major points to tackle in this type of set up.

The application of forced flow convection for the distribution of nutrients in the culture seems a very efficient way to ensure a maximum spread within the brain tissue. Based on this observation, a novel design was proposed, in which the brain is perfused by means of suction from an outlet placed at the bottom of the culture chamber. This mechanism may be also advantageous for anchoring the tissue without any extra help, like a nylon mesh or a coating to promote adhesion, although this need to be proved yet.

Unfortunately, several factors could have been the cause of the death of brain slices in the single experiment (due to time constraints) that was carried out: bubbles in the tubing, or maybe lack of attachement to the silicon substrate. Despite this, the experience conveyed also valuable information, such as the need of small tubing to optimize the set up, or the importance of devising a reliable sealing mechanism. Bubbling is an issue that cannot be set aside either: during the brain slice experiment, it hindered the progress of the set up, and worse than that, it did eventually appear in the system. An important and very positive outcome of this test, though, is the demonstration that the perforated MEA chip allows perfusion through it without any clogging. It was a first test of the chip, and the results were fully satisfactory. The use of the chip as the culture substrate could facilitate greatly the recording of signals during culture, and even though these results have been already published in literature, those attempts didn't aim at long time culture and just a simple vial was used as a culture chamber. With the solution proposed here, it is possible to integrate the MEA chip in the perfused-culture system, which optimizes the conditions for long-time cultures with uninterrupted electrical recordings.

As a closure, it should be stated that the possibilities of the last design presented seem very promising. Based in previous works in literature, the mechanism is unlikely to fail. Its design incorporates a MEA chip to allow long term recordings without interrupting the culture. It is only due to time constriction that the system hasn't been tested further to prove its benefits.

Chapter 5

Movable electrodes

For signal measurements in brain slices, the use of three dimensional electrodes in MEA systems adapts this technology to the particularities of brain slice cultures to improve the quality of recordings. This is so since the presence of neuronal networks arranged in different layers demands structures able to insert themselves within the tissue.

As it has been discussed in previous sections, and demonstrated in literature [24], the use of out-of-plane electrodes improves the recordings of neuronal activity in the brain slices. The penetration inside the tissue avoids dead cell layers and closes the distance between the active cells and the surface of the electrode. On top of that, there is better discrimination of real signals from noise, due to the increase in surface area in comparison with planar electrodes.

Nevertheless, the rigidity of MEA systems impedes any possibility of repositioning of the electrodes; once the brain slice is placed on the array, the recording sites are permanent and the electrodes take measurements in a static position.

It would be advantageous to be able to reposition the electrodes if desired. In the event of a specific neuronal site not signalling, the electrodes could record activity from alternative areas to obtain meaningful data. Such a system would also allow the probing of different layers of the same tissue, which until now is not possible to do, since all devices applied to electrophysiology can only obtain recordings from the same z-plane of the tissue. In the case of a system with movable electrodes, new different layers in the tissue would be accessible, with the added advantage of a minimum handling of the brain slice.

To the knowledge of the author, the incorporation of such a type of mechanism in an electrophysiological system is new (leaving aside micropipettes for patch-clamping, which are actuated manually and record one cell at a time). As such, a careful study of the options for the adequate implementation is needed, in order to choose a suitable mechanism. This study was

done as a Master's project at DTU Nanotech [88], which was co-supervised by me. For details of different implementations of actuation methods and their comparison, the reader is referred to the above mentioned thesis. Here, only a brief description of the methods will be given, in order to understand the reasons for the final choice of method and the actuation mechansim itself.

In the MEMS industry, several actuation methods are available. All the mechanisms are based in well known phenomena. The choice of method depends strongly on the application intended, in its restrictions and requirements. The main actuation mechanisms that will be briefly described are piezoelectric, electrostatic and bimetallic, as the most currently used. Additionally, a pneumatic actuation, widely applied in microfluidic systems, is studied and compared with the previous actuations.

In order to choose an appropriate actuator for the integration with the MEA array of three dimensional electrodes, the following conditions need to be taken into account:

- The temperature of the culture environment cannot be altered
- The nature of the signals to be recorded is electrical, and all external artifacts that could corrupt the recordings of these signals should be avoided
- The minimum displacement that the actuator should be able to deliver is about 20 μm. This value is based on the consideration of having a meaningful movement inside the tissue that would ensure the repositioning of the electrodes into a new layer of cells.
- The moving mechanism must be reversible.

5.1 Actuation mechanisms

5.1.1 Piezoelectric actuation

Whether it is due to genetics or to instructive table conversation, is unknown, but yet again the Curie family had an important breakthrough in science when brothers Pierre and Jacques Curie demonstrated the existence of piezoelectric phenomena in 1880 [89]. Their results paved the way to the understanding of piezoelectricity, and nowadays microphones, accelerometers, ultrasonic transducers, etc. apply this effect as a a sensing principle.

Piezoelectric materials have the ability to convert electrical energy into mechanical displacement (and inversely). When a voltage is applied to the material, it causes a crystallographic deformation in its structure, which translates into an elongation or a shortening of the material.

They are interesting materials for the fabrication of sensors due to their large electrical response to a small strain. In the inverted direction, that is, in the presence of an applied electrostatic force, the perspectives are not so

bright: their strain response is very modest, in the range of 0.1 to 0.2 %, although new combinations of piezoelectric materials have been reported to rise this percentage of up to 1 % [89]. This condition demands a very high driving voltages for displacements of more than a few micrometers, and it is for this reason that they are not usually applied to generate motion.

The use of bimorphs can palliate this shortcome, as reported in [90, 91]. A bimorph is made of a cantilever bonded on each of its sides to piezoelectric materials that respond in opposite directions to an applied electrical field across the cantilever (figure 5.1). The cantilever bends downwards as a consequence of this, with a deflection movement that is very sensitive to small changes in the piezoelectric elements' lengths.

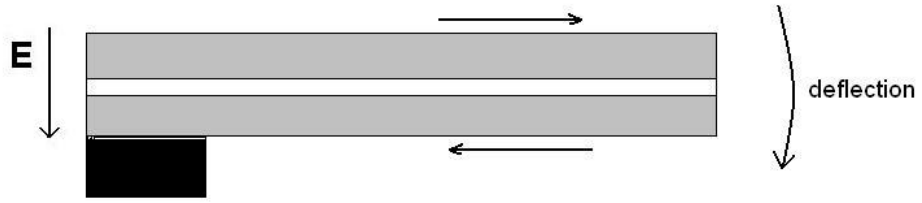

Figure 5.1: The use of a bimorph structure increases the displacement range of a piezoelectric material.Two piezoelectric materials are bonded on each side of the cantilever, and at the application of an electrical field E across the beam they expand in opposite directions. This motion forces the cantilever to bend downwards

The piezoelectric actuation offers a great precision and repeatibility, but one of the downsides of this method, when considering its integration in the MEA fabrication, is the use of a piezoelectric material in the clean room. Piezoelectric materials have a restricted use in most machines and would hinder an easy incorporation in the process flow. Other concerns involved are the biocompatibility of these materials, which should be tested, and the range of deflection that they can provide, as mentioned previously. Yes, it is true that this last problem can be compensated, but the use of cantilevers would complicate the fabrication process and its performance should be tested too. On top of that, the use of electrical fields for the actuation method could interfere with the measurement of the electrical signals coming from the brain slices, and therefore impede a good quality in the recordings.

5.1.2 Electrostatic actuation

Electrostatic forces have been used extensively in MEMS. Electrostatic actuators present the advantage of easy integration in a fabricated device, since the only requirement for the material used is to be conductive, which

is already given by utilizing metal layers in the fabrication process. There is a whealth of applications shown in literature, the most common ones being tunable capacitors, microswitches and micromirrors.

Although there are several varieties of electrostatic actuators, mainly the straight configuration or the comb configuration, all are based in the same actuation principle. The mechanism is based in the application of a voltage between a cantilever or a fixed beam and a second electrode that is separated by a distance from the first. This creates an electrostatic force that deflects the cantilever towards the fixed electrode, in opposition to the spring force of the structure. The straight configuration is by definition, a simple design of two parallel plates as explained, which form a capacitance that governs the displacement equations.

The deflection movement is not linear in relation to the applied voltage, and this makes it usually slightly more difficult to control than other methods. Nevertheless, this fact offers the advantage of giving the maximum force delivered at the end of the motion range, which in the present case would be at the moment of entering in contact with the tissue culture. This would ensure a fast penetration and firm penetration that would minimize the damage in the brain slices.

This method is easy to include in a clean room fabrication process. The materials involved are compatible with other MEMS fabrication steps, and the design itself would be easy to incorporate with the electrodes, since those could be one side of the capacitor actuator system, whereas the second side could be placed as a substrate for the culture site, on top of the electrode array. Another advantage of using this actuation method is that its control is easy and offers a good precision over the motion range. The displacement is regulated by the voltage applied to the electrodes that form the capacitive system, and therefore a simple voltage controller would provide a reliable control over the actuator.

Despite the advantages of this technique, there is a main concern when applying the electrostatic actuator to the MEA system. Due to the nature of the actuation (electrical), it could create interferences with the signals recorded from the cells in culture (cross-talk). This would result in serious detriment in the quality of recordings, which defeats the purpose of developing three dimensional electrodes. The introduction of an additional source of noise, as this would surely be, would cancel out the benefits of having electrodes with good signal-to-noise ratio.

5.1.3 Bimetallic actuation

This type of actuation is based in the difference in the thermal expansion coefficients of two different materials. The mismatch in the coefficients provokes a thermal stress in the structure, which translates into a deflection.

The bimetallic actuator is made of a stack of two materials, usually in the shape of a cantilever, with the same length. The materials need to present different heat expansion coefficients. When the whole structure is heated (usually by an electric current), the cantilever will bend according to the bending moment generated by the difference in thermal expansion of the two materials. The cantilever needs to be designed according to the desired deflection, since the motion will depend on the geometrical parameters of the actuator, mainly the thickness of the two layers, but it is a good actuation method if large deflections are desired.

One of the disadvantages, though, is that in order to obtain a fixed position once the deflection has reached a desired point, the temperature needs to be kept at that value. This is not a very energy-efficient mechanism if current is used as the heating element.

In any case, the most important point to keep under consideration when applying this actuation method is the temperature effect in the rest of the system. It is imperative to ensure that it won't affect the environment of the brain silce culture.

5.1.4 Pneumatic and phase change actuation

Although sometimes described separately, pneumatic and phase change actuators use the same principle. The concept driving the actuation is based in the deflection of a membrane by a difference in pressure applied to it. The difference between the two subcategories, as they could be called, is that the first introduces pressure in a sealed system as the actuation mechanism, whereas the change actuation method needs a material that modifies its phyisical state, expanding in volume and therefore applying pressure to the system.

Pneumatic actuators have been used in MEMS for the design of pressure sensors. The larger the membranes are the smaller the pressure that needs to be applied in order to obtain large deflections. The deflection of an entire array of electrodes will not move uniformly all the electrodes, since there will a maximum deflection at the center of the membrane. This should be taken into account if it were to be used as the final actuation mechanism. The fabrication of this type of mechanism is very straight forward and would be easy to integrate in the fabricaiton process of the electrode array. It simply needs a membrane, and a cavity underneath that could be connected to a pressure controller in order to regulate the pressure that moves the membrane.

It should be considered, though, that a pressure controller doesn't provide a good control over the parameters of the actuator as it is the case of an electrically driven mechanism.

Nevertheless, some alternatives can be used instead of the application of

direct pressure to obtain a deflection in the membane. The change in pressure inside a cavity can be achieved by means of the expansion of a material, like a thermally expanding material or a hydrogel. These alternatives have been used extensively in microfluidics, for applications in valves. The concept is based in the same principle as mentioned before: a membrane is deflected so that it obstructs the opening of a microchannel, thereby interrupting the flow. The field of microfluidics has used the properties of phase changing polymers to achieve these deflections. These polymers increase their volume up to 30 % with temperature, and this will introduce a change in pressure that behaves as the activating parameter of the mechanism. As in the case of the bimetallic actuator, care needs to be taken into controlling accurately the temperature on the chip to ensure that it doesn't disturb the culture environment. Apart from this fact, the pneumatic actuation is a simple solution that offers a straight forward integration. Only a membrane and a cavity for the material that is phase changing is required.

5.1.5 Choice of actuator

As mentioned at the start of the chapter, a very extensive work was done by [88] for testing and comparing different actuation mechanisms. The conclusions on the suitability of the actuators for the final integration with the electrode array were extracted from that work.

It must be remarked that the mentioned study was done with the idea of implementing a moving mechanism for each individual electrode, and the final conclusions were based upon a displacement target of 10 μm. Although this is a slight divergence from the aim in the present work (moving the whole array, with a displacement of about 20 μm), the results hold as a measure of the possibilities of each actuation mechanism and their easiness of integration in the final system. Nevertheless, this difference in scope was taken into account during the final choice of actuator, and it will be discussed.

From the commented actuation mechanisms, the piezoelectric one was discarded after the first calculations.This method wouldn't be able to achieve the minimum deflection required. In the analytical investigation, even with the use of a cantilever as means of amplification of the movement (as it was explained previously), the maximum deflection of a material with a strain of 0.2 % was not higher than 5 μm. The electrostatic actuator was also inefficient in delivering the necessary movement range, and for the aimed displacement (in the case-study, 10 μm), a voltage of 100 V was required, which is not realistic for an electrical device.

Two more mechanisms were tested, a bimetallic actuator and a phase change actuator. Both mechanisms are valid for the purpose of the investigation, achieving the required displacement without any problem. For the case of the bimetallic actuator, cantilevers in between 400 and 500 μm in

length had the right dimensions to provide 10 μm of vertical motion while keeping the electrodes at a temperature not higher than 36.8 °C. During the introduction of the actuation methods, it was mentioned that the temperature level was a main concern for the use of this actuator. This fact was investigated, and the results showed that the length of the cantilever affects directly the temperature of the electrode. By choosing an appropriate length, the increase in temperature can be controlled. Nevertheless, the use of long cantlivers may restrict the dimensions of the array of electrodes, and should be taken into account.

The phase change actuator was tested by using polyethylene glycol (PEG). In particular, PEG8000 was the polymer used in all the experiments, with a melting point at 65 °C and a volumetric expasion at that temperature of 30 %. For the realization of the experiments, a thin layer of PDMS was used as the membrane for the deflection. This was done for ease of fabrication, but PDMS is not a suitable material due to its considerably high thermal conductivity. If used in a final design with the electrode array, the heat for expanding the PEG would transfer to the electrodes, since they would be placed on top of the membrane, and this heat would consequently arrive to the culture environment.

Conclusion

From the two possible actuation methods to use, the phase change actuator was chosen due to its easy integration in the main fabrication process of the electrode array. It basically implies the addition of a membrane and a cavity underneath, as it will be explained in the following sections. In contrast, the fabrication of cantilevers with electrodes, as it would be required by the bimetallic actuator, is not trivial and this solution was discarded. On top of that, the complication of the cantilevers presence is not justified in the case of a displacement of the total group of electrodes. The bimetallic actuation method is very promising for the individual movement range, but the calculations performed during the analysis of the method aren't adjusted for the concept of moving a surface area as broad as the whole chip.

In conclusion, the phase actuation method is the most suitable candidate for the integration of a movable mechanism for an array of electrodes. This concept will be taken into practice by first, fabricating the device, and second, measuring the obtained deflection.

5.2 Analytical examination of design

The mechanism of a phase change actuator is based in the thermal expasion of a material, as it is shown in figure 5.2. The volumetric increment of

the fluid increases the pressure exerted over a membrane, thus provoking its deflection.

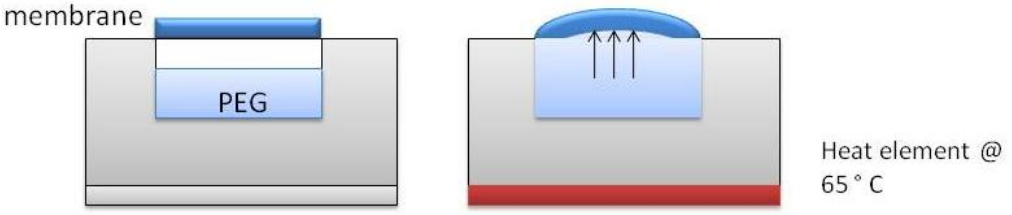

Figure 5.2: Phase-change actuation mechanism. A fluid contained in a reservoir is heated to its melting point. In the case of the experiments, PEG expands at 65 °C about 30 % of its volume. The increase in volume produces a pressure in the membrane placed above the reservoir. The membrane will deflect as a consequence of it.

Several factors need to be considered for the design of the actuator, namely the maximum stress that the membrane stands before rupture, and the relationship between the expanded volume and the pressure exerted. The applied pressure needs to be such that a deflection of at least 20 μm should be reached. It is then necessary to establish what is the relationship between the pressure and the movement of the membrane.

The following calculations have been made by considering a reservoir of 8 mm^3 of volume (a cube of 4x4 mm of side by 0.5 mm of height). This is due to the fact that the area of the array of electrodes is a square of the same dimensions. The idea of the design is to fabricate the membrane lying underneath this array, and therefore it makes sense to take these magnitudes as a guidance for preliminary calculations. The height is not chosen arbitrarily either: it corresponds to the thickness of a single wafer, and as it will be explained in detail later, the cavity will be fabricated through the depth of a wafer.

Based on the previous experience when testing the different actuators, the material used for these experiments will be based on the expansion of PEG. As explained before, this polymer has the convenient property of expanding to a 30 % of its original volume when heated past its melting point of 65 °C. Its parameters will be therefore used for the analytical calculations that are shown in the next section.

As for the material of the membrane, silicon oxide is considered for its good thermal isolation and the availability in standard fabrication processes for MEMS. It is important that the material of the membrane doesn't allow the heat to go through it. In this way, it serves as a barrier between the heated liquid-actuator and the culture space for the brain slice, which cannot be affected by any change in its temperature.

5.2.1 Theoretical deflection of a membrane

To calculate a deflection in a square membrane, which is fixed in all its sides (as it is the case), upon the effect of an external pressure, the theory of plates developed by Timoshenko in the 50's [92] gives a range of equations that predict these parameters. The theory establishes two different regimes, depending on the range of the deflection: large deflections and small deflections. It is considered to be in the small deflection mode if the movement is much smaller than the thickness of the membrane. This isn't the case in the situation at hand, where a thin membrane should provide a motion of at least 20 μm. Therefore, the dynamics of the movement will be considered to fit into the large deflection type.

In accordance to the theory of plates by Timoshenko [92], the pressure P necessary to produce a (large) maximum deflection w_0 on a square membrane can be estimated by:

$$P(h) = \frac{E}{(1-\nu)}\frac{h^3}{a^4}w_0\left[\frac{1}{12\alpha(1+\nu)} + C\frac{w_0^2}{h^2}\right] \tag{5.2.1}$$

where the linear component belongs to the case of a small deflection, and the cubic component is added in the presence of large deflections.

E and ν are, respectively, the Young's modulus and Poisson's ratio of the material used for the membrane. For a square membrane, a is its side length and h its thickness.

As for the coefficients α and C, their values are given as follows (for square membranes). For small membrane deflections (when $w_0 \ll$ h), Timoshenko gave the value of $\alpha = 1.2610\ 10^{-3}$. C was calculated by [93] for the regime of large deflections, and it is given by the expression:

$$C = 21.62(1.41 - 0.292\nu)$$

In the case of a membrane of silicon oxide, $\nu = 0.42$, which leaves C with a value of 27.8.

Figure 5.3 shows the dependency of the pressure with the thicknes of the membrane. For the calculations, it was considered to have a minimum displacement of 20 μm at the center of a square membrane of 4x4 mm.

On the other hand, it is important to consider the design restrictions imposed by the bending limits of a thin membrane. This limit is dictated by the yield stress of the material used for the fabrication of the membrane. If this limit is overcome, the membrane stops streching and breaks. According to [88], it is safe to ensure a stress over the membrane that won't reach half of the yield stress value, in order to compensate for possible thickness variations in the material. In this case, the pressure limit is given as:

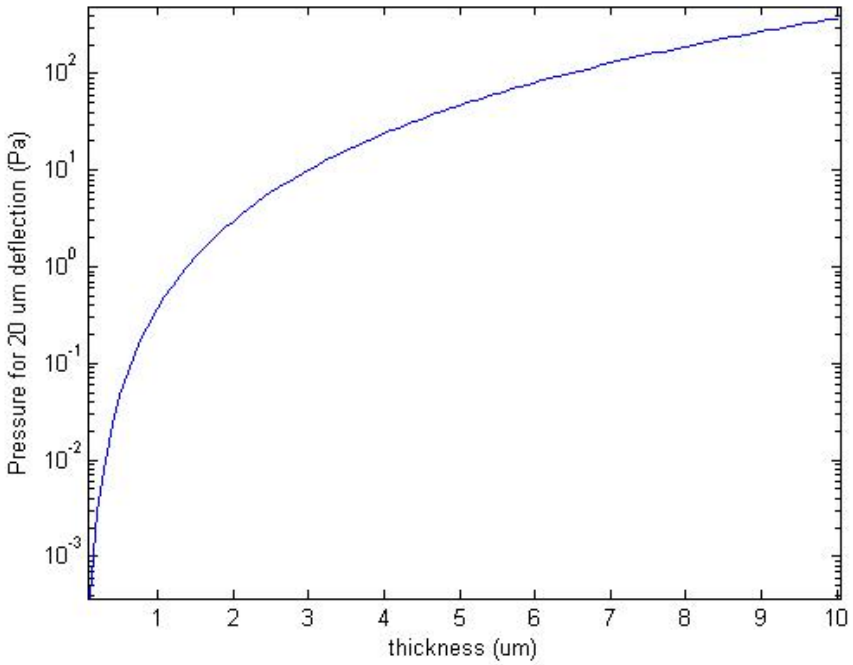

Figure 5.3: Plot of the pressure required to deflect 20 μm a square membrane of 4 mm of width, as a function of the thickness of the membrane

$$P_{limit}(h) = \frac{\sigma_{limit}}{A}\frac{h^2}{a^2} \tag{5.2.2}$$

where A = 0.294 is a correction factor and σ_{limit} is the maximum safe stress for the membrane.

Furthermore, the design of the membrane should take into consideration the robustness of the system when being handled. The membrane should be able to withstand a gravity pull of 200g (with g as the normal gravity pull). Equation 5.2.3 translates this force into pressure:

$$P_g = 2000\rho g h \tag{5.2.3}$$

For silicon oxide, $\rho = 2.5$ g/cm^3 and $\sigma_{limit} = 8$ GPa [88].

Having all these factors in mind, it is very useful to observe figure 5.4, where the three values of the pressures given by 5.2.1, 5.2.3 and 5.2.2 are represented together. The plot shows cleary how the upper limit given by the yield stress of the membrane is never reached by the pressure needed to cause a deflection of 20 μm, which is a good indication that the design is feasible.

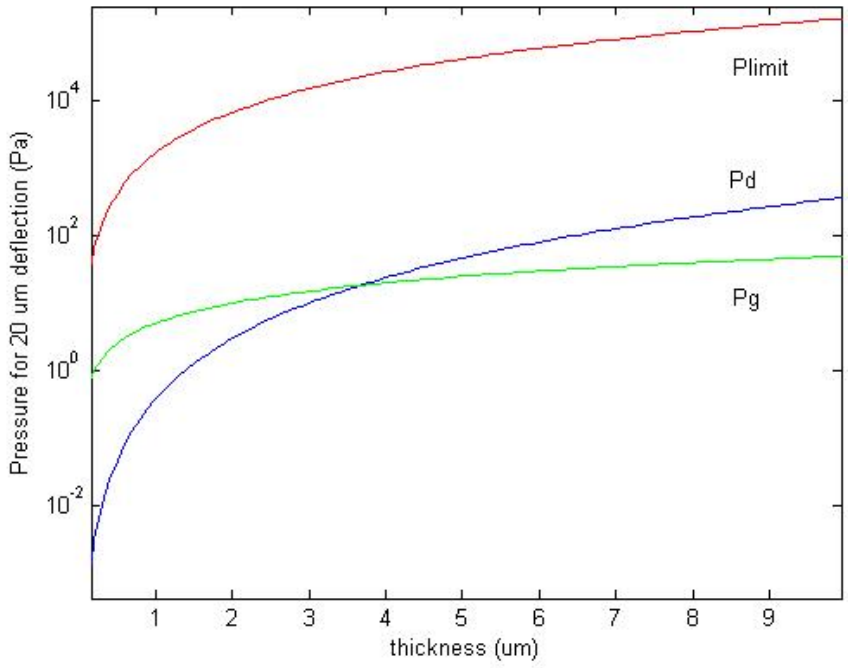

Figure 5.4: The pressures represented agains the thickness of the membrane show the limit value P_{limit} that shouldn't be reached, and P_d and P_g the deflection pressure and gravity pull pressure, respectively

5.2.2 Theoretical pressure due to phase change

Tait's equation is an empirical PVT relationship for polymer liquids. This equation is widely used to represent high-pressure density data for liquids [94]. In the case of the current analytical calculations, it is useful for the relation of the pressure to a certain volume of the polymer PEG, which is the expanding material of the actuator. Tait' equation is given by the following expression [95]:

$$V(P,T) = V(0,T)\left\{1 - Cln\left[1 + \frac{P}{B(T)}\right]\right\} \tag{5.2.4}$$

where P is the pressure (in bar), T the temperature (in °C and V the specific volume of the polymer (in cm^3/g), which is the inverse of the density. For polymers, C is a coefficient usually taken as a universal constant, C = 0.0894 (dimensionless). In the case of PEG (according to [95]),

$$V(0,T) = 0.8766e^{7.087\times e^{-4}T}$$

and the Tait's coefficient

$$B(T) = 2077e^{-3.947\times e^{-3}T}$$

which is obtained experimentally. For T = 65 °C, then, V(0,T) = 0.91 cm^3/g and B(T) = 1639 (dimensionless).

Assuming that the original volume of PEG was 8 mm^3 (for a reservoir of 4x4 mm of area and 0.5 mm of height), it implies that the mass of the polymer contained inside is

$$m = \rho V = 9.6\ \mu g$$

After applying a T = 65 °C, the volume of the polymer will expand a 30 %. This means that now the density of the material has changed to

$$\rho = \frac{m}{V_{exp}} = \frac{9.6}{10.4} = 0.92 g/cm^3$$

with the value V_{exp} being the expanded volume of PEG. Therefore, the specific volume of PEG is taken as

$$V(P,65) = 1.083\ cm^3/g$$

Substituting these values in equation 5.2.4, one can obtain the pressure exerted by the volume of PEG:

$$P = B(T)\left\{e^{\left(1-\frac{V(P,T)}{V(0,T)}\right)\frac{1}{C}} - 1\right\} \tag{5.2.5}$$

In the case of the given parameters, 5.2.5 gives a result of P = 143.6 MPa.

Let's recall what these calculations were necessary for. In the previous section, a plot of pressure vs. thickness of a membrane showed the values of pressure in order to obtain a delfection of 20 μm. By calculating the pressure exerted by the expansion of the polymer, as it has just been shown, it is now possible to compare the values from both calculations in order to check the feasibility of the deflection in relation to the volume of PEG. In accordance with figure 5.3, the value of the presssure obtained is more than sufficient to deflect a membrane of 8 μm in thickness.

5.3 Fabrication of a phase change actuator

The integration of the actuation method with the MEA is simple. This is one of the main advantages of using phase change actuation as the moving mechanism, as it will be seen during the explanation of the added steps to the already designed sequence of the electrode fabrication.

Considering the design of the actuator itself, the elements that need to be integrated are:

- a membrane underneath the electrode array that can deflect and thereby move the electrodes placed on top
- a cavity filled with PEG, situated underneath the membrane
- a sealing surface to close the cavity after loading the polymer

As the reader is reminded, the electrodes were fabricated in a SOI wafer (chapter 2, section 2.2). At the end of the process, pillar-electrodes stand on top of a surface of silicon oxide. This thin layer of oxide is part of the SOI wafer, and is used conveniently for the fabrication of electrodes. This is so because the presence of the SiO_2 isolates the electrodes from each other automatically.

Using this layer as the membrane of the actuator reduces the complexity of the integration in the design. It also helps in obtaining a compact device, without the need of external parts, and it doesn't increase the cost of the fabrication in regard to more materials for the extra steps, as they are already used during the previous fabrication.

As for the addition of the cavity, this step is very straight forward. Since the cavity needs to be placed underneath the oxide membane, it should be etched in the silicon substrate at the back of the SOI wafer. An SOI wafer is in fact two wafers bonded by an isolation layer (in this case made of silicon oxide), and the one at the back is usually thicker than the one at the top. The silicon at the back needs to be etched with the shape of the cavity, until the hole reaches the oxide membrane. In this way, the system will have the electrodes placed on top of the membrane, and a cavity filled with PEG will operate from the other side of the chip.

Finally, a sealing surface should be placed at the opening of the cavity in order to form a closed reservoir. The original design incorporated two channels to fill the cavity with PEG from outside, with the help of a syringe. The idea of including these channels in the design had the purpose of providing full control of the volume of PEG deposited in the cavity. After the filling, they could be sealed easily with epoxy or any other obstructing material.

In order to incorporate the channels to the design, a single wafer was needed. The idea behind it was to bond the SOI wafer with the single wafer with channels in order to provide a perfectly sealed chip, since the bonding of two silicon surfaces is quite strong.

5.3.1 Fabrication flow

The fabrication of the phase change actuator was done in the pursuit of a Master's thesis that was supervised by me. During this project, the phase actuator was fabricated and tested. Any details that the reader could be missing in this work can be found in [96].

The main steps of the fabrication process are shown in figure 5.5. Two parallel processes are run. The fabrication of a membrane and a reservoir for the polymer is done in a SOI wafer, which was previously processed for obtaining of the electrodes. Another wafer is used for the creation of channels. Once they are finished with their own processing, these two wafers will be bonded together to obtain a sealed device.

Membrane and cavity fabrication

The device layer of an SOI wafer, with 350 μm in total thickness, is used as the material for the process. The SOI wafer is patterned with a positive photolithography (resist of 4.5 μm of thickness in order to stand the etching process) that defines the sites of the cavities. Those are squares of 4x4 mm that should lie exactly at the same location as the array of electrodes (but on the opposite side of the wafer). By doing a back side alignment, the matching of the structures on both sides is ensured. Explained very simply, a back side alignment consists of comparing the top and bottom image of the wafer by using two microscopes, one on each side, and moving the wafer until it sits perfectly in line with the features of the mask for photolithography.

Once the photolithography is done, the wafer is placed in the ASE to etch the cavity, until the buried layer of oxide starts showing. This releases the layer to form a thin membrane.

The etch process was the one provided by the manufacturer for deep trenches, *deepetch*, which was already commented in chapter 2. The process was characterized to have an etch rate of 5.5 μm/min, which meant that the process was left to run for 1 hour. Nevertheless, precautions need to be

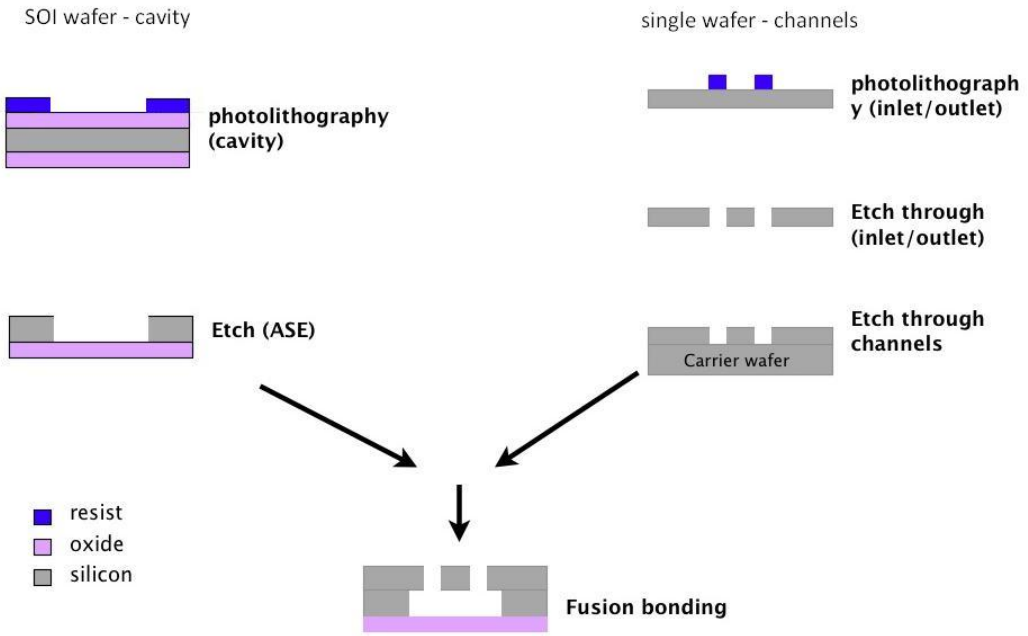

Figure 5.5: Fabrication steps of phase change actuator. On the left hand side, an SOI wafer, where the electrodes had been etched already (not shown here for simplicity), goes through a photolithography step that defines the dimensions of the cavity for the PEG. Following this, the wafer is etched almost completely, until reaching the layer of SiO_2 that is buried in the wafer. On the right hand side, a single wafer goes through all the steps for the fabrication of the channels. In the same fashion as for the cavity, the holes for the channels are defined with a photolithographic step, and then etched in silicon until the hole goes all the way through. Finally, these structures are aligned and bonded to form a sealed cavity underneath the oxide membrane.

taken in order to avoid the tear of the membrane due to the pressure of the ASE chamber during the process. This problem can be easily avoided by placing a carrier wafer underneath the SOI wafer, as a means of support of the membrane throughout the etching.

Two different thicknesses of the membrane were fabricated, which was helpful for testing experimentally their effect on the final displacement of the electrodes. A membrane of silicon oxide of 8 μm in thickness and another one made of a combination of oxide and silicon, with a total thickness of about 60 μm, were obtained.

The main point of fabricating the thick version, though, was to avoid the fragility of the thin membrane. It was seen that the yield of fabricated thin membranes was very poor, and they also broke easily afterwards, just by dipping them in an ultrasonic bath to remove the remaining resist. Therefore, it is recommended, for the sake of robustness of the system, to aim for thicker membranes.

It is important to remark that the sequence in which the electrode and membrane are fabricated influences greatly the results. In principle, nothing would impede a prior fabrication of the membrane and later include the etching of the electrodes, since both processes are done in different sides of the wafer. Despite this, the fact of having a membrane when etching three dimensional electrodes has disastrous effects. This is most probably due to the fact that the membrane starts oscillating during the etching, therefore interfering in the fabrication of the pillars. This effect can be seen in figure 5.6, where the electrode site appears ill defined and the electrode destroyed. By fabricating first the electrodes, the process was reliable and it was possible to integrate both, the electrodes and the cavity, in the SOI wafer. Figure 5.7 shows the electrodes obtained in this way. The cavity was etched underneath afterwards, and used for testing the whole device.

Fabrication of channels

As mentioned earlier, the design was meant to be sealed by the bonding of a wafer that had an inlet and an outlet to insert the PEG in a controllable manner. This is done with a positive photolithography and a posterior dry etch process that continues until the holes are made through the whole wafer. In fact, this process needs to be stopped since etching in the ASE with holes is not allowed. Therefore, a carrier wafer is attached to the wafer with the (almost) holes and finally etched completely. This process is very straight forward and doesn't present any issues.

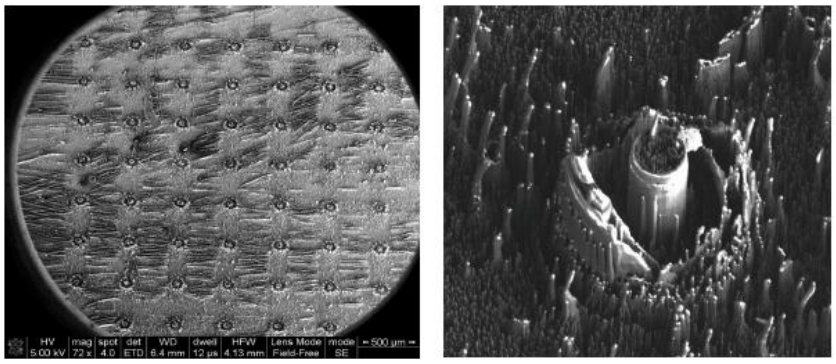

Figure 5.6: Destroyed electrodes during the final integration with the membrane. The presence of the membrane during the etching of the electrodes destroyed the structures of the pillars, most likely due to vibrations. Left: full view of the array. Right, detail of an electrode site

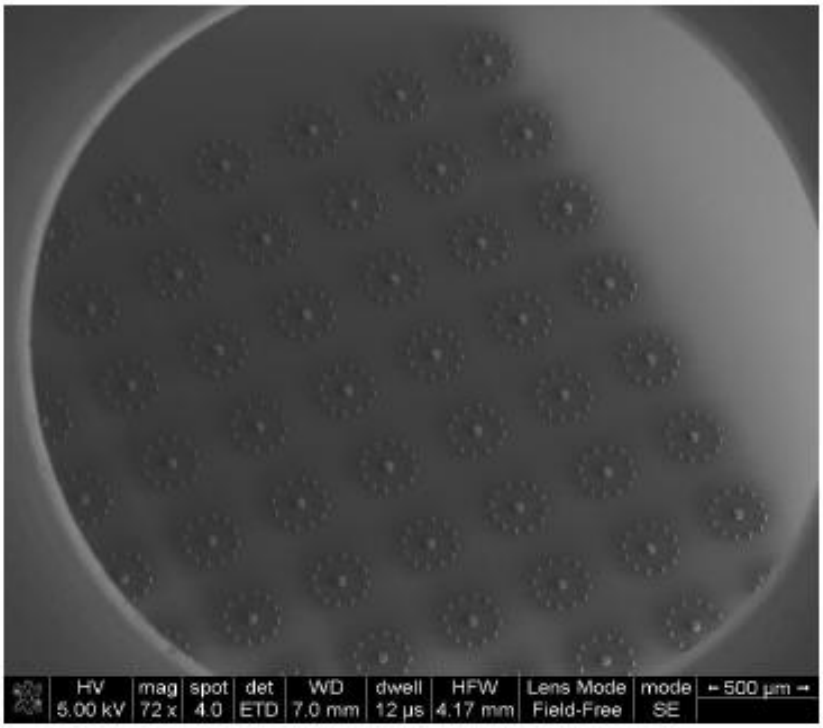

Figure 5.7: It was possible to integrate the electrodes with the fabrication of a cavity if the pillars for the electrodes were etched before proceeding with the etchig of the cavity. The picutre shows the electrodes thus obtained, which had a heigth of 60 μm. This wafer was used afterwards for the fabrication of the cavity at the back, and use in the final testings of the chip.

Sealing

As a final step, the two wafers so processed are bonded by fusion bonding. This technique won't be commented. The experimental details can be consulted at [96], but it will be mentioned that it allows to bond permanently silicon to silicon or silicon to oxide.

Despite several tries and a thorough cleaning of the surfaces, the bonding wasn't successful. The most likely reason for this is the non-uniformity of the wafer surfaces after having being etched in the ASE.

Although other attempts and alternatives were tried, it was not possible to realize the bonding; therefore, it was decided to seal the reservoir of the PEG, already etched in the system, without the disponibility of any channel. Therefore, the cavity was to be filled before the sealing process. The steps to fill the cavity are done as follows:

1. A syringe filled with PEG is heated to the melting point of the polymer
2. The MEA chip is placed on top of an icing block (figure 5.8), and the cavity filled quickly with PEG. The fact of keeping the system cool allows the PEG to solidify from the bottom of the cavity to the top
3. With a razor blade, the excess of PEG is removed from the surface of the chip. The PEG solidifies inmediately due to the change in temperature

Once the filling process is finished, the cavity needs to be filled. This needs to be done with a material that is heat conductive. The reason for this is that the PEG needs to be heated when the actuator is required to produce a deflection, and therefore the heat should go through the sealing layer. The sealing of the cavity is then done with a single silicon wafer. Silicon is highly heat conductive, and therefore suitable for the purpose. Therefore, squares of silicon of the same size as the chip were diced. In order to seal this surface to the surface of the actuator, a thin layer of PDMS is spun onto the silicon wafer and activated by plasma to promote the adhesion. After clamping this layers to the chip, the system is sealed and ready for use.

5.4 Measurement of membrane deflection

Optical focus readout

It is possible to measure the deflection of the membrane with the simple help of an optical microscope. Heights of objects can be measured by focusing on them and using the focus units as a measuring scale. For this, it is required to calibrate previously the focus units in order to be able to convert them into length units. This is done by focusing on an object of known dimensions. This

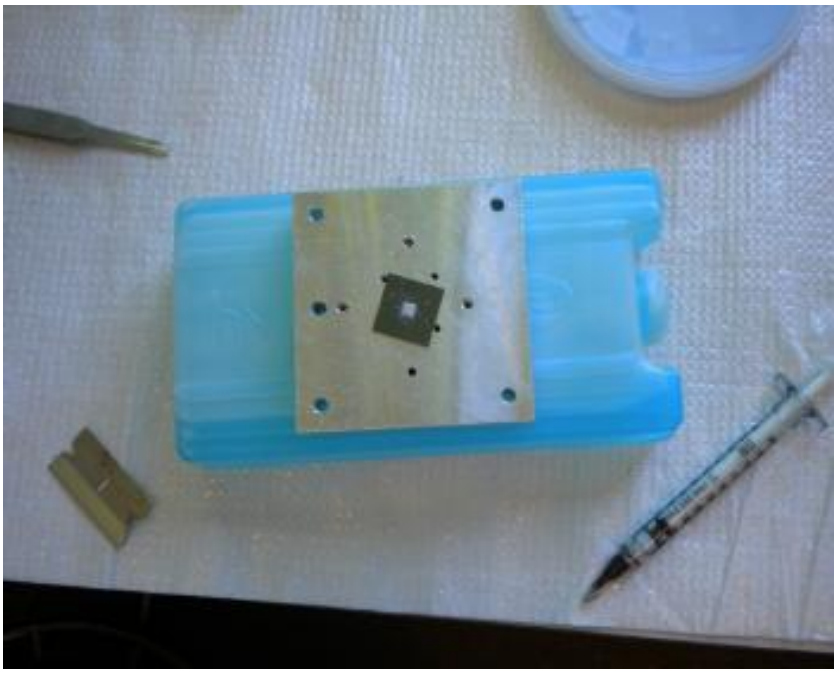

Figure 5.8: Filling cavity with PEG

measuring technique allows the measurement of distances in the z direction as small as 2.5 μm [88].

For the characterization of the membrane actuation, the following set up was prepared: a custome-made holder (figure 5.9) was made to hold the chip steady while at the same time allowing to heat it. The holder is made of two aluminium parts that screw together, with an opening on the top to allow the visualization of the deflection of the membrane. The bottom of the holder is placed on a hot plate, which is used to heat the chip from underneath by passing a current through it. The temperature is controlled by connecting a temperature sensor to the plate, which ensures the reaching of the melting point of the polymer (65 °C).

The holder is placed on an optical microscope (figure 5.10). The focus is adjusted on the center of the membrane and a particular point at the side. These same measurements are repeated after heating up the system to 65 °C, adjusting again the focus to the necessary range. To calibrate the microscope focus, a 9 μm sample is placed on the microscope and the focus adjusted. This gives the translation factor of focus units into heights.

For the membrane made of silicon oxide of 8 μm of thickness, a deflection of 79 μm was measured. In the case of the combined membrane of silicon + silicon oxide, which had a total thickness of 60 μm, the displacement measured was 12 μm.

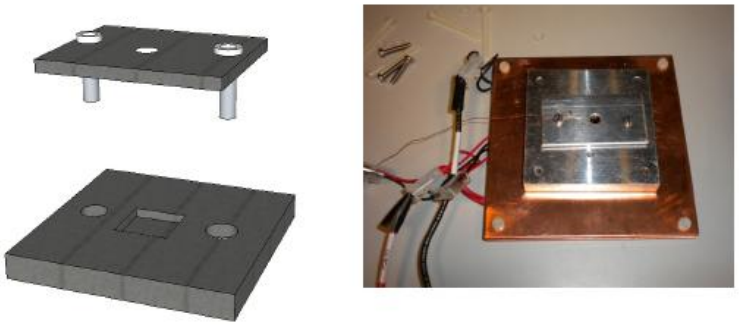

Figure 5.9: Holder for the actuation mechanism [96]

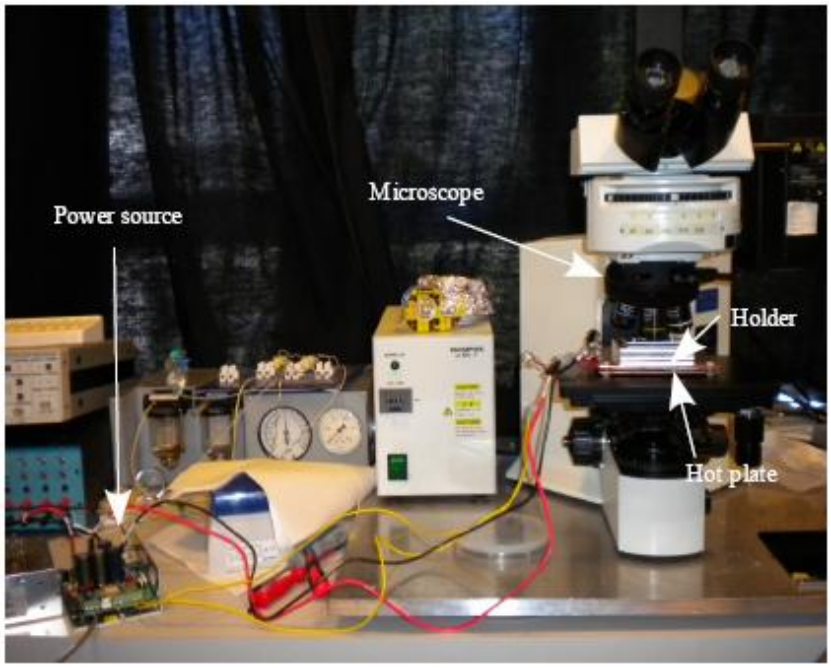

Figure 5.10: Set up to measure deflection of the MEA chip. The microscope is focused on a point on the surface of the membrane before and after heating the actuating polymer PEG. A holder made of aluminium keeps the device in place during the measurements. The holder is connected to a temperature controller in order to ensure that the temperature is set to the right value (from [96])

5.5 Summary and conclusions

The fabrication and integration of an actuation mechanism to move the array of three dimensional electrodes was realized. The use of a phase change actuator proved a good solution in regard to ease of integration with the flow of the process already designed for the MEA itself. The only additon required is a reservoir and a sealing mechanism on top of it. Previously to the sealing, though, a manual filling of the polymer PEG is required.

The performance of the system was measured for two different thickness of the membrane that deflects. The displacement obtained for a membrane of 8 μm, although smaller than the one predicted by the simulations (the experimental 80 μm against the theoretical of 250 μm), is considered an excellent result as it is possible to obtain such large deflections.

As for the measurement of deflection in a more rigid, thicker membrane (60 μm of silicon and oxide), the results were quite poor in comparison with the first ones already commented. In any case, a more modest displacement of this membrane was expected, in contrast with the thiner one, since silicon has a much higher Young' modulus than oxide (185 GPa against 70 GPa for SiO_2), and the total thickness of the final membrane was 7.5 times thicker than the first one tested. The main purpose of fabricating such a thick membrane was to ensure the feasibility of the fabrication process and to do a test on the mechanism of the actuation method, which proved functional. The range of deflection can be incremented by modifying slightly the dimensions of the design, be it the thickness of the membrane or the reservoir itself. In order to ensure a proper fitting of the design, though, simulations with the change of parameters should be carried out.

5.5.1 Outlook

As a first experimental test, this work proved very successful. Nevertheless, the system lacks of control in the deflection movement, which is an important issue. The deflection is caused by the volumetric expansion of the polymer PEG, and therefore the fixed volume in the reservoir determines the amount of pressure transferred to the membrane placed on top. This limitation could be avoided by the addition of a microchannel structure to the design, in order to control the volume introduced in the PEG chamber.

Another important feature for an optimal integration of a final system is the addition of a heating mechanism on-chip, so that no external hot plate would be required. This could be done with the design of a resistive heat element at the bottom of the reservoir, where heat could be generated by current.

Chapter 6

Conclusions

6.1 Conclusions

The use of MEAs in electrophysiology has many advantages and is most suitable for experiments on brain slices, due to its ability for recording simultaneously at multiple sites of a network and stimulate local areas of the tissue. However, one of the disadvantages of using this technique in comparison to patch-clamp is that the amplitude of the signal recorded is usually much lower, and with additional noise picked-up from the environment and the electronics.

A novel type of 3D electrode

The main part of this work aimed at obtaining a novel type of electrode for the improvement of performance of MEAs in experiments on brain slices. The starting point of this project was based on the idea projected by [24, 30] of replacing conventional planar electrodes with three dimensional structures. It was proven, both theoretically and experimentally, that three dimensional electrodes improved the quality of recording. This fact is due to the ability of the electrodes to penetrate the tissue, avoiding a dead cell layer that usually surrounds the brain slice and thus reaching active sites of the tissue.

For the fabrication of three dimensional structures, silicon was the material of choice due its biocompatibility and robustness, but most importantly due to the availability of microfabrication technology resources at Danchip, @DTU Nanotech. The fabrication of the electrodes was achieved after trying different techniques of silicon dry etching, and learning the effects of different parameters on the process. The choice of this technique was based on the belief that it would simplify the process of obtainment of high aspect ratio pillars, as it is a technique tailored for that specific purpose. Nevertheless, the optimization of the fabrication process proved to be not so straight forward and different methods to control unwanted effects in the process had

to be developed. The final fabricated electrodes present a height of about 60 μm and very sharp tips, of approximately 1 μm, but the most interesting feature of these structures is their particular profile, which was a pronounced scalloping shape. It is hypotezised that this profile may help in the promotion of attachment of the tissue to the surface of the electrode without the need of any external anchoring, but this idea will have to be tested before any further comment.

In comparison with the aforemention works, the fabricated electrodes present improved impedance values that were measured in different experiments. The characterization of the electrodes showed also a decrease in the impedance of 1.5 against similarly fabricated planar electrodes, thus confirming the expected behaviour reported by [24].

The electrodes were also tested mechanicaly by inserting them into a thick layer of PDMS, showing no tear or wear after several experiments where they were displaced in both a perpendicular and transversal direction within the PDMS surface. However, despite these results, an unexpected effect appeared consistently in the electrodes: after fabrication, and even without them being used, many of them were cleaved off from the surface of the chip. This is most probably due to the fact that they are fabricated on a silicon oxide surface, and it may be that the electrode structures, which are made of silicon, are not well attached to this substrate. Additionally, the depostion of silicon nitride as a final passivation layer may have increase the stress on the electrode structures, therefore contributing to their breaking.

Culture chamber

A second aim of the project was to integrate a culture system on-chip, in order to allow for long term recordings of brain slices *in vitro* without the need to disturb the tissue and change the sterility conditions of the culture.

After a thorough analysis of the traditional culture techniques and the alternatives given by the microfluidic community, it was clear that the integration of the interface culture method together with the chip would promote a thick slice to grow and survive for a long period. Thick slices are preferable for network activity studies, since the connectivity of cells is best preserved and presents more similarities with the real structure of the brain tissue.

Two different designs were proposed, with different aims. In the first, focus was placed into optimizing the shape of the chamber (lemon-shape chamber) in order to avoid dead volumes. This is desirable for a uniform distribution of nutrients that guarantees equal feeding rate to all areas of the culture. In the second, a perfusion top down was suggested as an alternative to standard methods. The suction of media from the bottom of the chamber force-feeds throughout the brain slice tissue and anchors it to the substrate, which is the MEA itself. Experiments with brain slices were performed with

both models, unsuccessfully, although the functionality of both models was shown. In the case of the lemon-shape chamber, it has been seen that it can be used successfully as a cell trap chamber. In the case of the suction model, the system was able to perfuse top-down throughout the MEA chip.

Movable electrodes

The ability to move the electrodes inside the brain tissue could be an advantageous feature. Electrophysiological experiments would have the possibility to change the sites of recording if necessary, or penetrate a different layer within the tissue in order to obtain complementary information to previous recordings. No similar work has been found in literature, and its realization was based in typical mechanisms used in the area microelectromechanical systems (MEMS). The choice of the actuation method was based in the desired deflection range and easiness of integration in the already fabricated MEA. A phase-change actuator was finally integrated in the chip and tested. The experiments showed very encouraging results, as a deflection of the array could be measured. This deflection depends strongly on the thickness of the membrane used in the design, as it was shown experimentally.

6.2 Outlook

First of all, careful investigation needs to be done with regard to the issue of the stability of the electrodes. This test wasn't done at the time of writing this thesis due to time constrictions, but the author is optimistic in the outlook of this analysis. If it were confirmed that the problem lies in the attachment of the electrodes to the substrate layer, a slight modification in the fabrication process would guarantee the avoidance of this issue. For instance, the use of an SOI wafer could be replaced by a single wafer. The issues related to the metalization of the electrodes in this type of wafer was solved during this project with a novel method that polymerizes the structures in order to make them conductive [49].

The most important step to follow after the finalization of this work is to test the performance of the MEA in a real electrophysiological experiment. Although this experiment was scheduled during this project, the issue of the breaking of the electrodes impeded its final realization.

With regard to the culture system, the author is inclined to believe that the suction model presents a great potential as a culture system. It has the advantage of integrating the MEA in its design, and the method of perfusion is devised to maximize the nutrients reaching all layers of the brain slice in culture. This avoids the common problem of isolation of the inner layers of the tissue from the nutrient flow, which leads to its death. From the

experience aqcuired during the testing, it was clear that with few minor improvements in the set up the system would succeed in culturing brain slices for a long period.

Last, the use of movable electrodes opens a new field within the MEA technology. The fabrication of the first prototype was very successful and the results are promising. However, for a final application it needs to be improved. There are some minor issues that need to be addressed, like the mechanism to control precisely the volume of the polymer-actuator that forces the displacement, or the integration of a heating system in the chip to obtain a compact system.

The filling of the cavity could be realized in a more controllable way by incorporating an inlet to allow a perfusion of the desired volume of the polymer. In fact, by having acces to the cavity in this way, it is feasible to vary the polymer volume in order to tailor the deflection of the sytem. As for the heating element, this could be done by simply patterning a metalic resistance at the bottom of the design. A currentpassing through this element would heat it up at a desired temperature.

Appendix A

Appendix

A.1 Journal publications

These section contains a list of the journal articles published or submitted during the submission of this thesis in January 2011:

- High aspect ratio electrodes for brain slice recordings. Patricia Vazquez, Maria Dimaki, Winnie E. Svendsen. Resubmitted at Journal of Microelectromechanical Systems
- Metallization of high aspect ratio, out of plane structures. Advances in sensors and Interfaces, 2009. Patricia Vazquez, Maria Dimaki, Winnie E. Svendsen.
- Three dimensional electrochemical system for neurobiological studies. Patricia Vazquez, Maria Dimaki and Winnie Edith Svendsen. Published in Proceedings of the 31st Annual International Conference of the IEEE Engineering in Medicine and Biology Society, p. 5870-5874, 2009
- Conducting Polymer 3D Microelectrodes. Luigi Sasso and Patricia Vazquez, Jaime Castillo-Leon, Jenny Emneus and Winnie E. Svendsen.
- Fabrication and Characterization of 3D Micro- and Nanoelectrodes for Neuron Recordings. Maria Dimaki, Patricia Vazquez, Mark Holm Olsen, Luigi Sasso, Romen Rodriguez-Trujillo, Indumathi Vedarethinam and Winnie E. Svendsen.

A.2 Conferences

- Polypirrole coating to enhance three dimensional electrodes for neurological studies.Patricia Vazquez, Luigi Sasso, Maria Dimaki, Winnie E. Svendsen . Conference on Electrochemical Science and Technology 2010, Denmark. Oral presentation

- Conductive polymer on three dimensional electrodes for neurological studies. Patricia Vazquez, Luigi Sasso, Winnie E. Svendsen. Advanced Nano Materials 2010, Agadir, Morocco. Oral presentation.
- Three dimensional electro and electrochemical systems for neurophysiological studies. Patricia Vazquez, Maria Dimaki, Winnie E. Svendsen. BMI workshop, Ystad, Sweeden, 2010. Poster contribution.
- 3D electrodes with polyaniline coating for neurophysiological studies. Patricia Vazquez, Luigi Sasso, Maria Dimaki, Winnie E. Svendsen. Biosensors 2010, Glasgow, Scotland. Poster contribution.
- Three dimensional system for neurobiological studies. Patricia Vazquez, Maria Dimaki, Winnie E. Svendsen. EMBC 2009, Minneapolis, USA. Poster contribution (accepted in proceedings).
- Metallization of high aspect ratio, out of plane structures. Patricia Vazquez, Maria Dimaki, Winnie E. Svendsen. IWASI 2009, Trani, Italy. Poster contribution (accepted in proceedings).
- Three dimensional electrodes for the study of neurotransmitters in a microfluidic system. P. Vazquez, P.; J. Castillo; M. Dimaki; W. E. Svendsen. Biosensors. 14-16 May 2008. Shanghai, China. Poster contributon.
- 3D electrodes for neurological studies. P. Vazquez, J. Moresco Lange, J. Castillo, W. E. Svendsen. Nano2Life meeting, Juanuary 2008, Champery, Switzerland. Poster contribution.
- Neurophysiology with three dimensional electrodes. P. Vazquez, W. E. Svendsen, M. Dimaki, J. Castillo. National conference DFS 2008. Poster contribution.
- Uncovering cells by microtechnology. Patricia Vazquez, J. M. Lange, J. Castillo, W. Svendsen. Nano2Life Autumn Meeting, Lund, October 2007

Bibliography

[1] J.L. McGaugh. "Time dependent processes in memory storage". *Science*, 153:1351–1358, 1966.

[2] Scoville W.B. "Loss of recent memory after bilateral hippocampal lesions". *J. Neurol. Neurosurg. Psychiatr.*, 20:11– 21, 1957.

[3] Shacter S. and Singer J. "Cognitive, social, and physiological determinants of emotional state". *Physiol. Rev.*, 69.:379–399, 1962.

[4] Pearce T.M and Williams J.C. "Microtechnology: meet neurobiology". *Lab on a Chip*, 7:30–40, 2006.

[5] Tranquilo J.V. *"Quantitative Neurophysiology"*. byMorgan & Claypool, 2008. Book on neurophysiology.

[6] Lodish H., Berk A., Zipursky S.L., Matsudaira P., Baltimore D., and Darnell J. *"Molecular Cell Biology"*. W.H. Freeman, 2000.

[7] Yamamoto C. and McIlwain H. "Electrical activities in thin sections from the mammalian brain maintained in chemically defined media in vitro". *J. of Neurochemistry*, 13:1333–1343, 1966.

[8] Corner M. A., van Pelta J., Woltersa P. S., Bakera R. E., and Nuytincka R. H. "Physiological effects of sustained blockade of excitatory synaptic transmission on spontaneously active developing neuronal networks - an inquiry into the reciprocal linkage between intrinsic biorhythms and neuroplasticity in early ontogeny". *Neuroscience and Biobehavioral Reviews*, 26:127–185, 2002.

[9] Baker R. E. abd Corner M. A. and van Pelt J. "Spontaneous neuronal discharge patterns in developing organotypic mega-co-cultures of neonatal rat cerebral cortex". *Brain research*, 1101:29–35, 2006.

[10] Shimono K, Baudry M., Panchenko V., and Taketani M. "Chronic multichannel recordings from organotypic hippocampal slice cultures: protection from excitotoxic effects of nmda by noncompetitive nmda antagonists". *J. of Neuroscience Methods*, 120:193–202, 2009.

[11] Gähwiler B.H., Capogna M., Debanne D., McKinney R.A., and Thompson S.M. "Organotypic slice cultures: a technique has come of age ". *Trends Neurosci.*, 20(10):471–447, 1997.

[12] Teyler T. J. and Fountain S. B. "Neuronal plasticity in the mammalian brain: relevance to behavioral learning and memory". *Child development*, 58:698–712, 1987.

[13] Eichenbaum H., Yonelinas A. R., and Ranganath C. "The medial temporal lobe and recognition memory". *Annual Reviews of Neuroscience*, 30:123–152, 2007.

[14] Fountain S. B., Y. L. T Ting, and Teyler T. J. "The in vitro hippocampal slice preparation as a screen for neurotoxicity". *Toxicology in vitro*, 6(1):77–87, 1992.

[15] Thomas Jr., Springer P.A., Loeb G.E., Berwald-Netter Y., and Okun L.M. "A miniature microelectrode array to monitor the bioelectric activity of cultured cells". *Exptl Cell Res.*, 74:61–66, 1972.

[16] Gross G.W., Rieske E., Kreutzberg G.W., and Meyera A. "A new fixed-array multi-microelectrode system designed for long-term monitoring of extracellular single unit neuronal activity in vitro ". *Neuroscience Letters*, 6(2-3):101–105, 1977.

[17] Pine J. "Recording action potentials from cultured neurons with extracellular microcircuit electrodes". *J. Neuroscience Methods*, 2:19–31, 1980.

[18] Oka H., Shimono K., Ogawa R., Sugihara H., and Taketani M. "A new planar multielectrode array for extracellular neuronal activity in vitro". *J. of Neuroscience and Methods*, 93:61–67, 1999.

[19] Hofmann F. and Bading H. "Long term recordings with microelectrode arrays: studies of transcription-dependent neuronal plasticity and axonal regeneration". *Journal of Physiology*, 99:125–132, 2006.

[20] Hafizovic S., Heer F, Ugniwenko T., Frey U., Blau A., Ziegle C., and Hierlemann A. "A cmos-based microelectrode array for interaction with neuronal cultures". *Journal of Neuroscience Methods*, 164(1):93–106, 2007.

[21] Greve F., Lichtenberg J., Kirstein K.U., Frey U., Perriard J.C, and Hierlemann A. "A perforated cmos microchip for immobilization and activity monitoring of electrogenic cells". *J. Micromechanics and Microengineering*, 17(3):462, 2007.

[22] Jones K.E., Campbell P.K., and Normann R.A. "A glass-silicon composite intracortical electrode array". *Annals of Biomedical Engineering*, 20:423–437, 1992.

[23] Thiébaud P., de Rooij N.F., Koudelka-Hep M., and Stoppini L. "Microelectrodes arrays for electrophysiological monitoring of hippocampal organotypic slice cultures". *IEEE transactions on biomedical engineering*, 44(11), 1997.

[24] Heuschkel M.O., Fejt Michael Raggenbass F.R., Bertrand M., and Philippe D.R. "A three-dimensional multi-electrode array for multi-site stimulation and recording in acute brain slices". *Journal of Neuroscience Methods*, 114(2):135–148, 2002.

[25] Stangl C. and Fromherz P. "neuronal field potential in acute hippocampus slice recorded with transistor and micropipette". *European Journal of Neuroscience*, 27:958–964, 2008.

[26] Novak J.L. and Wheeler B.C. "Multisite hippocampal slice recording and stimulation using a 32 element microelectrode array". *Journal of Neuroscience Methods*, 23(2):149–159, 1988.

[27] Merril D.R., Bikson M., and Jefferys J.G.R. "Electrical stimulation of excitable tissue: design of efficacious and safe protocols ". *J. Neuroscience Methods*, 141:171–198, 2005.

[28] Hanein Y., Schabmueller C.G.J, Holman G., Lücke P.L., Denton D. D., and Böhringer K.F. "High-aspect ratio submicrometer needles for intracellular applications". *Journal ofMicromechanical Engineering*, 13:91–95, 2003.

[29] Choi Y. "A three-dimensional coupled microelectrode and microfluidic array for neuronal interfacing ". PhD. thesis, 2005.

[30] Thiebaud P., Beuret C., de Rooij N. F., and Koudelka-Hep M. "Microfabrication of Pt-tip microelectrodes". *Sensors and Actuators B-Chemical*, 70(1-3):51–56, 2000.

[31] Marc J. Madou. *"Fundamentals of microfabrication"*. CRC Press, 2002. Book on microfabrication.

[32] Jansen H. V., de Boer M. J., Unnikrishnan S., Louwerse M. C., and Elwenspoek M. C. "Black silicon method X: a review on high speed and selective plasma etching of silicon with profile control: an in-depth comparison between Bosch and cryostat DRIE processes as a roadmap to next generation equipment". *Journal of Micromechanics and Microengineering*, 19(3):41, 2009.

[33] Tsujimoto K., Tachi S., Ninomiya K., Suzuki K., and Okudaira S. "New side wall protection technique in microwave plasma etching using a chopping method". *18th. Conf. Solid State Devices and Materials*, page 229, 1986.

[34] Laermer F and Schilp A. "Verfahren zum anisotropen ätzen von silicium ". Patent, 1994.

[35] Gomez S., Belen R. J., Kiehlbauch M., and Aydil E. S. "Etching of high aspect ratio structures in Si using SF_6O_2 plasma". *Journal of Vacuum Science & Technology A*, 22(3):606–615, 2004.

[36] Kiihamaki J. and Franssila S. "Pattern shape effects and artefacts in deep silicon etching". *45th National Symposium of the American Vacuum Society*, 1999.

[37] Ayon A. A, Braff R., Lin C. C., Sawin H. H., and Schmidt M. A. "Characterization of a time multiplexed inductively coupled plasma etcher". *Journal of the Electrochemical Society*, 146(1):339–349, 1999.

[38] Oehrleina G. S. and Kurogi Y. "Sidewall surface chemistry in directional etching processes". *Materials Science and Engineering*, 24:153–183, 1998.

[39] Coburn J. W. and Winters H. F. "Plasma-assisted etching in microfabrication". *Annual Reviews of Materials Science*, 13:91–116, 1983.

[40] Jansen H., de Boer M., Legtenberg R., and Elwenspoek M. "The Black silicon method: a universal method for determining the parameter setting of a fluorine-based ractive ion etcher in deep silicon trench etching with profile control". *Journal of Micromechanics and Microengineering*, 5:115–120, 1995.

[41] Roxhed N.G.P.S.G. "A method for tapered deep reactive ion etching using a modified bosch process". *J. Micromechanics and Microengineering*, 17:1087–1092, 2007.

[42] May G. S. and Sze S. M. *"Fundamentals of semiconductor fabrication"*. Wiley, 2004. Book on microfabrication.

[43] Ng H.B. and Shearwood C. "A systematic approach to fabricate high aspect ratio silicon microneedles for transdermal drug delivery". *Progress in biomedical optics and imaging*, 8(50), 2007.

[44] Schultze J.W., Osaka T., and Datta M. *"Microelectronic Packaging"*. CRC press, 2005.

[45] K. Seshan. *"Handbook of Thin-Film Deposition Processes and Techniques - Principles, Methods, Equipment and Applications"*. William Andrew Publishing, 2002.

[46] Vazquez P., Dimaki M., and Svendsen W.E. "Metallization of high aspect ratio, out of plane structures". *3rd International Workshop on Advances in Sensors and Interfaces, IEEE*, pages 193–196, 2009.

[47] Hangarter C.M., Bangar M., Mulchandani A., and Myung N.V. "Conducting polymer nanowires for chemiresistive and FET-based biochemical sensors". *J. Mater. Chem*, 20:3131–3140, 2010.

[48] Bartlett P.N. and Cooper J.M. A. "A review of the immobilization of enzymes in electropolymerized films". *J. Electroanal. Chem*, 362:1–12, 1993.

[49] Sasso L., Vazquez P., Vedarethinam I., Castillo-Leon J., Emneus J., and Svendsen W.E. "Conductive polymer 3D microelectrodes". *Sensors*, 10(12):10986–11000, 2010.

[50] Wang Joseph. *"Analytical Electrochemistry"*. John Wiley and sons, 2000. pg 20.

[51] Bard A.J and Faulkner L.R. *"Electrochemical methods: fundamentals and applications"*. Wiley, 2001. Book on electrochemistry.

[52] W.-S. Huang, B.D. Humphrey, and MacDiarmid A.G. "Polyaniline, a novel conducting polymer. morphology and chemistry of its oxidation and reduction in aqueous electrolytes". *"J. Chem. Soc., Faraday Trans. 1"*, 82:2385–2400, 1986.

[53] Karyakin A.A., Bobrova O.A., Lukachova L.V., and Karyakina E.E. "potentiometric biosensors based on polyaniline semiconductor films". *Sensors and actuators*, 33:34–38, 1996.

[54] George P.M., Lyckman A.W., LaVan D.A., Hegde A., Leung Y., Avasare R., Testa C., Alexander P.M., and Langer R. Sur M. "Fabrication and biocompatibility of polypyrrole implants suitable for neural prosthetics". *Journal of Biomaterials*, 26:3511–3519, 2004.

[55] Bagotsky V.S. *"Fundamentals of Electrochemistry edn 2nd. New Jersey"*. Wiley Interscience, 2006.

[56] Borkholder D.A. "Cell based biosensors using microelectrodes ". *PhD. thesis*, 2005.

[57] Trujillo R. "high speed micro fluidic devices for particle counting on a chip ". *PhD. thesis*, 2005.

[58] Zoltowski P. "On the electrical capacitance of interfaces exhibiting constant phase element behaviour ". *Journal of Electroanalytical Chemistry*, 443:149–154, 1998.

[59] Sharp A. A. "I]n vivo penetration mechanics and mechanical properties of mouse brain tissue at micrometer scales ". *IEEE Transactions on Biomedical Engineering*, 56(1):45–53, 2009.

[60] Shergold O. A and Fleck N. A. "Mechanisms of deep penetration of soft solids, with application to the injection and wounding of skin ". *Proc. R. Soc. London Ser. A-Math. Phys. Eng. Sci.*, 460(2050):3037–3058, 2003.

[61] Azar Toufic and Hayward Vincent. "Estimation of the fracture toughness of soft tissue from the needle insertion ". *Proc. Biomedical Simulation*, 5104:166–175, 2008.

[62] Davis Shawn P., J. Landis Benjamin, Adams Zachary H., Allen Mark G., and Prausnitz Mark R. "Insertion of microneedles into skin: measurement and prediction of insertion force and needle fracture force". *Journal ofBiomechanics*, 37:1155–1163, 2003.

[63] Armani D., Liu C., and Aluru N. "Re-configurable fluid circuits by PDMS elastomer micromachining". *Mems '99: Twelfth Ieee International Conference on Micro Electro Mechanical Systems, Technical Digest*, pages 222–227, 1999.

[64] Rambani Koma, Vukasinovic Jelena, Glezer Ari, and Potter Steve M. "Culturing thick brain slices: an interstitial 3D microperfusion system for enhanced viability". *J. of Neuroscience Methods*, 180:243–254, 2009.

[65] Teyler T.J. "Brain slice preparation: hippocampus". *Brain research bulletin*, 5:391–403, 1980.

[66] Bergold P.J. and Casaccia-Bonnefil P. "Preparation of organotypic hippocampal slice cultures using the membrane filter method ". *Methods in Molecular Biology*, 72:15–22, 1997.

[67] Beggs J.M and Plenz D. "Neuronal avalanches are diverse and precise activity patterns that are stable for many hours in cortical slice cultures". *The Journal of Neuroscience*, 24(22):5216 â€“5229, 2004.

[68] Freshney R. Ian. *"Culture of animal cells"*. John Wiley and sons, 2005. Book on cell culture, pg 436-438.

[69] Choi Y. and McClain M.A. "Three dimensional mems microfluidic perfusion system for thick brain slice cultures". *Biomed Microdevices*, 9:7–13, 2007.

[70] Skrede K.K and Westgaard R.H. "The transverse hippocampal slice: a well defined cortical structure maintained *in vitro*". *Brain research*, 35:589–593, 1971.

[71] Young W. K. and Beebe D.J. "Fundamentals of microfluidic cell culture in controlled microenvironments". *Chem. Soc. Rev*, 39:1036â€“1048, 2010.

[72] Zheng W., Wang Z., Zhang W., and Jiang X. "A simple PDMS-based microfluidic channel design that removes bubbles for long-term on-chip culture of mammalian cells". *Lab on a Chip*, 10:2906–2910, 2010.

[73] Kim L., Toh Y., Voldman J., and Yu H. "A practical guide to microfluidic perfusion culture of adherent mammalian cells". *Lab on a Chip*, 7:681–694, 2007.

[74] Hogue M.J. "Human fetal brain cells in tissue culture: their identification and motility". *J. Exp. Zool.*, 106:85–107, 1947.

[75] Gähwiler. "Organotypic monolayer cultures of nervous tissue ". *Journal of neuroscience methods*, 4(4):329–342, 1981.

[76] Stoppini L., Buchs P.A., and Muller D. "A simple method for organotypic cultures of nervous tissue". *J. of Neuroscience Methods*, 37:173–182, 1991.

[77] Berdichevsky Y., Sabolek H., Levine J.B., Staley K.J., and Yarmush M.L. "microfluidics and multielectrode array-compatible organotypic slice culture method ". *J. of Neuroscience Methods*, 178:59–64, 2009.

[78] Blake A.J., Pearce T.M., Rao N.S., Johnson S.M., and Williams J.C. "Multilayer pdms microfluidic chamber for controlling brain slice microenvironment ". *Lab Chip*, 7(7):842–849, 2008.

[79] Wu C., Luk W. P., Gillis J., Skinner F., and Zhang L. "Size does matter: Generation of intrinsic network rhythms in thick mouse hippocampal slices". *J. of Neurophysiology*, 93:2302–231, 2004.

[80] Egert U., Schlosshauer B., Fennrich S., Nisch W., Fejtl M., Knott T., Müller T., and Hamerle H. "A novel organotypic long-term culture of the rat hippocampus on substrate-integrated multielectrode arrays". *Brain Research Protocols*, 2:229–242, 1998.

[81] Tscherter A., Heuschkel M. O., Renaud P., and Streit J. "spatiotemporal characterization of rhythmic activity in rat spinal cord slice cultures". *European Journal of Neuroscience*, 14:179–190, 2001.

[82] van Bergen A., Papanikolaou T., Schuker A., Möller A., and Schlosshauer B. "Long term stimulation of mouse hippocampal slice culture on microelectrode array". *Brain research protocols*, 11:123–133, 2003.

[83] "Alpha Med Scientific". Commercial MEA.

[84] Thiébaud P., Beuret C., Koudelka-Hep M., Bove M., Martinoia S., Grattarola M., Jahnsen H., Rebaudo R., Balestrino M., Zimmer J., and Dupont Y. "An array of pt-tip microelectrodes for extracellular monitoring of activity of brain slices". *Biosensors and Bioelectronics*, 14(1):61–65, 1999.

[85] Jahnsen H., Kristensen B.W., Thiébaud P., Noraberg J., Jakobsen B., Bove M., Martinoia S., Koudelka-Hep M., Grattaola M., and Zimmer J. "Coupling of organotypic brain slice cultures to silicon-based arrays of electrodes". *Methods: A Companion to Methods in Enzymology*, 18:160–172, 1999.

[86] Weber E. "cellcheck internal report ", 2010.

[87] Bonde C., Noraberg J., Noer H., and Zimmer J. "Ionotropic glutamate receptors and glutamate transporters are involved in necrotic neuronal cell death induced by oxigen-glucose deprivation of hippocampal slice cultures". *Neuroscience*, 136:779â€“794, 2005.

[88] Brandt K. "Movable 3 dimensional nano electrodes". *Master thesis, @ DTU Nanotech*, 2009.

[89] Hak M.G. *"MEMS applications"*. Taylor & Francis, 2006. Book on MEMS actuators.

[90] Corey D.P. and Hudspeth A.J. "Mechanical stimulation and micromanipulation with piezoelectric bimorph elements". *Journal of Neuroscience Methods*, 3:183–202, 1980.

[91] Oh K.W. and Ahn C.H. "A review of microvalves". *J. of Micromechanics and Microengineering*, 16:16–39, 2006.

[92] Timoshenko S.P. *"Theory of plates and shells"*. Mc Graw-Hill, 1959. Book on membrane theory.

[93] Bonnotte E., P. Delobelle P., Bornier L., Trolard B., and Tribillon G. "Two interferometric methods for the mechanical characterization of thin films by bulging tests". *J. of Mater. Res.*, 12(9), 1997.

[94] Dymond J. K. and Malhotra R. "The tait's equation: 100 years on". *Internation Journal of Thermophysics*, 9(6):941–951, 1988.

[95] Rodgers P.A. "Pressure-volume-temperature relationships for polymeric liquids: A review of equations of state and their characteristic parameters for 56 polymers". *J. of Applied Polymer Science*, 48:1061–1080, 1993.

[96] Altamura2010. "phase change actuation for neural recordings in tissue slices". *Master thesis, @ DTU Nanotech*, 2010.

List of Figures